

Intergenerational neural mediators of early-life anxious temperament

Andrew S. Fox^{a,b,c,1}, Jonathan A. Oler^{a,c}, Alexander J. Shackman^d, Steven E. Shelton^a, Muthuswamy Raveendran^e, D. Reese McKay^f, Alexander K. Converse^b, Andrew Alexander^{b,g}, Richard J. Davidson^{a,b,c,h}, John Blangeroⁱ, Jeffrey Rogers^e, and Ned H. Kalin^{a,b,c,h,1}

^aHealthEmotions Research Institute, Department of Psychiatry, University of Wisconsin–Madison, Madison, WI 53719; ^bWaisman Center, University of Wisconsin–Madison, Madison, WI 53705; ^cDepartment of Psychiatry, University of Wisconsin–Madison, Madison, WI 53719; ^dDepartment of Psychology, University of Maryland, College Park, MD 20742; ^eDepartment of Genetics, Baylor College of Medicine, Houston, TX 77030; ^fDepartment of Psychiatry, Yale School of Medicine, New Haven, CT 06519; ^gDepartment of Medical Physics, University of Wisconsin–Madison, Madison, WI 53705; ^hDepartment of Psychology, University of Wisconsin–Madison, Madison, WI 53706; and ⁱDepartment of Genetics, Texas Biomedical Research Institute, San Antonio, TX 78245

Edited by Huda Akil, University of Michigan, Ann Arbor, MI, and approved June 9, 2015 (received for review May 4, 2015)

Understanding the heritability of neural systems linked to psychopathology is not sufficient to implicate them as intergenerational neural mediators. By closely examining how individual differences in neural phenotypes and psychopathology cosegregate as they fall through the family tree, we can identify the brain systems that underlie the parent-to-child transmission of psychopathology. Although research has identified genes and neural circuits that contribute to the risk of developing anxiety and depression, the specific neural systems that mediate the inborn risk for these debilitating disorders remain unknown. In a sample of 592 young rhesus monkeys that are part of an extended multigenerational pedigree, we demonstrate that metabolism within a tripartite prefrontal-limbic-midbrain circuit mediates some of the inborn risk for developing anxiety and depression. Importantly, although brain volume is highly heritable early in life, it is brain metabolism—not brain structure—that is the critical intermediary between genetics and the childhood risk to develop stress-related psychopathology.

anxiety | primate | heritability | positron emission tomography | brain volume

Parents with anxiety and depressive disorders are considerably more likely to have children with an extremely anxious temperament (AT) (1–3). Extreme-AT children have heightened behavioral and physiological reactivity to potential threat and have a markedly increased risk to develop anxiety and depressive disorders (4, 5). These disorders emerge as inborn tendencies and environmental factors converge to disrupt the neural systems that mediate adaptive anxiety; as many as 50% of children with extreme-AT develop a psychiatric disorder (6). In addition to environmental influences that facilitate the cross-generational transfer of psychopathology (e.g., parent–child interactions), genetic variance accounts for ~35% of the likelihood that a child will develop an anxiety disorder (7, 8). The neural substrates of AT are distributed throughout the brain and range from primitive brainstem structures to primate-specific cortical subfields. Multiple brain regions causally contribute to AT, and damage to any one of these regions is sufficient to decrease, although not abolish, anxiety (9–14). Thus, the inherited risk to develop stress-related psychopathology likely manifests via its effects on multiple components of the neural circuit underlying AT. Here we use a genetic correlation approach to identify brain regions where function and structure contribute to the intergenerational transmission of AT. Genetic correlation analyses are crucial for identifying regions that are likely to mediate the genetic contributions to AT, and to distinguish them from regions that, although heritable, rely on an independent set of genetic variations.

The recent evolutionary divergence of humans and rhesus monkeys is reflected in their shared capacity for higher-order cognition, complex social behavior, and homologous neural circuits, which make the young rhesus monkey an ideal model for

understanding the neural substrates of childhood AT. Our group developed and validated a paradigm for studying the neural bases of primate AT that combines [18-F] deoxyglucose positron emission tomography (FDG-PET) imaging with behavioral and neuroendocrine responses to a potentially threatening human intruder making no eye contact (NEC) with the monkey. The NEC context is designed to elicit naturalistic adaptive defensive behaviors and captures the evolutionarily conserved tendency of high-AT individuals to inhibit behaviors that otherwise could attract the attention of potential predators. Because it measures brain metabolism over ~30 min, FDG-PET imaging is ideally suited to examine the sustained neural responses that underlie trait-like measures, such as AT. Following FDG injection, the monkey is placed in the NEC context. As FDG is taken-up into metabolically active cells, the monkey behaves freely in the NEC context, revealing its anxious disposition. The post-NEC PET scan measures the integrated brain metabolism that occurred during exposure to the ethologically relevant NEC context.

To identify the brain regions that underlie the parent-to-child transmission of psychopathology, it is critical to understand the pattern of cosegregation between the AT phenotype and its neural circuit alterations within the family tree. This approach first requires demonstrating that the phenotype is heritable, identifying

Significance

According to the World Health Organization, anxiety and depressive disorders are a leading source of disability, affecting hundreds of millions of people. Children can inherit an extremely anxious temperament, which is a prominent risk factor for the later development of anxiety, depression, and comorbid substance abuse. This study uses high-resolution functional and structural imaging in our well-established developmental nonhuman primate model to identify the heritable neural substrate that underlies extreme childhood anxious temperament. Using a large multigenerational family pedigree, genetic correlation analyses revealed a tripartite neural circuit where metabolism likely shares a genetic substrate with early-life dispositional anxiety. Interestingly, we found that brain function—not structure—is the critical intermediary between genetics and the childhood risk to develop stress-related psychopathology.

Author contributions: A.S.F., S.E.S., R.J.D., J.R., and N.H.K. designed research; A.S.F., J.A.O., S.E.S., M.R., J.R., and N.H.K. performed research; A.S.F., D.R.M., A.K.C., A.A., and J.B. contributed new reagents/analytic tools; A.S.F., J.A.O., and A.J.S. analyzed data; and A.S.F., J.A.O., A.J.S., and N.H.K. wrote the paper.

The authors declare no conflict of interest.

This article is a PNAS Direct Submission.

Data deposition: The full voxelwise maps are available in [Dataset S1](#).

¹To whom correspondence may be addressed. Email: asfox@wisc.edu or nkalin@wisc.edu.

This article contains supporting information online at www.pnas.org/lookup/suppl/doi:10.1073/pnas.1508593112/-DCSupplemental.

Regional AT-related brain metabolism

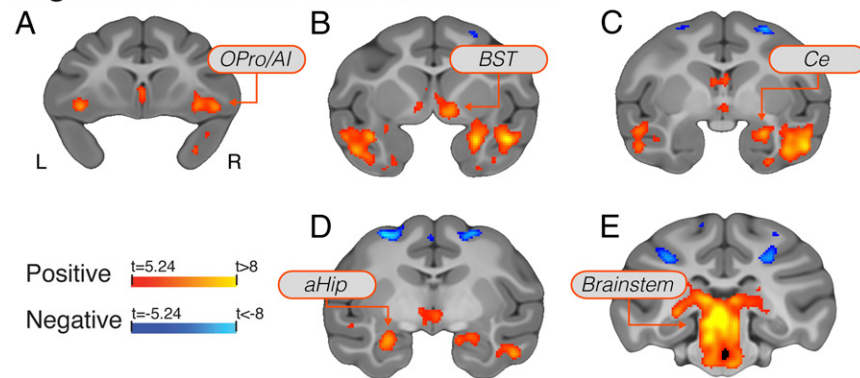


Fig. 1. Regions where brain metabolism was significantly associated with individual differences in AT ($P < 0.05$, Šidák-corrected for multiple comparisons across the whole-brain). Regions include the OPro/AI (A), subgenual anterior cingulate, temporal cortex, BST (B), Ce (C), aHip (D), and brainstem regions including the PAG (E).

brain regions associated with the phenotype, and determining which of these brain regions are heritable. Once this is accomplished, a genetic correlation analysis between brain function/structure and the phenotype is critical to identify the neural mediators of the heritable parent-to-child transfer of risk.

Following this strategy in a large familial sample of young rhesus monkeys, we (i) demonstrate the heritability of AT, (ii) identify neuroimaging measures that predict AT, (iii) assess the heritability of the relevant brain structural and functional measures, and finally, (iv) perform the relevant genetic correlation analyses between the neuroimaging measures and AT. To this end, NEC FDG-PET and structural brain imaging were performed in our large sample of 592 young rhesus monkeys from a large multigenerational pedigree (age: mean = 1.88 y; 327 males/265 females). Paralleling work in children, the monkey AT phenotype encompasses behavioral (freezing), communicative (decreased cooing), and physiological (increased cortisol) responses to potential threat. Specifically, our composite measure of AT was operationalized as the mean of the monkey's relative freezing levels, inhibition of coo vocalizations, and plasma cortisol concentration (15–18). In humans, the features of AT, extreme behavioral inhibition, and heightened cortisol levels are early risk factors for the later development of anxiety and depressive disorders (6, 19–21). Children who respond to strangers and novel situations with excessive apprehension or physiological arousal are likely to modify their behavior in ways that are maladaptive and over time are indicative of stress-related psychopathology. Similar to humans, monkeys with extreme AT appear to be functionally impaired across laboratory and naturalistic social settings, making the rhesus monkey model of AT ideal for understanding the pathophysiology that underlies the risk to develop anxiety and depression (21).

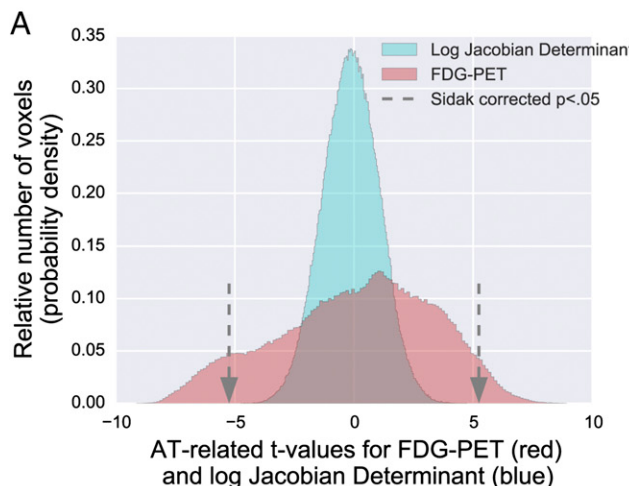
Heritability of AT was estimated as the proportion of variation in the phenotype explained by the coefficient of relatedness in the extended multigenerational pedigree (see ref. 22 and *Methods* for details). This extended pedigree approach is powerful because it accounts for the phenotypic similarity of both close and distant relationships (see *SI Appendix, SI Methods* for details). In this preadolescent sample, there was no significant effect of sex on AT ($t = 0.830$, $P = 0.407$), but there was a significant decrease in AT with age ($t = -10.013$, $P < 0.001$). Accordingly, all analyses controlled for nuisance variance in age, age², sex, and the age \times sex interaction. Results demonstrated that the AT phenotype is heritable (AT: $h^2 = 0.29$, $P < 0.0001$), consistent with prior findings in young monkeys as well as the heritability estimates for human anxiety and anxiety disorders (7, 23, 24).

To identify brain regions where metabolism contributes to the cross-generational transmission of AT, it is first necessary to identify the regions where these measures predict variation in the anxious phenotype. Voxelwise robust regressions were performed between AT and FDG-PET. Results revealed significant relations between metabolism and AT ($P < 0.05$ Šidák-corrected; also see *SI Appendix, Results and Discussion*) in regions of the orbital frontal (OFC) and anterior insular (AI) cortices [including orbital proisocortex (OPro/AI), as well as cytoarchitectonic areas 11/13/47], amygdala [including the central nucleus of the amygdala (Ce)], anterior hippocampus (aHip), bed nucleus of stria terminalis (BST), as well as midbrain regions that encompass the periaqueductal gray (PAG) (Fig. 1 and *SI Appendix, Table S1*; full voxelwise maps are available in *Dataset S1*). Importantly, these AT-related regions include areas that causally contribute to AT in mechanistic studies, including: orbital-prefrontal cortical areas involved in emotional valuation (25); the extended amygdala, an interface between emotions and their behavioral and physiological expression (26); and brainstem regions, including PAG, which are the downstream effectors required for the expression of defensive responses (27).

In parallel, to identify regions where brain volume was associated with AT, voxelwise analyses were performed to identify regions where brain volume predicted AT. Regional brain volume was measured using the log-Jacobian determinant of the nonlinear transformations to template space. Remarkably, there were no voxels in which brain volume significantly predicted AT [Šidák correction, $P > 0.05$, or false-discovery rate (FDR) $q > 0.05$ corrected] (Fig. 2A; full voxelwise maps are available in *Dataset S1*). Cross-validation analyses examining the predictive utility of brain volume to predict AT or its components using elastic-net regression and supervised learning yielded the same conclusion (see *SI Appendix, Results and Discussion* and Figs. S2 and S3 for details). Thus, at least early in life, variation in the expression of AT does not involve altered regional brain volume.

The heritability of brain metabolism was identified using voxelwise heritability analyses of FDG-PET that were performed by harnessing the computational resources of the Open Science Grid's distributed high-throughput computing system (*Methods*). Results demonstrated significant heritability of glucose metabolism across the brain (Fig. 2B). We observed significantly heritable metabolic activity in nearly every AT-related region (FDR $q < 0.05$, corrected within regions where metabolism significantly predicted AT) (Fig. 3 and *SI Appendix, SI Results and Discussion* and *Table S1*). Within these AT-related heritable regions there was substantial variability in the magnitude of heritability estimates, with peak heritability estimates of 26%

Distributions of AT-related t-values for brain volume and metabolism



Distributions of heritability estimates for brain volume and metabolism

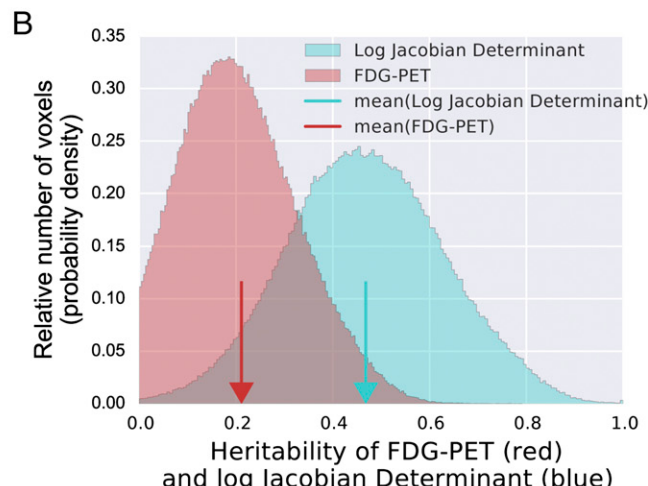


Fig. 2. Histograms of voxelwise AT-related brain metabolism (red) and brain volume (blue) demonstrate significant relationships for brain metabolism but not brain volume (A). Gray arrows represent the threshold for reaching significance at a Šidák-corrected $P < 0.05$. Histograms of heritability estimates for brain metabolism (red) and brain volume (blue) demonstrated significant heritability for many voxels of both measures, and on average greater heritability of brain volume (see main text for details) (B). Red and blue arrows indicate the mean heritability estimates for FDG-PET and the log-Jacobian determinant, respectively.

in the amygdala, 53% in the hippocampus, and 57% in the BST region. Estimates were as low as 9% in the superior temporal sulcus (full voxelwise maps are available in [Dataset S1](#)).

We assessed the heritability of regional brain volume using the same approach. Interestingly, brain volume was generally more heritable than brain metabolism ($\chi^2 > 1,000$, $P < 0.001$), with the average h^2 for brain volume ~ 0.5 , whereas the average h^2 for regional brain metabolism was ~ 0.2 . Within the specific subset of brain regions where metabolism predicted AT, variation in volume was significantly heritable (full voxelwise maps are available in [Dataset S1](#)). For example, volume in the AT-related amygdala and OFC regions was more than 60% heritable. Nevertheless, the surprising result that brain volume did not predict that AT provides compelling evidence that these highly heritable early-life structural differences do not mediate the intergenerational transmission of the risk for anxiety and depressive disorders.

Demonstrating significant heritability of AT-related brain regions does not implicate these regions in the intergenerational transfer of AT. Because of the importance of identifying regions where brain metabolism and AT similarly fell through the family tree, we performed voxelwise genetic correlation analyses. Genetic correlation analyses are crucial for dissociating brain regions that share an overlapping genetic basis with AT from heritable regions where metabolism is driven by genes that are unrelated to the AT-phenotype. We computed bivariate genetic correlations (ρ_g) between AT and heritable AT-related brain metabolism. Results demonstrate significant genetic correlations with AT in regions that encompass portions of the OFC/AI, extended amygdala, and brainstem (Fig. 4 and [SI Appendix](#), Fig. S4 and Table S2). To our knowledge, these data provide the first evidence for a coheritable substrate for AT and AT-related brain metabolism in a circuit, wherein the extended amygdala links prefrontal regulatory mechanisms to brainstem effector sites that initiate anxiety-related responses. Metabolism within this tripartite neural circuit is likely to share a genetic substrate with AT through which it mediates the inherited risk to develop stress-related psychopathology.

To precisely identify the locations of peak activations within the identified tripartite prefrontal-limbic-midbrain circuit, we used

high-precision diffeomorphic registration and chemoarchitectonic imaging (*Methods*). High-precision diffeomorphic registration allowed us to localize significant regions on a superresolution template brain, which reflects the mean rhesus monkey brain anatomy with submillimeter precision in well-aligned areas. This integrative approach revealed that the OFC/AI cluster included regions of agranular orbital and insular cortices, with the peak ρ_g located in OPro/AI (Fig. 4A). To refine the localization of subcortical clusters, we leveraged *in vivo* chemoarchitectonic imaging of dopamine D2/D3 receptor binding ([F-18]fallypride; $n = 33$) and serotonin transporter binding ([C-11]DASB; $n = 34$) derived from an independent sample of young rhesus monkeys (28, 29). Using D2/D3 receptor binding to demarcate the ventral striatum, we localized the peak ρ_g within the extended amygdala to be specifically located in the BST region between the anterior commissure and the ventral striatum (Fig. 4B). In addition to the peak-region in the BST, the extended amygdala cluster encompassed portions of the subtenuclular extended amygdala immediately

Heritable regional AT-related brain metabolism

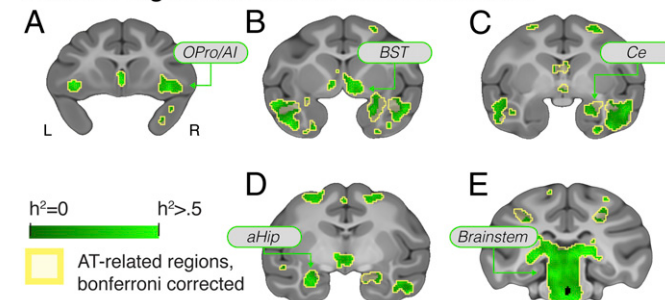
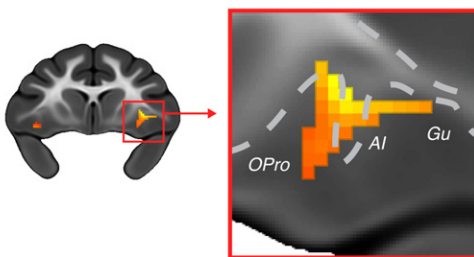


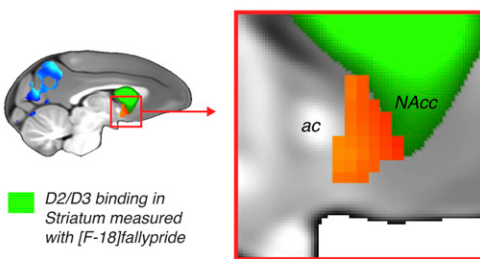
Fig. 3. Voxelwise heritability of brain metabolism demonstrated that nearly every region that significantly predicted AT was also significantly heritable ($q < 0.05$, FDR-corrected within AT-related regions). Regions include the OPro/AI (A), subgenual anterior cingulate, temporal cortex, BST (B), Ce (C), aHip (D), and brainstem regions including the PAG (E).

AT-related regional brain metabolism sharing a genetic substrate with AT

Anatomic localization of OPro/AI



Chemoarchitectonic Localization of BST



Chemoarchitectonic Localization of PAG

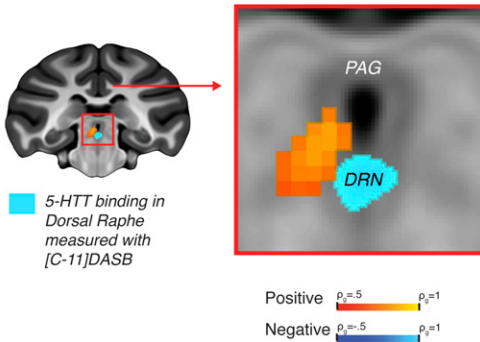


Fig. 4. Regions where brain metabolism demonstrated significant genetic correlation with AT, thus sharing a genetic substrate, include: the OPro/AI (Top), BST (Middle), and the PAG (Bottom). Using high-resolution anatomical and chemoarchitectonic imaging in a separate group of monkeys, regions were precisely localized as: agranular OPro/AI (Top); the BST region lying between the anterior commissure (ac) and the [18-F] fallypride identified D2/D3-rich ventral striatum that includes the nucleus accumbens (green; NAcc) (Middle); and the vIPAG-region in the gray matter surrounding the ventricle, superior to the [11-C] DASB identified serotonin transporter-rich DRN (Bottom).

posterior to the shell of the nucleus accumbens. Using serotonin transporter binding to pinpoint the dorsal raphe nucleus (DRN), we localized the peak ρ_g within the brainstem cluster to the ventrolateral PAG (vIPAG), slightly superior and lateral to the DRN in the gray matter that encircles the ventricle (Fig. 4C).

To understand whether metabolism in the brain regions that are genetically correlated with AT are themselves genetically correlated, we performed interregion bivariate genetic correlations. We observed significant genetic correlations in metabolism between the BST and both the PAG ($\rho_g = 0.56, P = 0.01$) and OPro/AI ($\rho_g = 0.63, P = 0.006$), but failed to find a significant correlation between the PAG and OPro/AI ($\rho_g = 0.40, P = 0.12$). These data, demonstrating significant genetic correlations in metabolism across the identified tripartite circuit, suggest that the molecular mechanisms that jointly influence the function of these regions may, in part, mediate the heritable components of

AT. These results pave the path for future molecular investigations of AT. For example, publicly available datasets can be leveraged to suggest potential molecular mediators of metabolism in these regions by identifying genes that are overexpressed in the BST-PAG or BST-OPro/AI compared with the rest of the brain (SI Appendix, SI Methods). These exploratory analyses can reveal candidate genes and molecular mechanisms that may partially mediate the cross-generational transfer AT by altering brain function within the tripartite prefrontal-limbic-midbrain circuit [e.g., somatostatin, neuropeptide Y, or the “neuropeptide hormone activity” (GO:0005184)] (Datasets S2 and S3). By identifying those brain regions that are genetically correlated with AT, informatics and molecular investigations can serve to help to prioritize future mechanistic studies aimed at altering the pathophysiology of anxiety.

Through a tripartite prefrontal-limbic-midbrain circuit, the OPro/AI, BST, and PAG regions work in concert to integrate and evaluate potentially threatening information to initiate and enact anxiety-related responses. Interestingly, this circuit, genetically correlated with individual differences in early-life anxiety, incorporates survival-related regions that span evolutionary history, where selective pressures shaped each stage of central nervous system development. The OPro/AI, BST, and PAG working together may also underlie the pathophysiology of anxiety and affective disorders (21, 30, 31). The primate OPro and AI are thought to be involved in predicting and maintaining affective representations of current and future events, which can be communicated to other AT-related brain regions to guide emotional responding (25, 32, 33). Increased OPro/AI activity may give rise to the excessive anticipatory anxiety associated with anxiety disorders (30, 34, 35). Furthermore, lesions to the monkey OFC that include the OPro/AI are sufficient to decrease anxiety-related behavior, as well as metabolism within the BST region (9, 10). The BST is required for the prolonged threat preparedness (16, 36–40) and is well-suited to integrate cortical affective inputs to coordinate emotional responses, via direct projections to the brain-stem regions required to mount defensive behaviors (31, 41). Although understudied in relation to human psychopathology, dysregulation of the BST likely underlies the hypervigilance characteristic of patients with extreme anxiety and anxiety disorders (31, 42). The evolutionarily old PAG is organized into functionally distinct columns that initiate specific behavioral and physiological responses, including those characteristic of anxiety, such as fleeing, inhibition of motoric activity, and increased passive coping (27, 43–45). It is likely that dysregulated PAG activity, in part, underlies the extreme behavioral inhibition, freezing behavior, and increased autonomic reactivity that is associated with panic symptoms that are common to anxiety disorders. Although temperamental anxiety is instantiated in distributed circuits throughout the brain, these new data specifically implicate the OPro/AI, BST, and PAG as key components that likely work together to mediate some of the inherited predisposition for extreme early-life temperamental anxiety.

Here, we identified previously unknown relationships between AT and metabolism in brain systems that regulate, initiate, and enact anxiety-related behavior that, when passed down from parent to child, likely result in early-life anxiety. We found that the genetic alterations underlying the inborn risk for anxiety and depressive disorders, which are only beginning to be identified, are likely instantiated within the molecular systems that alter metabolism within the OPro/AI, BST, and PAG. Furthermore, we demonstrated the utility of combining empirical data from this study with large-scale publicly available gene-expression databases to gain insight into the molecular systems underlying the heritable components of AT. Regions that do not share a genetic substrate with AT, including the amygdala and aHip, likely play a role in mediating environmental influences, such as caregiver-style, trauma, and other critical socio-emotional environmental

factors on AT. Surprisingly, although early-life regional brain volume was highly heritable, we did not find any evidence linking it to early life anxiety. By identifying the neural systems that share a genetic substrate with AT and likely mediate a part of the genetic risk to develop stress-related psychopathology, these data provide a novel framework for understanding the relationship between genetic variation and early-life anxiety. Elucidating how inherited molecular alterations affect brain function in this tripartite anxiety circuit will help guide the development of novel interventions aimed at helping families with debilitating anxiety enhance the mental health of their at-risk children.

Methods

For this study, 592 young rhesus monkeys that were part of a large multi-generational pedigree were phenotyped with well-established behavioral, physiological, and brain-imaging methods. Each animal was injected with FDG and exposed to the potentially threatening NEC context in which a human intruder presents their profile to the monkey for 30 min before receiving a PET scan. This paradigm allows us to obtain simultaneous measurements of our composite AT measure and integrated regional brain metabolism during exposure to the NEC context. On a separate day, a structural T1-weighted MRI scan was acquired on each animal. Based on the T1-weighted MRI, the log-Jacobian determinant of the transformation to standard space was computed as to measure relative brain volume. Brain imaging measures were regressed against AT to identify AT-related brain regions. Heritability of local brain volume and brain metabolism was estimated at each voxel based on each pair of animals' degree of relatedness. Bivariate heritability estimates were similarly computed to examine the

degree to which AT and regional brain metabolism share a genetic substrate. All experiments were performed according to the federal guidelines of animal use and care and with the approval of the University of Wisconsin-Madison Institutional Animal Care and Use Committee. More information can be found in *SI Appendix, SI Methods*.

ACKNOWLEDGMENTS. Authors thank E. Ahlers, B. Christian, L. Friedman, E. Larson, K. Mayer, T. Oakes, M. Riedel, P. Roseboom, J. Storey, B. Postle, W. Li, R. Jenison, D. Tromp, N. Vack, H. Van Valkenberg, and the staffs of the Harlow Center for Biological Psychology, HealthEmotions Research Institute, Waisman Center, Waisman Laboratory for Brain Imaging and Behavior, University of Wisconsin Department of Psychiatry, and the Lane Imaging Laboratory for aid in data collection and conceptualization; Maria Jesson for her essential work in processing anatomical images; and Sneka Raveendran for valuable assistance in developing the pedigree information. This research was performed using the computer resources and assistance of the University of Wisconsin-Madison Center For High Throughput Computing in the Department of Computer Sciences, which is supported by the University of Wisconsin-Madison, the Advanced Computing Initiative, the Wisconsin Alumni Research Foundation, the Wisconsin Institutes for Discovery, and the National Science Foundation, and is an active member of the Open Science Grid, which is supported by the National Science Foundation and the US Department of Energy's Office of Science. Research was supported in part by National Institutes of Health (NIH) Award P51OD011106 to the Wisconsin National Primate Research Center, University of Wisconsin-Madison. This research was conducted in part at a facility constructed with support from Research Facilities Improvement Program Grants RR15459-01 and RR020141-01. The authors of this work were supported by the NIH Grants R21MH91550, R01MH81884, R01MH46729, P50MH84051, P50MH100031, R21MH092581; HealthEmotions Research Institute; and the University of Maryland.

- Battaglia M, et al. (1997) Physiological and behavioral responses to minor stressors in offspring of patients with panic disorder. *J Psychiatr Res* 31(3):365–376.
- Rosenbaum JF, et al. (1988) Behavioral inhibition in children of parents with panic disorder and agoraphobia. A controlled study. *Arch Gen Psychiatry* 45(5):463–470.
- Rosenbaum JF, et al. (2000) A controlled study of behavioral inhibition in children of parents with panic disorder and depression. *Am J Psychiatry* 157(12):2002–2010.
- Hirshfeld DR, et al. (1992) Stable behavioral inhibition and its association with anxiety disorder. *J Am Acad Child Adolesc Psychiatry* 31(1):103–111.
- Kagan J (1997) Temperament and the reactions to unfamiliarity. *Child Dev* 68(1):139–143.
- Clauss JA, Blackford JU (2012) Behavioral inhibition and risk for developing social anxiety disorder: A meta-analytic study. *J Am Acad Child Adolesc Psychiatry* 51(10):1066–1075.e1.
- Hettema JM, Neale MC, Kendler KS (2001) A review and meta-analysis of the genetic epidemiology of anxiety disorders. *Am J Psychiatry* 158(10):1568–1578.
- Tambs K, et al. (2009) Structure of genetic and environmental risk factors for dimensional representations of DSM-IV anxiety disorders. *Br J Psychiatry* 195(4):301–307.
- Fox AS, et al. (2010) Orbitofrontal cortex lesions alter anxiety-related activity in the primate bed nucleus of stria terminalis. *J Neurosci* 30(20):7023–7027.
- Kalin NH, Shelton SE, Davidson RJ (2007) Role of the primate orbitofrontal cortex in mediating anxious temperament. *Biol Psychiatry* 62(10):1134–1139.
- Kalin NH, Shelton SE, Davidson RJ (2004) The role of the central nucleus of the amygdala in mediating fear and anxiety in the primate. *J Neurosci* 24(24):5506–5515.
- Chudasama Y, Izquierdo A, Murray EA (2009) Distinct contributions of the amygdala and hippocampus to fear expression. *Eur J Neurosci* 30(12):2327–2337.
- Murray EA, Izquierdo A (2007) Orbitofrontal cortex and amygdala contributions to affect and action in primates. *Ann N Y Acad Sci* 1121:273–296.
- Machado CJ, Bachevaller J (2008) Behavioral and hormonal reactivity to threat: Effects of selective amygdala, hippocampal or orbital frontal lesions in monkeys. *Psychoneuroendocrinology* 33(7):926–941.
- Fox AS, et al. (2012) Central amygdala nucleus (Ce) gene expression linked to increased trait-like Ce metabolism and anxious temperament in young primates. *Proc Natl Acad Sci USA* 109(44):18108–18113.
- Fox AS, Shelton SE, Oakes TR, Davidson RJ, Kalin NH (2008) Trait-like brain activity during adolescence predicts anxious temperament in primates. *PLoS ONE* 3(7):e2570.
- Oler JA, et al. (2009) Serotonin transporter availability in the amygdala and bed nucleus of the stria terminalis predicts anxious temperament and brain glucose metabolic activity. *J Neurosci* 29(32):9961–9966.
- Oler JA, et al. (2010) Amygdalar and hippocampal substrates of anxious temperament differ in their heritability. *Nature* 466(7308):864–868.
- Essex MJ, Klein MH, Slattery MJ, Goldsmith HH, Kalin NH (2010) Early risk factors and developmental pathways to chronic high inhibition and social anxiety disorder in adolescence. *Am J Psychiatry* 167(1):40–46.
- Gagne JS, Vendlinski MK, Goldsmith HH (2009) *Handbook of Behavioral Genetics*, ed Kim Y-K (Springer, New York), pp 251–267.
- Fox AS, Kalin NH (2014) A translational neuroscience approach to understanding the development of social anxiety disorder and its pathophysiology. *Am J Psychiatry* 171(11):1162–1173.
- Almasy L, Blangero J (1998) Multipoint quantitative-trait linkage analysis in general pedigrees. *Am J Hum Genet* 62(5):1198–1211.
- Calboli FCF, et al. (2010) A genome-wide association study of neuroticism in a population-based sample. *PLoS ONE* 5(7):e11504.
- Bouchard TJ, Jr, Loehlin JC (2001) Genes, evolution, and personality. *Behav Genet* 31(3):243–273.
- Wallis JD (2012) Cross-species studies of orbitofrontal cortex and value-based decision-making. *Nat Neurosci* 15(1):13–19.
- Alheid GF, Heimer L (1988) New perspectives in basal forebrain organization of special relevance for neuropsychiatric disorders: The striatopallidal, amygdaloid, and corticopetal components of substantia innominata. *Neuroscience* 27(1):1–39.
- Bandler R, Shipley MT (1994) Columnar organization in the midbrain periaqueductal gray: Modular for emotional expression? *Trends Neurosci* 17(9):379–389.
- Christian BT, et al. (2009) Serotonin transporter binding and genotype in the non-human primate brain using [C-11]DASB PET. *Neuroimage* 47(4):1230–1236.
- Christian BT, et al. (2009) The distribution of D2/D3 receptor binding in the adolescent rhesus monkey using small animal PET imaging. *Neuroimage* 44(4):1334–1344.
- Grupe DW, Nitschke JB (2013) Uncertainty and anticipation in anxiety: An integrated neurobiological and psychological perspective. *Nat Rev Neurosci* 14(7):488–501.
- Fox AS, Oler JA, Tromp DPM, Fudge JL, Kalin NH (2015) Extending the amygdala in theories of threat processing. *Trends Neurosci* 38(5):319–329.
- An X, Bandler R, Ongür D, Price JL (1998) Prefrontal cortical projections to longitudinal columns in the midbrain periaqueductal gray in macaque monkeys. *J Comp Neurol* 401(4):455–479.
- Ghashghaei HT, Hilgetag CC, Barbas H (2007) Sequence of information processing for emotions based on the anatomic dialogue between prefrontal cortex and amygdala. *Neuroimage* 34(3):905–923.
- Williams LE, et al. (2015) Fear of the unknown: Uncertain anticipation reveals amygdala alterations in childhood anxiety disorders. *Neuropsychopharmacology* 40(6):1428–1435.
- Paulus MP, Stein MB (2006) An insular view of anxiety. *Biol Psychiatry* 60(4):383–387.
- Davis M, Walker DL, Miles L, Grillon C (2010) Phasic vs sustained fear in rats and humans: Role of the extended amygdala in fear vs anxiety. *Neuropsychopharmacology* 35(1):105–135.
- Kalin NH, Shelton SE, Fox AS, Oakes TR, Davidson RJ (2005) Brain regions associated with the expression and contextual regulation of anxiety in primates. *Biol Psychiatry* 58(10):796–804.
- Mobbs D, et al. (2010) Neural activity associated with monitoring the oscillating threat value of a tarantula. *Proc Natl Acad Sci USA* 107(47):20582–20586.
- Somerville LH, Whalen PJ, Kelley WM (2010) Human bed nucleus of the stria terminalis indexes hypervigilant threat monitoring. *Biol Psychiatry* 68(5):416–424.
- Walker DL, Toufexis DJ, Davis M (2003) Role of the bed nucleus of the stria terminalis versus the amygdala in fear, stress, and anxiety. *Eur J Pharmacol* 463(1–3):199–216.
- Davis M, Whalen PJ (2001) The amygdala: Vigilance and emotion. *Mol Psychiatry* 6(1):13–34.
- Straube T, Mentzel H-J, Miltner WHR (2007) Waiting for spiders: Brain activation during anticipatory anxiety in spider phobics. *Neuroimage* 37(4):1427–1436.
- Fendt M, Fanselow MS (1999) The neuroanatomical and neurochemical basis of conditioned fear. *Neurosci Biobehav Rev* 23(5):743–760.
- Nashold BS, Jr, Wilson WP, Slaughter DG (1969) Sensations evoked by stimulation in the midbrain of man. *J Neurosurg* 30(1):14–24.
- Satpute AB, et al. (2013) Identification of discrete functional subregions of the human periaqueductal gray. *Proc Natl Acad Sci USA* 110(42):17101–17106.

Supplementary Information: Intergenerational neural mediators of early-life anxious temperament

Andrew S. Fox^{a,b,c,1}, Jonathan A. Oler^{a,c}, Alexander J. Shackman^d, Steven E. Shelton^a, Muthuswamy Raveendran^e, D. Reese McKay^f, Alexander K. Converse^b, Andrew Alexander^{b,g}, Richard J. Davidson^{a,b,c,h}, John Blangeroⁱ, Jeffrey Rogers^e, and Ned H. Kalin^{a,b,c,h,1}

^aHealthEmotions Research Institute, University of Wisconsin–Madison, Madison, WI 53709; ^bWaisman Center, University of Wisconsin–Madison, Madison, WI 53709; ^cDepartment of Psychiatry, University of Wisconsin–Madison, Madison, WI 53709; ^dDepartment of Psychology, University of Maryland, College Park, MD 20742; ^eDepartment of Genetics, Baylor College of Medicine, Houston, TX 77030; ^fDepartment of Psychiatry, Yale School of Medicine, New Haven, CT 06519; ^gDepartment of Medical Physics, University of Wisconsin–Madison, Madison, WI 53709; ^hDepartment of Psychology, University of Wisconsin–Madison, Madison, WI 53709; and ⁱTexas Biomedical Research Institute, San Antonio, TX 78245

Including:

- Supplementary Results/Discussion (with Figures) (pg. 2-6)
- Supplementary Methods (pg. 6-12)
- Supplementary References (pg. 12-13)
- Supplementary Legends (pg. 14)
- Supplementary Tables (pg. 15-17)

Ned H. Kalin, M.D.
Chair Department of Psychiatry
HealthEmotions Research Institute
University of Wisconsin-Madison
6001 Research Park Blvd
Madison, WI 53719, USA
(608) 263-6079 office
(608) 263-9340 fax
nkalin@wisc.edu

Andrew S. Fox, Ph.D.
HealthEmotions Research Institute
University of Wisconsin-Madison
6001 Research Park Blvd
Madison, WI 53719, USA
(608) 301-5531 office
(608) 263-9340 fax
asfox@wisc.edu

Supplemental Results & Discussion

Brain metabolism and the components of AT

To ensure that the relationship between the composite measure of AT and brain metabolism was not primarily determined by an individual component of the composite AT phenotype, we performed three separate voxelwise regressions between NEC-related FDG-uptake and freezing, cooing, and cortisol. Results demonstrated significant relationships between brain metabolism and each AT-component, i.e. freezing, cooing and cortisol (Fig S1a, all Šidák corrected p's<.05). We then sought to determine if the three components of AT were likely to share a neural substrate by examining the spatial correlation of AT-relatedness across voxels. Although the components of AT are not highly related (see (1)), spatial correlations across voxels demonstrate a similar pattern of brain-phenotype relationships between components of AT (Fig S1b, $r^2_{[Freezing,Cooing]}=.71$; c, $r^2_{[Freezing,Cortisol]}=.37$; d, $r^2_{[Cooing,Cortisol]}=.40$; all p's<.0001). While the scatter plots reveal some phenotype specific voxels, most of the regions that we highlight commonly relate to each of our three anxiety-related measures. Consistent with our previous research, these data suggest that the components of AT are, in part, associated with a shared neural substrate for anxiety-related responding (1, 2). For these reasons, we have focused on AT as a whole. It will be critical for future research to further differentiate general AT-related regions, from those that specifically relate to a particular phenotypic expression of anxiety.

Cross-validation analysis of imaging-AT relationships

To obtain reliable estimate of the utility of brain metabolism and local brain volume in predicting extreme early-life AT, we performed supervised learning analyses with repeated cross-validation. These analyses use every brain voxel as a predictor and AT as the outcome variable. Analyses were performed separately for brain metabolism (i.e. FDG-PET) and local brain volume (i.e. log jacobian determinant). Prior to statistical analysis, each voxel was residualized for the potentially confounding effects of age, sex, site, MRI scanner, prior exposure to NEC, scan order, and affine registration parameters. These residuals were used as predictors in regression analyses.

AT-component related brain volume and metabolism

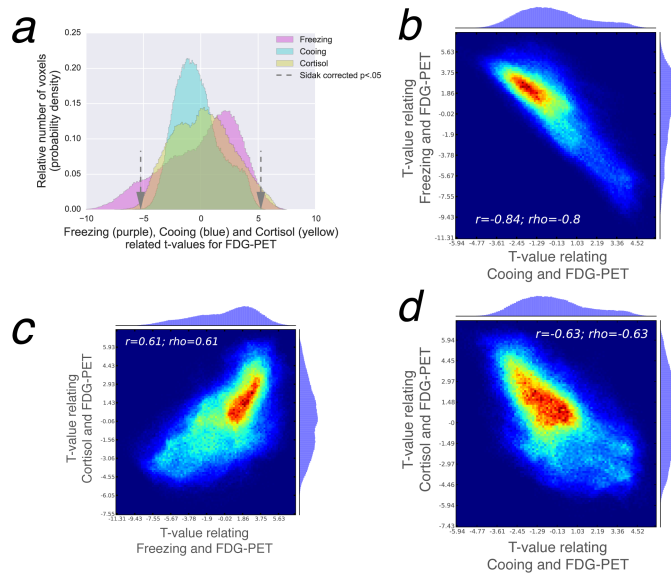


Figure S1: Histograms displaying the distribution of t-values reflecting the relationship between brain metabolism and each component of AT, i.e. freezing, cooing, and cortisol can be seen in (a). Grey arrows represent the threshold for reaching significance at a Šidák corrected $p<.05$. Although the components of AT are not highly related (see (1)), spatial correlations across voxels demonstrate a similar pattern of brain-phenotype relationships between components of AT (b, $r^2_{[Freezing,Cooing]}=.71$; c, $r^2_{[Freezing,Cortisol]}=.37$; d, $r^2_{[Cooing,Cortisol]}=.40$; all p's<.0001).

Receiver operating characteristic curve for brain metabolism and brain volume in predicting extreme AT

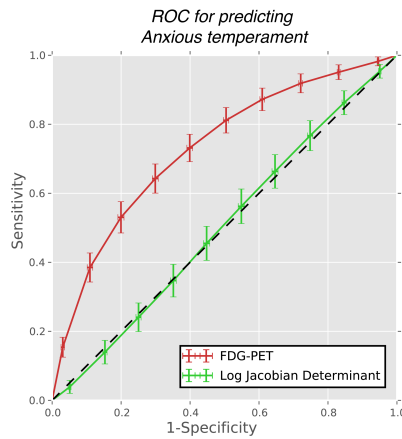


Figure S2: ROC curves using FDG-PET (red) and log jacobian determinant (green) to predict AT using elastic net regularized regressions. The dashed black line indicates chance predictions, and curves that near the upper left corner represent better predictors of AT.

the correlation coefficient between the predicted and actual AT values in the test sample. To estimate the amount of variance that could be predicted, this procedure was repeated 1000 times.

To determine the utility of brain metabolism and brain volume in predicting extreme AT, we performed cross-validation analyses to determine the sensitivity and specificity of our AT-prediction. Receiver operating characteristic (ROC) curves were computed for classification of individuals into a high-AT groups defined at various percentiles (i.e. 0, 5, 15, 25, 35, 45, 55, 65, 75, 85, 95, 100). Sensitivity was computed as the number of correctly predicted AT-individuals divided by the total number of high-AT individuals in the test-set, while specificity was measured as the number of correctly predicted non high-AT individuals divided by the total number of non high-AT individuals in the test-set. Predictive measures should ideally result in high sensitivity and specificity. Complementing our univariate analyses in the full sample, cross-validation of extreme-AT prediction demonstrated significant predictive validity for FDG-PET, but not for the log jacobian determinant (Fig S2). Similar analyses were performed to examine the relationship between neuroimaging measures and the components of AT (i.e. Freezing, Cooing, and Cortisol). Like to AT, examination of the relationship between neuroimaging measures and each of AT's components revealed significant predictive validity for FDG-PET, but not for the log jacobian determinant (Fig S3).

These results indicate that there is valuable AT-related information in the FDG-PET data, but fail to support the hypothesis that early-life AT is associated with altered regional brain volume.

Cross-validation techniques were used to compute voxelwise parameter estimates in a training dataset and use those parameter estimates to examine a test dataset. The training (four-fifths: n= 473) and test (one-fifth: n=119) samples were randomly drawn from the set of 592 subject scans. Supervised learning was performed using an elastic net regularized regression to estimate the best-fitting set of voxels and parameter estimates to predict AT in the training sample, using AT as the dependent measure and all voxels as predictors (3). These voxels and parameter estimates were then used to compute the estimated levels of AT in each subject in the test sample. When the number of predictors is greater than the number of samples, standard regression techniques will fail, as the set of linear equations becomes over-parameterized and rank-deficient. Regularized regression techniques provide a reasoned method for selecting which voxels best predict the AT phenotype and how to optimally weight them. Elastic net regularization combines the LASSO and ridge-regression approaches to prevent over-fitting of the data and punish overly-sparse solutions. Elastic net regularization was used to 'lightly' regularize the regression (i.e. lasso & ridge parameters $\lambda_1=.001$, $\lambda_2=.009$, respectively). The amount of variance explained was defined as the square of

Receiver operating characteristic curve for brain metabolism and brain volume in predicting the components of AT

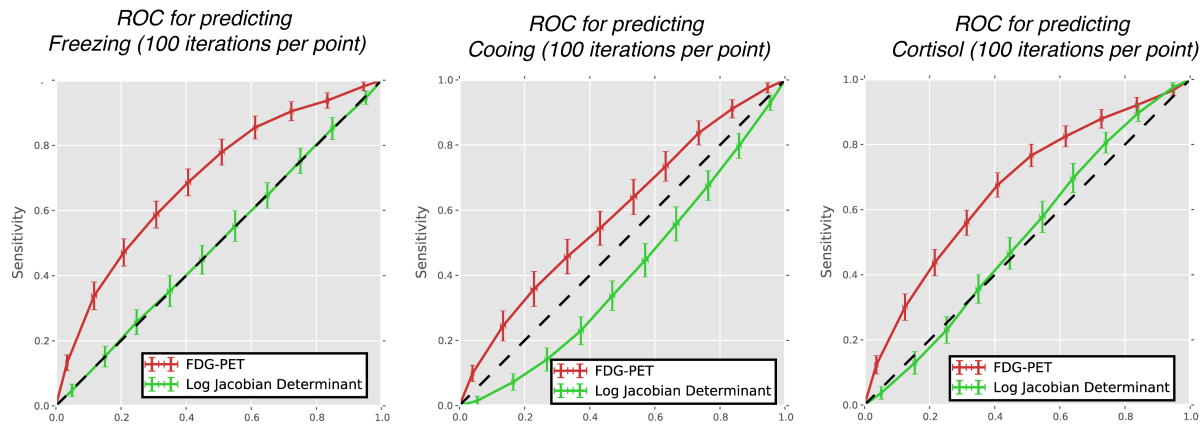


Figure S3: ROC curves using FDG-PET (red) and log jacobian determinant (green) to predict Freezing (left), Cooling (middle) and Cortisol (right) using elastic net regularized regressions. The dashed black line indicates chance predictions, and curves that near the upper left corner represent better predictors of AT.

Heritability of brain metabolism

The FDG-PET findings in this manuscript replicate and extend our previously published work, which were performed in the initial subjects from this sample ($n=238/592$; (4)). In $n=238$ we found heritability differed across AT's neural substrates. Of particular interest, we found that anterior hippocampal metabolism was heritable, whereas Ce metabolism was not. This finding replicates in the non-overlapping portion of the present sample ($n=354/592$; FDR $q < .05$). Power analyses revealed that we had a $\sim 35\%$ chance of detecting a voxel that was 25% heritable as different from zero in the initial sample, whereas in the combined $n=592$ sample we obtained $\sim 95\%$ power for this same test. In $n=592$, although some Ce voxels failed to reach significance, we also identified heritable voxels within the Ce-region (i.e. peak h^2 in Ce: $p=.0003$). Consistent with our prior work, the peak hippocampal metabolism was observed to be nearly twice as heritable (e.g. peak h^2 in aHip=.50). The differential heritability of ATs neural substrates provides important information that can help us to understand the biology of anxiety. In particular, these data suggest that different genetic pathways are likely to influence the function of the amygdala and anterior hippocampus. Moreover, by extending these results to include genetic correlation analyses, we can begin to identify those regions that are most likely to mediate the heritable risk to develop anxiety and depressive disorders (See main text as well as Figure S4).

AT-related regional brain metabolism shares a genetic substrate with AT

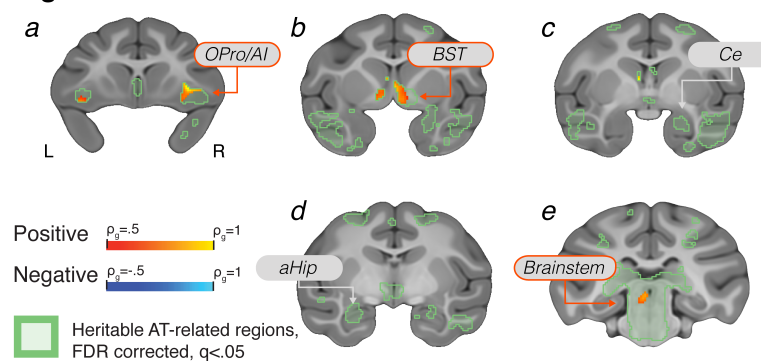


Figure S4: Regions where brain metabolism showed a significant genetic correlation with AT include include orbital proisocortex/anterior insula (OPro/AI; shown in [a]), bed nucleus of the stria terminalis (BST; shown in [b]), and periaqueductal gray (PAG; shown in [e]), with no significant results in central nucleus of the amygdala (Ce; shown in [c]), anterior hippocampus (aHip; shown in [d]) or other brainstem regions (shown in [e]).

Identifying candidate genes using publically available databases

To begin the process of identifying molecules that might mediate the heritable component of the risk to develop anxiety and depressive disorders, we examined regional variation in the levels of gene expression from publically available human brain data. Specifically, we compared gene expression in regions genetically correlated with both AT and each other, to gene expression in the rest of the brain. By virtue of their preferentially high expression in brain regions that mediate the intergenerational transfer of AT, these genes are candidates for future mechanistic studies aimed at identifying the molecular underpinnings of the heritable risk to develop anxiety and depressive disorders. All analyses were performed based on microarray-measured gene expression in the human brain using the differential expression tool at <http://human.brain-map.com>, provided by the Allen Institute for Brain Science (AIBS)(5). These analyses are not intended to implicate genetic variation within these genes in AT. Rather, these analyses based on our non-human primate brain imaging data aim to provide researchers with a list of potential molecular systems within the tripartite OPro/AT-BST-PAG circuit that may contribute to the intergenerational transmission of anxiety. Because our between-region genetic correlation analyses revealed significant genetic correlations in the metabolism between BST and both PAG and OPro/AI, we targeted differential gene expression searches to those genes preferentially expressed in regions most homologous to our BST-PAG and BST-OPro/AI clusters. Specifically, independent differential gene expression searches were performed in the corresponding BST-PAG (i.e. central gray of the midbrain similar to PAG, and left bed nucleus of stria terminalis ["CGMB BST-L"] versus all gray matter ["GM"]) and BST-OPro/AI regions (i.e. posterior orbital gyrus similar to OPro, short insular gyrus similar to AI, and left bed nucleus of stria terminalis ["POrG SIG BST-L"] versus all gray matter ["GM"]) of the human brain. These tests were used to identify the top 200 genes with the greatest fold-change increase in expression between POrG, SIG, & BST-L compared to the rest of the brain (Dataset S2a), and a similar list of the top 200 genes with the greatest fold-change increase in expression in PAG & BST-L compared to the rest of the brain (Dataset S2b). We restricted these exploratory analyses to genes that showed greater expression in target areas compared to the rest of the brain, as interpreting relatively decreased expression as unrelated to the heritability of AT would require: 1) accepting that these are true null findings, and 2) assuming that lack of expression in human brains during adulthood implies that these molecules do not play a role in the cross-generational transfer of AT. Analyses revealed several well-known molecules implicated in stress-related psychopathology (e.g. serotonin transporter [SLC6A4], corticotropin-releasing hormone [CRH]), as well as several promising targets for stress-related intervention (e.g. neuropeptide Y [NPY], somatostatin [SST], and serotonin receptor 2C [HTR2C]), and several molecules that represent novel candidates for examination in relation to AT (Dataset S2). Based on our genetic correlation analyses, the genes in these lists are reasonable candidates for contributing to the function of the tripartite OPro/AI-BST-PAG circuit and the heritable components of AT.

In order to assess the relevance of these gene lists to anxiety, and to identify broader anxiety-relevant molecular processes, we performed gene ontology analyses using Enrichr (6). Specifically, using gene set enrichment analyses, we examined the relative number of genes identified in Dataset S2 that belong to curated gene-sets with known functions (7). These analyses revealed an over-representation of genes in the Biological Processes (n=75; Dataset S3a), Cellular Component (n=15; Dataset S3b), and Molecular Function ontologies (n=25; Dataset S3c). Specific over-represented ontologies include, "neuropeptide hormone activity" (GO:0005184), "synapse part" (GO:0044456), and "behavioral fear response" (GO:0001662). These informatics-based proposals for molecular processes contributing to the function of the tripartite prefrontal-limbic-midbrain circuit, provide a "proof-of-concept" for combining our large-scale brain imaging studies in non-human primates with publically-available neurogenetic datasets to gain translational insight. A deeper understanding of the mechanisms and regulators of regional gene expression will

continue to refine these candidates for the molecules responsible for the heritable risk to develop anxiety and depressive disorders.

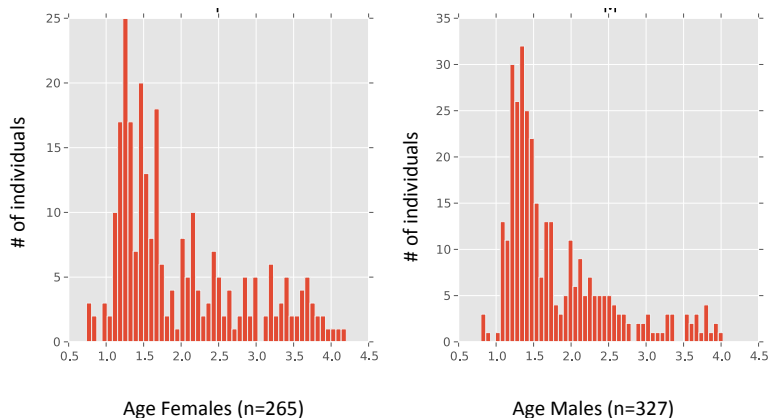
Supplementary Methods

Method overview

Each animal was injected with FDG and exposed to the NEC-context in which a human intruder presents their profile to the monkey for 30-minutes prior to receiving a PET scan. This paradigm allows us to obtain a measurement of integrated regional brain metabolism during exposure to the NEC-context. Brain metabolism was regressed against AT to identify AT-related brain regions. Heritability of local brain volume and brain metabolism was estimated at each voxel based on each pair of animals' degree of relatedness. Bivariate heritability estimates were similarly computed to examine the degree to which AT and regional brain metabolism share a genetic substrate. All experiments were performed according to the federal guidelines of animal use and care and with the approval of the University of Wisconsin Madison Institutional Animal Care and Use Committee.

Subjects

Five hundred and ninety-four young rhesus monkeys that were part of a large multi-generational pedigree were phenotyped for brain metabolism and stress-related behaviors. Paternity tests were performed when paternity was in question, which resulted in 2 animals being excluded from all analyses, resulting in five hundred and ninety-two animals included in all analyses (Age: $\mu=1.88$, $sd=0.78$; 327M/265F; see histogram below). All animals were mother-reared, and pair-housed in a vivarium on a 12 hour light/dark cycle with a 6 am light onset at the Harlow Primate Laboratory and the Wisconsin National Primate Research Center. All studies were performed during the light cycle. We attempted to test every young rhesus monkey at the University of Wisconsin-Madison's Harlow Lab and Primate Center that was available for study. The availability of animals during the period data collection determined the final sample size. Animals that underwent prior drug administration or surgery were excluded. Although, a small number of animals underwent prior behavioral testing at some point in their lives as a part of experiments in other laboratories, these effects were considered to be random with respect to the effects of interest, part of the environmental influences, and were, therefore, not specifically examined. The typical life span of a rhesus macaque is approximately 25, and since most animals are weaned between 6 months and 1 year and begin puberty when they are between 3 and 4 years old, the majority of animals are considered to be roughly equivalently aged to pre-pubescent children between 3-12 years old.



Multi-generational family pedigree

Subjects were part of a large multi-generational pedigree of 1928 animals across 8 generations. Scanned subjects from this pedigree consisted of 592 animals, with 350,464 possible relationships. The structure of this multi-generational pedigree consists of: 2 parent-offspring pairs, 28 full-sibling pairs, 44 other pairs of 1st degree relatives, 11 avuncular pairs, 1340 half sibling pairs, 1388 other pairs of 2nd degree relatives, 3293 pairs of 3rd degree relatives, 6991 pairs of 4th degree relatives, 73138 pairs of animals related less than 4th degree, and 83419 unrelated pairs.

No-Eye-Contact (NEC) context

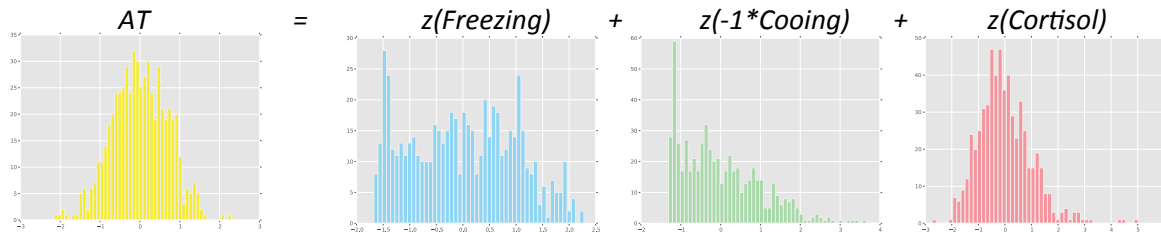
In the NEC-context of the human intruder paradigm a potentially threatening human intruder stands ~2.5 meters away and presents their profile to the monkey while making no-eye-contact (NEC) for 30 minutes (4, 8). In contrast to being alone or exposed to a human intruder staring at the monkey, the NEC context reliably elicits freezing behavior.

Measuring glucose metabolism using [18-F] deoxyglucose PET

Subjects received an intravenous injection of FDG immediately prior to the 30-minute NEC-context. Following 30-minute exposure to the NEC-context, whole blood was collected for quantifying cortisol and subjects were anesthetized with a 15mg/kg intramuscular injection of ketamine, intubated, and placed in the PET scanner. Anesthesia was maintained using 1-2% isoflurane gas. FDG and attenuation scans were acquired using a Siemens/Concorde microPET P4 scanner (9). Images were reconstructed using standard filtered-backprojection techniques with attenuation- and scatter-correction. This technique results in FDG-PET scans that represent the integrated brain metabolism throughout NEC-exposure. FDG-PET images were transformed to standard space as described below, and intensity-normalized so that the mean brain value was equivalent across individuals. A 2mm FWHM smoothing kernel was applied to account for variation in brain anatomy and registration.

Anxious Temperament (AT) measurements during NEC

AT estimates were computed based on behavior and physiology during NEC exposure as in other published work (1, 2, 4, 10). Behavior was measured during NEC exposure by a trained rater blind to pedigree information. Freezing was defined as a lack of movement for greater than 3-seconds, and was scored in seconds per 5-min of NEC exposure (30-min total). Mean freezing scores were log-scaled, and standardized after removing the linear effects of age and sex. Cooing was measured as the frequency of coo-vocalizations during each 5-min period of NEC-exposure. Mean cooing frequencies were square-root transformed, and standardized after removing the linear effects of age and sex. Plasma cortisol ($\mu\text{g}/\text{dL}$) was quantified based on samples taken immediately after NEC-exposure. Cortisol was quantified in duplicate using the DPC Coat-a-count radioimmunoassay (Siemens, Los Angeles, CA). Cortisol values were standardized after removing the linear effects of age, sex, and the time-of-day in which samples were taken. A composite measure of AT was computed as the combination of standardized freezing, reductions in cooing and cortisol measures. More specifically, freezing minus cooing plus cortisol all divided by three, as can be seen in the histograms below.



Measuring local brain volume using Magnetic Resonance Imaging (MRI)

Magnetic resonance images (MRI) were collected within 2 months of NEC-exposure. MRI was collected under anesthesia (see above) using a General Electric Discovery 3T scanner (GE Inc., Fairfield, CT) and standard quadrature extremity coil. Anatomical scans were obtained with a 3D T1-weighted, inversion-recovery, fast gradient echo prescription (TI/TR/TE/Flip/NEX/FOV/Matrix/Bandwidth: 600ms/8.65ms/1.89ms/10°/2/140mm/256×224/61.1 kHz) with whole brain coverage (128 slice encodes over 128 mm) reconstructed to 0.27×0.27×0.5 mm on the scanner). Each MRI scan was manually segmented into brain and non-brain tissue. T1-brain images were then transformed to standard space (methods described below), and transformation parameters were saved. The transformations to standard space were decomposed into linear (affine) and non-linear (warp) maps. The proportion of volumetric change between each animal's original scan and template space was quantified as the absolute value of the jacobian determinant of the non-linear transformation. This procedure is akin to computing the number of original-space voxels that became a single voxel in template space. To put volumetric expansions and reductions on the same scale, data were log transformed. Importantly, this procedure accounts for individual differences in total brain volume. This procedure produced a single map for each subject representing the relative volume at each voxel in the brain. These log jacobian determinant maps were smoothed by 2mm in standard space, and used for statistical computations.

Study-specific template creation and individual-subject registration

We created a study-specific template because this unique dataset of 592 young rhesus monkey T1-anatomical scans together constitutes our best estimate of the macro-structure of the young rhesus monkey brain anatomy. Study-specific T1-anatomical template creation was performed using an iterative procedure using Advanced Normalization Tools (ANTS; [http://sourceforge.net/projects/advants/](http://sourceforge.net/projects/advants;); (11, 12)). Each subject's T1-anatomical image was first aligned to a predefined template-space using a non-linear symmetric diffeomorphic image registration in ANTS. Nonlinear registration was performed using a symmetric diffeomorphic image registration and a .25 gradient step-size; a pure cross correlation cost-function with window radius 2 and weight 1; the similarity matrix was smoothed with sigma=2; and this process was repeated at 4 increasingly fine levels of resolution with 30, 20, 20, and 5 iterations at each level respectively. The average of all 592 individual-subject T1's in 'template-space' was computed and taken to be the study-mean. Similarly, the non-linear deformation-field was also averaged and taken to be the deformation-mean. The deformation-mean was inverted and 15% of this deformation was applied to the study-mean, to obtain the first iteration of the study-specific template. To maintain comparability to other studies, and to printed brain atlases, the affine transformation was *not* inverted and applied to the study-mean. The same procedure was performed by aligning each subject's T1-weighted anatomical image to the initial study-specific template. After averaging the images and deformations, a new study-specific template was created by applying 15% of the newest mean-deformation to the newest study-mean. This process was repeated 4 times, to obtain a final study-specific template. Each subject's original T1-anatomical images were then aligned to this study-specific template using the ANTS non-linear registration, as previously described. Each animal's FDG-PET image was aligned to its T1-anatomical image using a rigid body mutual information warp, and the transformation from T1 to template-space was then applied to the FDG-PET image.

Measuring serotonin transporter binding using [11-C] DASB

Serotonin transporter binding was measured using the radioligand [*11-C*]DASB in a sample of 34 animals. Data from these [*C-11*]DASB-PET scans have been previously published (13, 14). Methods for acquisition were fully described in (13). Reconstructed DASB binding estimates were transformed to the n=592 study-specific template using ANTS. Methods are identical to those described above, and transformations were applied to the DASB images.

*Measuring dopamine D2/D3 receptor binding using [*18-F*]Fallypride*

Dopamine D2/D3 receptor binding was measured using the radioligand [*18-F*]Fallypride, in a set of 33 animals. Data from these [*18-F*]Fallypride-PET scans and full methods have been previously published (15). Reconstructed Fallypride binding estimates were re-transformed to the n=592 study-specific template using ANTS. Methods are identical to those described above, and transformations were applied to the Fallypride images.

Statistical analysis: Voxelwise correlations

Voxelwise robust regressions between AT and brain metabolism were performed using fMRIStat (<http://www.math.mcgill.ca/keith/fmrifstat/>) and robustfit in MATLAB (<http://www.mathworks.com/>) (16). To account for potential confounds, all regressions entered potentially the confounding variables age, sex, MRI scanner, prior exposure to NEC, and order of acquisition. We implemented Šidák correction for multiple comparisons to examine AT to brain correlations (17).

Statistical Analysis: Spatial Correlations

To assess the similarity of the spatial relationships between voxelwise maps, we performed spatial correlations. Each image was converted to a vector, masked for voxels within the brain, and the two vectors were correlated using Pearson's and Spearman's correlations.

Statistical analysis: Heritability analyses

Heritability analyses were performed using SOLAR (<http://solar.txbiomedgenetics.org/>) based on pedigree information (18). Heritability analyses always controlled for age, age², sex and the age x sex interaction. Heritability analyses were performed at each voxel in the brain for both FDG-PET and log jacobian determinant with the help of the center for high-throughput computing at the University of Wisconsin-Madison and the Open Science Grid (OSG). Heritability analyses were computed as described below, and we corrected for multiple comparisons using the False Detection Rate (FDR) technique (19).

To estimate the heritability of a single trait (i.e. AT or brain metabolism at a single voxel), we first computed the trait's covariance matrix, which we will call Ω , where location i,j in the matrix is filled with the covariance in X between subject i and subject j .

$$\Omega_X = Cov[X, X] = \begin{bmatrix} cov(X_1, X_1) & cov(X_1, X_2) & \dots & cov(X_1, X_n) \\ cov(X_2, X_1) & cov(X_2, X_2) & \dots & cov(X_2, X_n) \\ \vdots & \vdots & \ddots & \vdots \\ cov(X_1, X_n) & cov(X_2, X_n) & \dots & cov(X_n, X_n) \end{bmatrix}$$

Where covariance is defined as:

$$cov[X_i, X_j] = E[(X_i - E[X_i])(X_j - E[X_j])]$$

and, at least in this case, the expectation can be defined as:

$$E[X] = \mu(X) = \frac{1}{N} \sum_{i=1:N} X_i$$

The relatedness matrix (Φ) can be computed based on the pedigree, as:

$$\Phi = \frac{1}{2} R$$

where R is the matrix of each pair of animals relationship to each other, with the r for a parent and a child $.5 = (2^{-1})$, r for siblings $.5 = (2^{-2} + 2^{-2})$, and so on according to the table below, and beyond.

Table for relatedness matrix:

r	relationship	degree of relationship
100%	identical twins; clones	0
50%	parent-offspring	1
50%	full siblings	2
37.5%	3/4 siblings or sibling cousins	2
25%	grandparent-grandchild	2
25%	half siblings	2
25%	aunt/uncle-nephew/niece	3
25%	double first cousins	4
12.5%	great grandparent-great grandchild	3
12.5%	first cousins	4
12.5%	quadruple second cousins	6
9.38%	triple second cousins	6
6.25%	half-first cousins	4
6.25%	first cousins once removed	5
6.25%	double second cousins	6
3.13%	second cousins	6
0.78%	third cousins	8
0.20%	fourth cousins	10

Using the covariance and relatedness matrices, one can estimate the putatively genetic and environmental variance of a quantitative phenotypic trait in the form:

$$\Omega \approx 2\Phi\sigma_g^2 + I_n\sigma_e^2$$

where:

Ω is the covariance matrix of the phenotype

Φ is the $n \times n$ kinship matrix for the pedigree

σ_g^2 is the variance in the trait due to additive genetic (g) effects

I_n is the $n \times n$ identity matrix

σ_e^2 is the variance due to unmeasured random effects, i.e. environmental (e)

It is worth noting that the variance attributed to the environment in this mode, is considered to be random for each subject, and not shared between subjects.

The variance parameters σ can be estimated by maximizing the likelihood function:

$$\mathcal{L}(\sigma_g^2, \sigma_e^2 | y) = -\frac{n}{2} \ln(2\eta) - \frac{1}{2} \ln(\Omega) - \frac{1}{2} (x - \mu_x)' \Omega^{-1} (X - \mu_X)$$

After estimating this model, the heritability (h^2) can be estimated based on the variance in genetic and environmental effects, by calculating:

$$h^2 = \frac{\sigma_g^2}{(\sigma_g^2 + \sigma_e^2)}$$

Computing the probability of this heritability and is computed by comparing the log likelihood of the model above and the difference between this model and another where σ_g^2 is constrained to equal 0, i.e.:

$$\chi_1^2[\sigma_g^2] = -2\mathcal{L}_{\sigma_g^2=0} + 2\mathcal{L}$$

Statistical analysis: Bivariate heritability analyses

Bivariate heritability analyses were performed using SOLAR (<http://solar.txbiomedgenetics.org/>) based on pedigree information (18, 20, 21). Bivariate heritability analyses always controlled for age, age², sex and the age by sex interaction. Bivariate heritability analyses examining the shared heritability of AT and FDG-PET were performed at each voxel in the brain as described below, and were corrected for multiple comparisons using the False Detection Rate (FDR) (19). Because there were no significant correlations between AT and the log-jacobian determinant, bivariate heritability was not performed on this dataset. Analyses were performed at the center for high-throughput computing at the University of Wisconsin-Madison and the Open Science Grid (OSG).

Bivariate heritability analyses are performed using methods similar to the heritability analyses detailed above, with a covariance matrix that represents both traits and their interaction. More specifically,

$$\Omega_B = \begin{bmatrix} \Omega_X & \Omega_{YX} \\ \Omega_{XY} & \Omega_Y \end{bmatrix}$$

Where Ω_X and Ω_Y are as Ω above, and the bivariate portions are:

$$\Omega_{XY} \cong 2\Phi\sigma_{g_{XY}}^2 + I_n\sigma_{e_{XY}}^2$$

with ϕ defined as before, and the variance of X, Y can be decomposed to its component parts:

$$\sigma_{XY}^2 = \sigma_X\sigma_Y\rho_{XY}$$

where $\rho_{g_{XY}}$ is the genetic correlation, that we have set out to estimate.

This can now be estimated using the same maximum likelihood estimation we described above:

$$\begin{aligned} \mathcal{L}(\sigma_{g_X}^2, \sigma_{e_X}^2, \sigma_{g_Y}^2, \sigma_{e_Y}^2, \rho_{e_{XY}} | X, Y) = & -n\ln(2\eta) - \frac{1}{2}\ln|\Omega_B| \\ & - \frac{1}{2}([\frac{X}{Y}] - \mu_{[\frac{X}{Y}]})' \Omega^{-1} ([\frac{X}{Y}] - \mu_{[\frac{X}{Y}]}) \end{aligned}$$

As before, the three parts of this function are: a distribution parameter (now for bivariate normal), the genetic and environmental components (now including a mean), and the mean.

Similar to the test above, the p-values for s can be computed by estimating the same model with $\rho = 0$.

$$\chi_1^2[\rho_g] = -2\mathcal{L}_{\rho_g=0} + 2\mathcal{L}$$

Computing: Center for High-Throughput Computing (CHTC) and the Open Science Grid

This research was performed using resources and the computing assistance of the UW-Madison Center For High Throughput Computing (CHTC) in the Department of Computer Sciences. The CHTC is supported by UW-Madison and the Wisconsin Alumni Research Foundation, and is an active member of the Open Science Grid, which is supported by the National Science Foundation and the U.S. Department of Energy's Office of Science. All jobs were submitted using HTCondor.

Data availability

Voxelwise maps representing the AT-relatedness and heritability of brain volume and brain metabolism, can be found in supplementary Dataset 1.

Supplementary References

1. A. J. Shackman *et al.*, Neural mechanisms underlying heterogeneity in the presentation of anxious temperament, *Proc. Natl. Acad. Sci. U.S.A.* **110**, 6145–6150 (2013).
2. A. S. Fox, S. E. Shelton, T. R. Oakes, R. J. Davidson, N. H. Kalin, Trait-Like Brain Activity during Adolescence Predicts Anxious Temperament in Primates, *PLoS ONE* **3** (2008), doi:10.1371/journal.pone.0002570.
3. H. Zou, T. Hastie, Regularization and Variable Selection via the Elastic Net, *Journal of the Royal Statistical Society. Series B (Statistical Methodology)* **67**, 301–320 (2005).
4. J. A. Oler *et al.*, Amygdalar and hippocampal substrates of anxious temperament differ in their heritability, *Nature* **466**, 864–868 (2010).
5. M. J. Hawrylycz *et al.*, An anatomically comprehensive atlas of the adult human brain transcriptome, *Nature* **489**, 391–399 (2012).
6. E. Y. Chen *et al.*, Enrichr: interactive and collaborative HTML5 gene list enrichment analysis tool, *BMC Bioinformatics* **14**, 128 (2013).
7. M. Ashburner *et al.*, Gene ontology: tool for the unification of biology. The Gene Ontology Consortium, *Nat. Genet.* **25**, 25–29 (2000).
8. N. H. Kalin, S. E. Shelton, M. Rickman, R. J. Davidson, Individual differences in freezing and cortisol in infant and mother rhesus monkeys, *Behav. Neurosci.* **112**, 251–254 (1998).
9. C. Tai *et al.*, Performance evaluation of the microPET P4: a PET system dedicated to animal imaging, *Phys Med Biol* **46**, 1845–1862 (2001).
10. A. S. Fox *et al.*, Central amygdala nucleus (Ce) gene expression linked to increased trait-like Ce metabolism and anxious temperament in young primates, *Proc. Natl. Acad. Sci. U.S.A.* **109**, 18108–18113 (2012).
11. B. B. Avants *et al.*, The optimal template effect in hippocampus studies of diseased populations, *Neuroimage* **49**, 2457–2466 (2010).
12. B. B. Avants *et al.*, A reproducible evaluation of ANTs similarity metric performance in brain image registration, *Neuroimage* **54**, 2033–2044 (2011).
13. B. T. Christian *et al.*, Serotonin transporter binding and genotype in the nonhuman primate brain using [C-11]DASB PET, *Neuroimage* **47**, 1230–1236 (2009).
14. J. A. Oler *et al.*, Serotonin transporter availability in the amygdala and bed nucleus of the stria terminalis predicts anxious temperament and brain glucose metabolic activity, *J. Neurosci.* **29**, 9961–9966 (2009).

15. B. T. Christian *et al.*, The distribution of D₂/D₃ receptor binding in the adolescent rhesus monkey using small animal PET imaging, *Neuroimage* **44**, 1334–1344 (2009).
16. T. D. Wager, M. C. Keller, S. C. Lacey, J. Jonides, Increased sensitivity in neuroimaging analyses using robust regression, *Neuroimage* **26**, 99–113 (2005).
17. Z. Šidák, Rectangular Confidence Regions for the Means of Multivariate Normal Distributions, *Journal of the American Statistical Association* **62**, 626–633 (1967).
18. L. Almasy, J. Blangero, Multipoint quantitative-trait linkage analysis in general pedigrees, *Am. J. Hum. Genet.* **62**, 1198–1211 (1998).
19. C. R. Genovese, N. A. Lazar, T. Nichols, Thresholding of statistical maps in functional neuroimaging using the false discovery rate, *Neuroimage* **15**, 870–878 (2002).
20. L. Almasy, T. D. Dyer, J. Blangero, Bivariate quantitative trait linkage analysis: pleiotropy versus co-incident linkages, *Genet. Epidemiol.* **14**, 953–958 (1997).
21. J. T. Williams, P. Van Eerdewegh, L. Almasy, J. Blangero, Joint multipoint linkage analysis of multivariate qualitative and quantitative traits. I. Likelihood formulation and simulation results, *Am. J. Hum. Genet.* **65**, 1134–1147 (1999).

Supplementary Legends

Legend Figure S1: Histograms displaying the distribution of t-values reflecting the relationship between brain metabolism and each component of AT, i.e. freezing, cooing, and cortisol can be seen in **(a)**. Grey arrows represent the threshold for reaching significance at a Šidák corrected $p < .05$. Although the components of AT are not highly related (see (1)), spatial correlations across voxels demonstrate a similar pattern of brain-phenotype relationships between components of AT **(b)**, $r^2_{[Freezing,Cooing]} = .71$; $c, r^2_{[Freezing,Cortisol]} = .37$; $d, r^2_{[Cooing,Cortisol]} = .40$; all p 's $< .0001$.

Legend Figure S2: ROC curves using FDG-PET (red) and log jacobian determinant (green) to predict AT using elastic net regularized regressions. The dashed black line indicates chance predictions, and curves that near the upper left corner represent better predictors of AT.

Legend Figure S3: ROC curves using FDG-PET (red) and log jacobian determinant (green) to predict Freezing (left), Cooing (middle) and Cortisol (right) using elastic net regularized regressions. The dashed black line indicates chance predictions, and curves that near the upper left corner represent better predictors of AT.

Legend Figure S4: Regions where brain metabolism showed a significant genetic correlation with AT include include orbital preisocortex/anterior insula (OPro/AI; shown in [a]), bed nucleus of the stria terminalis (BST; shown in [b]), and periaqueductal gray (PAG; shown in [e]), with no significant results in central nucleus of the amygdala (Ce; shown in [c]), anterior hippocampus (aHip; shown in [d]) or other brainstem regions (shown in [e]).

Legend Table S1: Clusters that are significantly related to AT ($p < .05$, Sidak corrected), as well as each local maxima in each cluster that fell in a cytoarchitectonically distinct region and was at least 2mm from the nearest peak.

Legend Table S2: Clusters that are: 1) significantly related to AT ($p < .05$, Sidak corrected), 2) significantly heritable (FDR $q < .05$ within AT-related regions), and 3) significantly co-heritable with AT (FDR $q < .05$ within AT-related heritable regions), as well as each local-maxima within each cluster that fell in a cytoarchitectonically distinct region and was at least 2mm from the nearest peak according to the Paxinos atlas. Importantly, because of the complexity of this analysis readers should not interpret point-estimates of rho-g or non-significant findings.

Supplementary Table S1: AT-related regions

Cluster Region	Direction of correlation	Cluster Hemisphere	Cluster volume (mm ³)	Peak							Heritability of peak				
				Region	Peak Hemisphere	Maximum t-value	p-value	x	y	z	h ²	p			
Anterior temporal lobe & Orbitofrontal Cortex	+	Right	1090 TPO	Right	8.0727	2.00E-15	21.25	2.5	-9.375		0	1			
				Ce	Right	7.6635	3.84E-14	12.5	2.5	-9.375	0.261337	0.000360489			
				TEa	Right	7.1609	1.22E-12	19.375	0	-12.5	0.174347	0.000328481			
				aHip	Right	7.0817	2.08E-12	15	-6.875	-10.625	0.257345	0.000152826			
				Opro	Right	6.4932	9.06E-11	16.25	9.375	-1.25	0.268771	0.000128925			
				TPPro	Right	6.3251	2.54E-10	21.25	6.875	-6.875	0.201427	0.00237447			
				Pir	Right	5.9655	2.13E-09	13.125	3.75	-4.375	0.188983	0.0121205			
				TLR(Area 36R	Right	5.6065	1.60E-08	13.75	3.75	-17.5	0.166364	0.00698572			
				TE1	Right	5.5715	1.94E-08	19.375	-2.5	-13.125	0.19479	0.000189722			
				ER	Right	5.4874	3.05E-08	11.875	1.875	-15	0.151739	0.00802457			
Brainstem, Thalamus, Hypothalamus	+	Bilateral	2167 PAG	Right	8.9211	3.03E-18	0.625	-15	-3.75	0.188205	0.0171766				
				PTg (region)	Left	8.2515	5.31E-16	-2.5	-13.75	-8.75	0.359567	3.81E-06			
				3N (region)	Right	7.5539	8.30E-14	0.625	-10.625	-6.875	0.513636	0			
				pHip	Left	7.2293	7.72E-13	-10	-16.875	1.25	0.188604	0.00589794			
				IPul	Left	6.8106	1.22E-11	-11.25	-14.375	-1.875	0.346932	1.25E-06			
				MVe (region)	Left	6.6964	2.53E-11	-1.875	-21.25	-15	0.369479	2.93E-05			
				SC	Right	6.6095	4.39E-11	5.625	-13.75	-13.75	0.263692	0.00019896			
				PH	Left	6.5273	7.33E-11	-1.25	-5.625	-4.375	0.324197	6.38E-06			
				PH	Right	6.385	1.76E-10	2.5	-5.625	-4.375	0.344087	2.09E-06			
				RLi (region)	Left	6.184	5.91E-10	-1.25	-8.75	-3.125	0.460485	1.79E-07			
				IPul	Right	5.979	1.97E-09	8.75	-13.75	0.625	0.490416	0			
				PR (region)	Left	5.9405	2.45E-09	-3.75	-8.125	-1.875	0.382055	5.36E-06			
				APul (region)	Left	5.7907	5.76E-09	-7.5	-13.125	6.875	0.36935	1.79E-07			
				MD	Right	5.6464	1.29E-08	1.25	-5.625	5	0.499351	5.96E-08			
				Anterior Temporal	Left	434 TPO	Left	7.1858	1.04E-12	-20	2.5	-12.5	0.153073	0.00567132	
				TEa	Left	6.4102	1.51E-10	-16.25	2.5	-14.375	0.242928	9.40E-05			
				TEM	Left	6.2393	4.25E-10	-22.5	-0.625	-12.5	0.188555	0.00140309			
				Pir	Left	5.8871	3.33E-09	-11.25	5	-10	0.155765	0.0173544			
				TPPro	Left	5.7371	7.77E-09	-19.375	7.5	-7.5	0.169864	0.014115			
				AA	Left	5.6471	1.28E-08	-11.875	3.125	-6.25	0	1			
				ST1	Left	5.4891	3.03E-08	-21.875	5.625	-6.875	0.250196	0.0013544			
Hippocampus	+	Left	172 aHip	Left	7.0474	2.61E-12	-11.25	-3.125	-9.375	0.294571	4.89E-05				
Extended Amygdala, Subgenual Cingulate	+	Right	155 BST	Right	6.742	1.90E-11	5.625	3.125	-1.875	0.269537	1.63E-05				
				Area 25	Right	6.3999	1.61E-10	1.25	8.75	1.875	0.40679	1.19E-07			
Temporal Cortex	+	Right	41 TEM	Right	6.0422	1.36E-09	28.125	-8.125	-4.375	0.229413	0.00238067				
Parietal Cortex	+	Right	31 PGa	Right	6.9724	4.27E-12	20	-9.375	-1.875	0	1				
Temporal Cortex	+	Left	35 TEM	Left	6.459	1.12E-10	-26.25	-10.625	-3.125	0.184614	0.00328374				
Orbitofrontal Cortex	+	Left	26 Area 47	Left	5.8177	4.94E-09	-16.25	14.375	4.375	0.12429	0.0409642				
				Area 13	Left	5.7168	8.70E-09	-10.625	14.375	5.625	0.164557	0.00539714			
Septum	+	Right	30 LS	Right	6.0748	1.13E-09	1.875	0	6.25	0	1				

Hippocampus	+	Right	16 Hip	Right	5.7616	6.78E-09	16.875	-10.625	-8.75	0.334407	5.90E-06
Visual Cortex,											
Parietal Cortex	-	Bilateral	7255 V1	Left	-9.1295	5.72E-19	-7.5	-20.625	13.75	0.187854	0.00480813
			PGM	Right	-8.9205	3.05E-18	9.375	-21.25	16.875	0.17998	0.00264174
			V4	Left	-8.7649	1.04E-17	-8.125	-18.75	13.125	0.158826	0.0188324
			PGM	Left	-8.7309	1.36E-17	-11.875	-26.875	0.625	0.335256	3.40E-06
			V1	Right	-8.5666	4.85E-17	6.25	-30.625	0	0.344527	6.56E-07
			V2	Left	-8.4085	1.63E-16	-5	-26.25	17.5	0.251739	9.38E-05
			LIP	Right	-8.2127	7.10E-16	10.625	-29.375	1.25	0.33002	4.05E-06
			V2	Right	-8.1754	9.37E-16	5	-34.375	-0.625	0.337413	4.17E-07
			PEa	Left	-8.0415	2.52E-15	-5	-36.25	1.25	0.30136	1.51E-05
			PEC	Right	-7.9715	4.21E-15	6.875	-33.75	8.75	0.348955	4.05E-06
			PEa	Right	-7.5088	1.14E-13	10.625	-35	1.875	0.329565	1.13E-06
			V3	Right	-7.3254	4.02E-13	2.5	-32.5	15.625	0.24428	2.72E-05
Superior Temporal											
Cortex	-	Right	78 MSTD	Right	-7.0493	2.57E-12	15	-21.875	6.875	0	1
Temporal Cortex	-	Left	83 TPOC	Left	-7.2556	6.47E-13	-12.5	-22.5	9.375	0.138651	0.0373646
Superior Temporal											
Cortex	-	Left	83 MSTD	Left	-6.1216	8.55E-10	-16.25	-24.375	10.625	0.231535	0.00296545
Motor Cortex	-	Left	497 Area 4	Left	-7.9745	4.11E-15	-12.5	-3.75	20	0.211055	6.09E-05
			Area 3	Left	-7.4147	2.18E-13	-6.875	-9.375	23.75	0.33474	0
Motor Cortex	-	Right	445 PE	Right	-7.8161	1.30E-14	11.25	-10.625	18.75	0.194055	0.00117958
			Area 3	Right	-7.2242	8.00E-13	7.5	-6.875	23.125	0.314775	0
			Area 4	Right	-7.1861	1.03E-12	10.625	-1.25	19.375	0.238066	1.31E-06

Supplementary Table S1: Clusters that are significantly related to AT ($p<.05$, Sidak corrected), as well as each local maxima in each cluster that fell in a cytoarchitectonically distinct region and was at least 2mm from the nearest peak.

Supplementary Table S2
Regions showing a significant genetic correlation with AT.

Region	Cluster	Peak									
		Direction of correlation	Cluster Hemisphere	Cluster volume (mm ³)	Region	Peak Hemisphere	Maximum rho-g	p-value	x	y	z
Brainstem		+	Left	5.3711	Left	Edinger Westphal/ Oculomotor Nucleus (3N)	0.64	0.0080	0	-10	-3.125
BST / Nucleus Accumbens		+	Left	7.5684	Left	BST	0.75	0.0005	-2.5	3.125	-1.25
BST / Subventricular extended amygdala / Nucleus Accumbens		+	Right	47.1191	Right	BST/Nacc	1.00	0.0006	1.25	4.375	0
Orbital/Insular Cortex		+	Right	32.7148	Right	13L	0.82	0.0005	16.875	11.25	1.875
		+			Right	OPro	1.00	0.0011	16.875	9.375	1.25
		+	Left	6.5918	Left	Opro	0.74	0.0023	-16.875	9.375	-2.5
		+			Right	47O	0.93	0.0024	20	11.25	-0.625
		+			Right	AI	0.80	0.0025	15.625	10	2.5
PAG		+	Left	15.1367	Left	PAG	0.86	0.0042	-0.625	-15.625	-3.75
White-matter		+	Right	8.7891	Right	White-matter near Area 47L and Area 45A	0.97	0.0024	18.75	15	6.25
Parietal Cortex		-	Left	5.3711	Left	MSTD	-0.94	0.0018	-11.875	-23.75	11.875
Visual and Parietal Cortex		-	Bilateral	1746.0938	Left	PEa (MIP)	-1.00	0.0000	-8.125	-23.75	16.875
Visual and Parietal Cortex		-			Right	PEa (MIP)	-1.00	0.0001	5.625	-21.875	13.125
		-			Right	V6	-0.73	0.0002	6.875	-30.625	3.75
		-			Right	V2	-0.72	0.0002	11.875	-31.25	0
		-			Right	PO (V6)	-1.00	0.0006	3.125	-33.75	7.5
		-			Left	PEa	-0.88	0.0009	-7.5	-16.25	13.125
		-			Left	V1	-0.69	0.0029	-11.25	-36.25	-1.25
		-			Right	V2	-0.63	0.0042	5	-36.25	5.625
Visual Cortex		-	Left	8.7891	Left	V2	-0.92	0.0006	-8.125	-20.625	-4.375
Visual cortex		-	Right	31.7383	Right	V1	-0.82	0.0038	5.625	-43.125	-5.625
Visual Cortex		-	Left	2.4414	Left	V3	-0.71	0.0071	-11.25	-22.5	-4.375

Supplementary Table S2: Clusters that are: 1) significantly related to AT ($p<.05$, Sidak corrected), 2) significantly heritable (FDR $q<.05$ within AT-related regions), and 3) significantly co-heritable with AT (FDR $q<.05$ within AT-related heritable regions), as well as each local-maxima within each cluster that fell in a cytoarchitectonically distinct region and was at least 2mm from the nearest peak according to the Paxinos atlas. Importantly, because of the complexity of this analysis readers should not interpret point-estimates of rho-g or non-significant findings.

Bridging psychology and genetics using large-scale spatial analysis of neuroimaging and neurogenetic data

Andrew S. Fox, Luke J. Chang, Krzysztof J. Gorgolewski, & Tal Yarkoni

Abstract

Understanding how microscopic molecules give rise to complex cognitive processes is a major goal of the biological sciences. The countless hypothetical molecule-cognition relationships necessitate discovery-based techniques to guide scientists toward the most productive lines of investigation. To this end, we present a novel discovery tool that uses spatial patterns of neural gene expression from the Allen Brain Institute (ABI) and large-scale functional neuroimaging meta-analyses from the Neurosynth framework to bridge neurogenetic and neuroimaging data. We quantified the spatial similarity between over 20,000 genes from the ABI and 48 psychological topics derived from lexical analysis of neuroimaging articles, producing a comprehensive set of gene/cognition mappings that we term the Neurosynth-gene atlas. We demonstrate the ability to independently replicate known gene/cognition associations (e.g., between dopamine and reward), and subsequently use it to identify a range of novel associations between individual molecules or genes and complex psychological phenomena such as reward, memory and emotion. Our results complement existing discovery-based methods such as GWAS, and provide a novel means of generating hypotheses about the neurogenetic substrates of complex cognitive functions.

Introduction

It is widely held that thoughts, feelings, and actions are reflected in macroscopic neural patterns that emerge from microscopic molecular processes that orchestrate the function of our nervous system. Although the basic concept of a matter-based mind is no longer a matter of serious scientific debate, the precise mapping between molecules and mental states remains largely a mystery. A major barrier to progress is that psychological and molecular processes unfold on vastly different spatial and temporal scales. In fact, the chasm between the two levels of description may be too wide to bridge directly, and has resulted in the emergence of multiple non-overlapping scientific fields. In the present work, we demonstrate the utility of distributed macroscopic neural patterns as a novel means of bridging the long-standing gap between psychological and molecular neurobiological levels of analysis.

Brain-wide macroscopic spatial patterns are ideal for linking cognitive and molecular processes because of their accessibility to multiple disciplines and levels of analysis (1–3). In recent decades, functional neuroimaging studies have identified highly consistent distributed brain networks that underlie mental states ranging from reward-seeking (4) to goal-directed thought (5) to autobiographical memory (6). Simultaneously, animal and human studies involving positron emission tomography, autoradiography, and *in situ* hybridization have demonstrated that many genes and the proteins they code for have predictable large-scale patterns of expression throughout the human brain (7–10). For example, in support of the role of dopamine in reward processing, it has been observed that genes encoding dopamine receptor proteins implicated in reward processing are highly expressed in consistent areas of the mammalian

striatum(11, 12). These regions are reliably activated in fMRI studies of reward processing (13, 14), and show extremely high concentrations of dopamine DRD2/DRD3 receptors in *in vivo* human imaging studies using positron emission tomography (PET)(15). The convergence of psychological and molecular processes at the level of large-scale, brain-wide spatial expression thus offers a powerful potential window into the molecular bases of cognition and affect.

In the work reported here, we introduce, validate, and apply a novel tool for mapping cognitive phenomena to molecular processes based on large-scale spatial analysis. We harness state-of-the-art neuroimaging and neurogenetics databases: Neurosynth, our recent framework for large-scale, automated synthesis of the published fMRI literature (16), and the Allen Human Brain Atlas (AHBA)(17), a brain-wide gene expression atlas derived from transcriptome-wide microarray assessments of human brain tissue. Here, we use this spatial integration of molecular and psychological processes (Neurosynth-gene) approach to independently replicate previous associations identified in the experimental literature, and to identify a large number of novel associations that have not been previously reported. This non-mechanistic approach can help guide researchers toward the most productive avenues for future research aiming to understand how complex psychological phenomena such as reward and memory processing emerge from the microscopic molecules of the brain.

Results

A common space for gene expression and functional activation

Our work builds directly on the Neurosynth framework (16, 18, 19). Neurosynth is an open framework for automated synthesis of published fMRI results, and enables researchers to produce high-quality estimates of the brain-wide neural correlates of major cognitive tasks and psychological states. The framework is ideal for understanding the relationship between psychological constructs and the brain, as it provides quantitative inferences about the

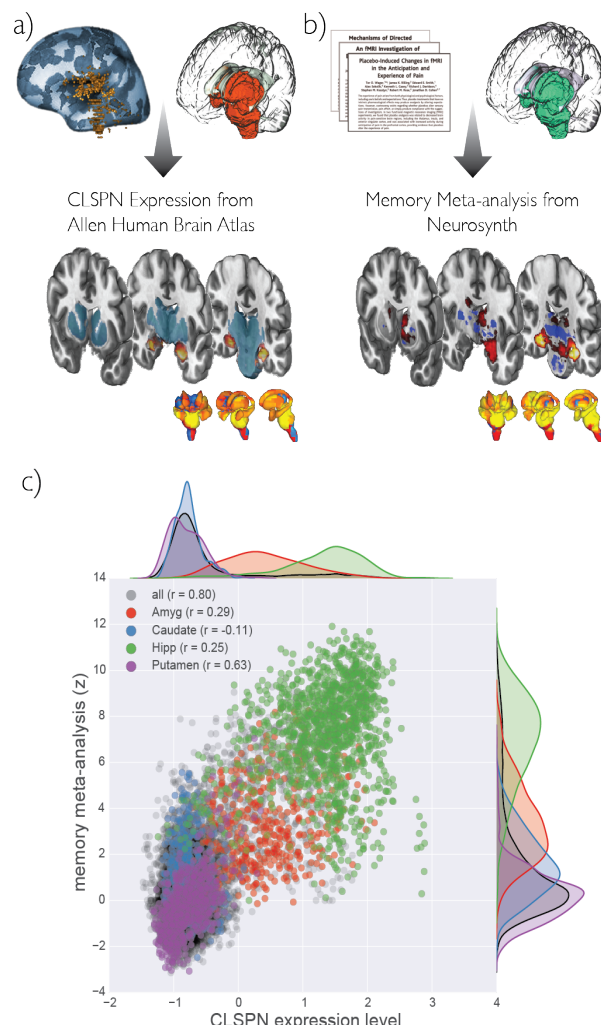


Figure 1. The Neurosynth-gene atlas uses spatial associations to link genes to cognitive processes, and is exemplified here by CLSPN gene expression from the AHBA and Memory meta-analysis map in Neurosynth. (a) Gene expression levels were extracted from the AHBA for subcortical structures and projected into standard space, shown here for the gene CLSPN. (b) Text mining is used to automatically generate "reverse inference" meta-analytic maps of fMRI studies within the same subcortical regions, exemplified here for the Memory topic. Patterns of gene expression and meta-analytic statistics are shown on both 2d slices and 3d renderings of subcortical structures (c) Scatter and kernel density estimation plots displaying spatial relationship between CLSPN expression levels and memory-related activation across all subcortical voxels. Different brain regions are represented in different colors.

consistency and specificity (20, 21) with which different cognitive processes elicit regional changes in brain activity. It can, for example, generate maps that estimate the relative

likelihood with which activation in a given brain region implies the presence of a particular psychological process such as reward or emotion, enabling “decoding” of entirely novel images in a relatively open-ended way (Figure 1a)(18, 22). Currently, Neurosynth provides whole-brain maps for several thousand distinct terms; in the present analyses we used a dimensionally-reduced set of 48 topics that reflect high-level psychological constructs such as Emotion, Memory and Reward (Fig 1b; Supplementary Table 1; Supplementary Figure 1; Supplementary Methods).

To bridge between large-scale functional activation and underlying molecular mechanisms, we integrated Neurosynth with data from the recently-released AHBA (23). The AHBA is a brain-wide gene expression atlas derived from transcriptome-wide microarray assessments of brain tissue from 3702 samples collected across 6 human donors. It provides a window into the distribution of human gene expression throughout the adult brain—an ability that has already led to novel insights (24). Gene expression is ideal for large-scale examinations of the molecular composition of neural tissue, as transcription of genes into RNA is a critical step in converting each cell’s DNA into the proteins that determine its function. Gene expression depends on genetic structure, the local molecular environment, and epigenetic factors, and, although each cell contains a full genome, patterns of gene expression are specific to particular cell types. Local regulation of gene expression is critical for determining the structure and function of neurons and glia by altering the composition of the cell, and thus gives rise to brain-region specific functions.

To quantify the spatial similarity between gene expression and functional activation maps, we transformed the gene expression data from the AHBA into the common stereotactic brain space used by Neurosynth. This process consisted of (i) normalizing brain-wide expression values separately for each gene averaged across probe-sets, (ii) mapping the reported coordinates for brain tissue used for microarray analyses to a standard neuroimaging template-space (i.e. Montreal Neurological Institute), and (iii)

smoothing the data to match the resolution of the Neurosynth maps (see Supplementary Methods for details). Because gene expression patterns differ substantially between subcortex and cortex (17), we conducted separate subcortical and cortical analyses. Here we focus exclusively on sub-cortical inferences, as the current spatial distribution of the AHBA samples was sparse in cortex (see Supplementary Methods; Supplementary Figure 2). Once the AHBA and Neurosynth maps were represented within the same standard brain space, we computed the spatial correlation between each gene expression map and each psychological topic map. The resulting matrix of 29,180 x 48 associations (i.e., genes x topics)—which we term the Neurosynth-gene atlas—provided a rich substrate for subsequent hypothesis testing and exploration of the relationship between specific genes or gene families and broad cognitive and affective processes.

To illustrate, Figure 1 displays the single strongest spatial correlation in the entire database—between expression of the gene CLSPN (claspin) and Memory-related brain activation—($r = .80$). Importantly, this correlation did not solely recapitulate anatomical boundaries (i.e., that CLSPN simply happens to be more strongly expressed in the hippocampus, which is known to be implicated in memory formation), as the positive correlation between patterns of CLSPN expression and memory-related activation is apparent both within and across multiple brain structures (Fig. 1C).

Strong corroboration of consensus neurotransmitter-cognition associations

The ability to search for candidate genes by psychological constructs (or for candidate psychological constructs by gene) presents a powerful tool for mapping between molecular and cognitive levels of analysis. The Neurosynth-gene atlas can be used for both top-down, theory-driven testing of hypotheses regarding the distribution of gene expression in the brain regions implicated in a specific cognitive process, as well as bottom-up, data-

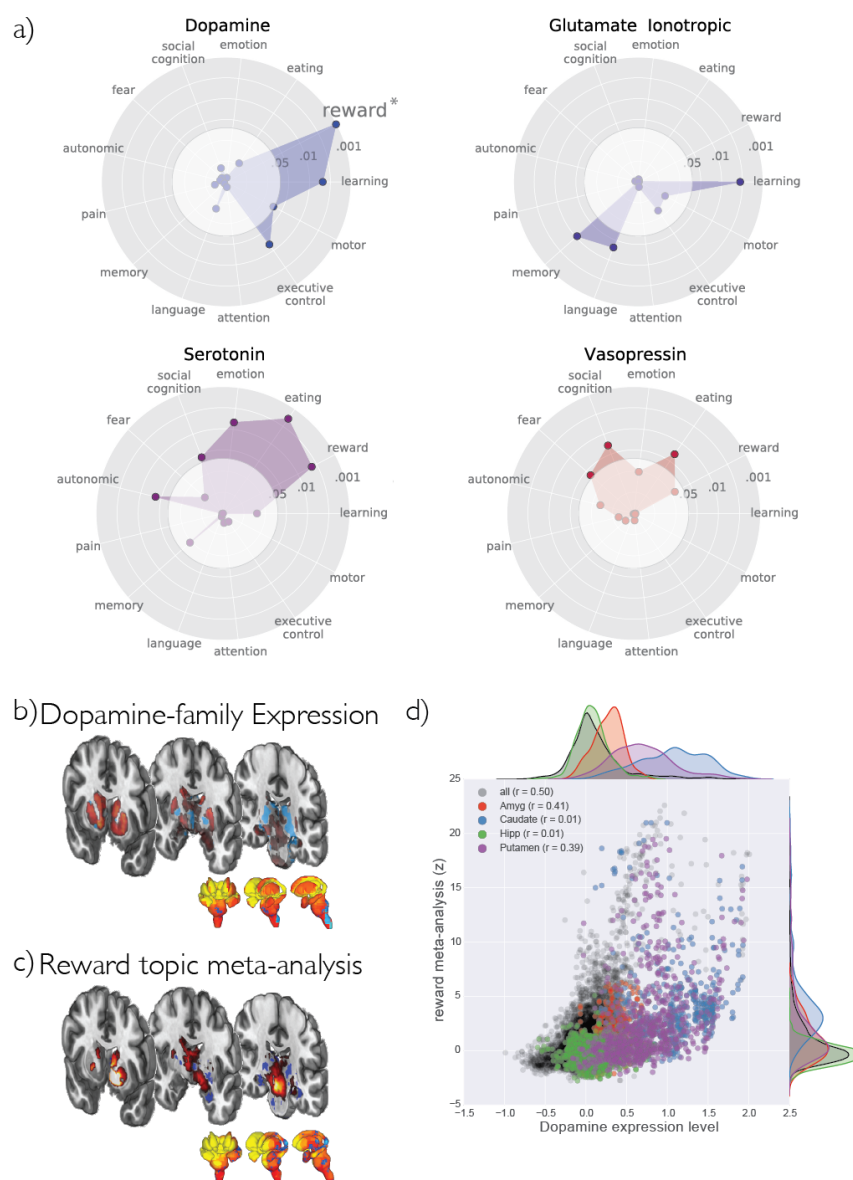


Figure 2. Neurotransmitter-genes are selectively associated with Neurosynth topics. Radar plots displaying statistical association between selected HGNC neurotransmitter receptor gene groups and selected Neurosynth topics (a) (for full results, see Supplementary Figure 4). Associations in the dark outer circle are significant at $p < .05$. Each statistical association represents the likelihood, relative to other neurotransmitters, that groups of neurotransmitter receptor genes are expressed in topic-related areas. For example, the dopamine-reward relationship (denoted with an asterisk) reflects the fact that patterns of gene expression in the Dopamine gene family (b) and the Reward-topic meta-analysis (c) are correlated across the brain (d).

driven hypothesis generation aimed at identifying novel gene-cognition relationships.

To demonstrate the utility of the Neurosynth-gene atlas, we first sought to corroborate existing relationships between

neurotransmitter systems and psychological processes—e.g., the well-established link between dopamine and reward (25), and the heavily-studied, though more contentious, relationship between the serotonin system and depression (26–28). Neurotransmitter systems are an ideal target for this kind of validation, as numerous studies have examined the psychological effects of specific pharmacological neurotransmitter receptor activation. Table 1 lists 16 frequently studied (though certainly not exhaustive) neurotransmitter/cognition associations—many of which have been reported in thousands of studies (e.g., dopamine/reward, serotonin/depression, and oxytocin/social behavior). To assess the relative strength of each of these associations, we first selected all individual genes contained in the corresponding HUGO Gene Nomenclature Committee (HGNC) neurotransmitter receptor group (e.g., DRD1, DRD2, etc.; see Supplementary Methods). We then computed the mean correlation with the target Neurosynth topic for all genes within each neurotransmitter group,

and used a permutation-based statistical approach to quantify the likelihood of obtaining an association of the observed strength purely by chance (see Supplementary Methods). The

#	Neurosynth-gene atlas found support		Receptor type	Putative cognitive function	Neurosynth topic map	mean r-value across subcorte	
	x	p				x	p
1	yes	Dopamine		reward	reward	0.23	0.0004
2	yes	Dopamine		working memory	working memory	0.08	0.03
3	no	Dopamine		motor function	motor processing	0.08	0.08
4	yes	Dopamine		ADHD	ADHD	0.14	0.002
5	yes	Serotonin		depression	depression	0.07	0.002
6	yes	Serotonin		emotion	emotion	0.05	0.02
7		Opioids		pain	pain	0.06	0.34
8	yes	Vasopressin/Oxytocin		social behavior	social processing	0.1	0.03
9	no	Acetylcholine (Muscarinic)		learning and memory	learning	0.01	0.33
					memory	-0.07	0.69
10	yes	Acetylcholine (Nicotinic)		working memory	working memory	0.05	0.02
11	yes	Acetylcholine (Nicotinic)		attention	attention	0.06	0.02
12	yes	Glutamate (Ionotropic)		learning and memory	learning	0.11	0.006
13	yes	Glutamate (Ionotropic)			memory	0.15	0.0005
14	yes	Neuropeptide Y		feeding	feeding	0.11	0.005
15	yes	Neuropeptide Y		Anxiety/Fear	anxiety	0.11	0.02
					fear	0.01	0.46
16	no	GABA		Anxiety/Fear	anxiety	-0.03	0.95
					fear	-0.03	0.95

Table 1. The Neurosynth-gene atlas was able to identify 12/16 frequently studied neurotransmitter-cognition associations. This non-exhaustive list was derived from PubMed abstracts related to neurotransmitters and cognitive science topics, verified and collated by ASF, LJC & TY. R-values indicate the mean partial correlation between genes in the gene-receptor family (e.g. Dopamine) in relation to the Neurosynth topic (e.g. reward) across the thousands of subcortical voxels. P-values were computed using a permutation analysis (see supplementary methods for details).

results supported 12 of the 16 hypothesized relationships (Table 1), effectively

“re-discovering” these known associations using the Neurosynth-gene atlas.

To assess the specificity of these associations and ensure that these positive results did not reflect broader relationships (e.g., that dopamine was spatially correlated with several cognitive processes because the latter were all themselves highly intercorrelated), we expanded our analysis to include all possible pairs of HGNC neurotransmitter receptor groups (37 in all; Supplementary Figure 3) and

Neurosynth topics. Most of the confirmed associations reported in Table 1 displayed a striking degree of specificity in this latter analysis (Figure 2). For example, while we had expected that dopamine receptor genes would be preferentially expressed in subcortical brain regions associated with reward, we did not necessarily expect the association to be highly selective, and had anticipated that a number of other neurotransmitters would also show strong associations with reward. Yet of 37 distinct neurotransmitter receptor families,

Reward was most strongly associated with the DRD family ($p=0.0004$), and the only other significantly associated neurotransmitter group was serotonin (a neurotransmitter also implicated in reward; $p=0.02$; Fig. 2; all neurotransmitter/topic relationships can be seen in Supplemental Figures 4 and 5). Examination of the spatial intercorrelations between Neurosynth topic maps further demonstrated low correlations between most maps (Supplementary Figure 6)--for example, the spatial intercorrelations between the Reward, Working Memory, and ADHD maps did not exceed 0.16, even though the DRD family was significantly associated with all three topics. Thus, these results validate the use of spatial expression mapping as a bridge between molecular genetics and human cognition by providing strong independent replications of associations that have previously been demonstrated using very different methodological approaches.

A discovery tool for gene-family-cognition associations
The successful replication of previously established association carries with it an important implication: if the present approach can successfully recapture known relationships, it is likely to also have considerable utility in testing other, more speculative, hypotheses, as well as in identifying entirely novel associations. Consistent with this notion, we observed a number of statistically reliable gene-cognition associations that, to our knowledge have not been previously reported, and yet are broadly consistent with existing literature (as seen in Supplementary Figure 5). For example, ‘Pain’ was associated with the Sphingosine gene

family, members of which have been suggested to play a role in pain signaling (29), and 'Social Cognition' was associated with the Trace Amine gene family, members of which have been linked to the processing of socially-relevant smells (30).

Next, we generalized our approach beyond neurotransmitter genes by conducting a comprehensive analysis of 397 gene families labeled in the HGNC. The results confirmed the striking selectivity of many of the neurotransmitter effects reported above. For example, of 397 gene groups, the single strongest spatial similarity to the Neurosynth Reward map was observed for the dopamine receptor family (i.e. DRD; $p < .0001$), and the single strongest similarity to the Emotion map was observed for the ionotropic serotonin receptor family (HTR3; $p < .0001$). Multiple comparison correction revealed other associations previously reported in the literature (Supplementary Figure 7). For example, the Neurosynth Memory map was significantly associated ($p < .001$) with the pattern of expression for genes that code for constituent proteins of the Actin-related protein 2/3 complex (Arp2/3), consistent with recent reports implicating the Arp2/3 complex in memory formation and forgetting (31–34).

Hierarchical clustering of gene/cognition associations

The preceding family-based analyses all assume strong prior knowledge about the grouping structure of individual genes. However, such a top-down approach risks overlooking any structure in the covariance of gene/cognition correlations that does not respect the boundaries of existing gene ontologies. For example, even within the DRD gene group—which displayed strong relationships with reward in the aggregate—there is known heterogeneity: the D4 dopamine receptor is known to show an affinity for other catecholamines besides dopamine (35, 36). A major advantage of a discovery tool like Neurosynth-gene is its potential to complement and inform existing ontologies by deriving novel, data-driven, gene clusters. To this end, we used hierarchical clustering to identify groups of neurotransmitter receptor genes that

exhibited similar profiles of association with Neurosynth topic maps irrespective of their nominal family membership in the HGNC ontology (Figure 3; full clustering results can be seen in Supplementary Figure 8). These analyses revealed that most, but not all, dopamine receptors concentrated together within a single cluster that loaded strongly on the Reward and Learning maps. Interestingly, DRD4 was not included in this cluster; instead, it fell into a cluster of genes that loaded on the Attention and Poly-modal Sensory topics. Moreover, these analyses provide insight into other, less-well understood neurotransmitters. For example, some (P2RY1 and P2RY11), but not all (P2RY12 and P2RY13), of the P2Y purinoceptors were concentrated within a Reward-related cluster, which is both consistent with the proposed role of P2Y in addiction, as well as the known heterogeneity within this system and the molecules bound by these receptors (37).

A discovery tool for individual gene-cognition associations

Finally, we turned to what is arguably the most tantalizing use of our gene-cognition mapping approach: the potential to conduct data-driven Neurosynth-gene atlas searches for associations between individual genes and specific cognitive or affective processes. One way to conduct such an exploration is to inspect the genes most strongly correlated with target cognitive and affective processes. Figure 4 displays the 10 individual genes most strongly associated with selected Neurosynth topics (for additional results, see Supplementary Figure 9). Not surprisingly, many of the gene-level findings recapitulated the family-level results (e.g. DRD3, seen in Supplementary Figures 9 and 10). For example, consistent with the family-level correlations for the DRD gene group, we identified a strong correlation across subcortex between DRD3 expression and Reward ($r = 0.55$). In fact, DRD3 expression was more strongly associated with Reward than all but two other genes (GUCA1A and GPR101). A similarly strong association ($r = .58$) was observed between learning and the A2A adenosine receptor gene, which animal models

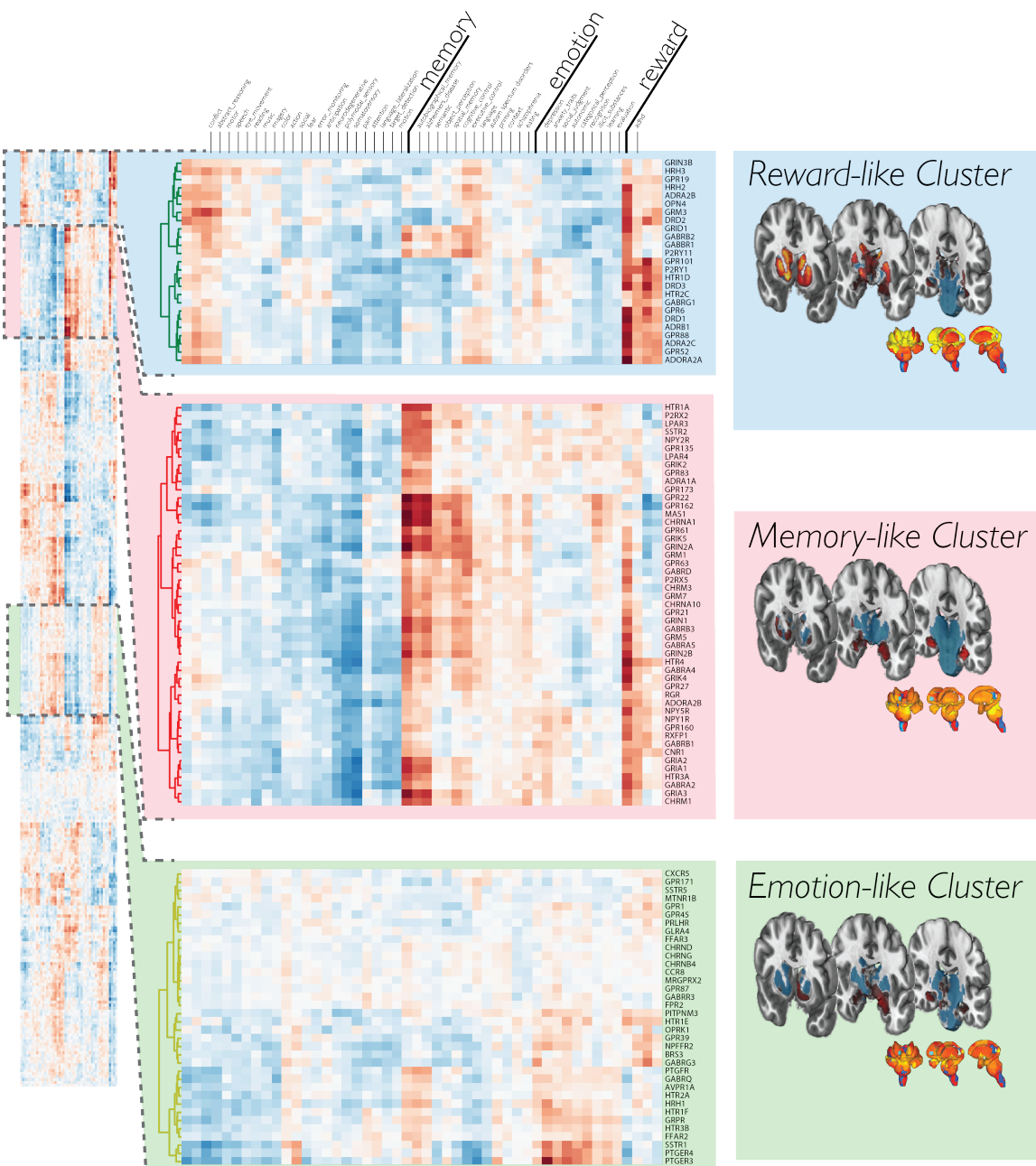


Figure 3. Hierarchical clustering of neurotransmitter receptor genes based on spatial similarity to Neurosynth topics, revealed clusters that span neurotransmitter groups. Clustergram for all 315 genes (left), with an expanded view displaying three example clusters (middle) that load highly on reward, memory, and emotion, respectively. Subcortical renderings of gene expression levels, averaged over all genes within each cluster can be seen on the right. The full clustergram can be seen in Supplementary Figure 8.

have implicated in multiple forms of learning and habit formation (Supplementary Figure 10) (38–40).

Importantly, in addition to these examples, we observed numerous other gene-level associations that were not subsumed by the family-level analysis yet converged with

prior theoretical and empirical work (for this and other example relationships depicted in scatter plots see: Supplementary Figure 10). Notable associations include Fear and SSTR1 (Somatostatin Receptor Type 1), which has been implicated in the genetics of panic disorder, used to treat patients with panic, and

implicated in animal models of fear (41–43); pain and LGALS1, a Galectin-1-coding gene implicated in the development of acute and chronic inflammation in knockout models (44–46); and motor control and several genes located within the spinal muscular atrophy gene region at 5q13.1—including SMN1 (Survival of Motor Neuron 1), the putative locus of causal effect (47–49).

Interestingly, we also identified a large number of gene-cognition relationships which are not obviously supported by the extant literature. These novel relationships are particularly exciting because they provide an impetus to investigate novel associations between psychological constructs and their molecular bases that might otherwise go unstudied. For example, if future research demonstrates a causal role for the aforementioned claspin-memory association (Figure 1), this would provide an unpredicted link between claspin-dependent processes and the formation of new memories. One might speculate, for instance, that the known role of claspin in the maintenance of genome integrity (50, 51) plays a critical role in the high-fidelity genome duplication that is required for memory-related hippocampal neurogenesis (52, 53).

Discussion

Understanding the molecular basis of human cognitive processes promises to illuminate the biology that embodies our thoughts and emotions. In this regard, identifying the genes that alter expression of the proteins that comprise cells and synapses—giving rise to the patterns of brain activation that underlie complex cognitive phenomena—is critical. Here we demonstrated that patterns of spatial covariation between gene expression and meta-analytic functional brain activity can provide a unique and powerful window into the relationships between genes and cognition. Our findings independently replicate numerous prior gene-cognition associations, and provide a novel discovery tool for identifying molecules that may participate in specific psychological or cognitive processes. This approach complements other discovery-based methods

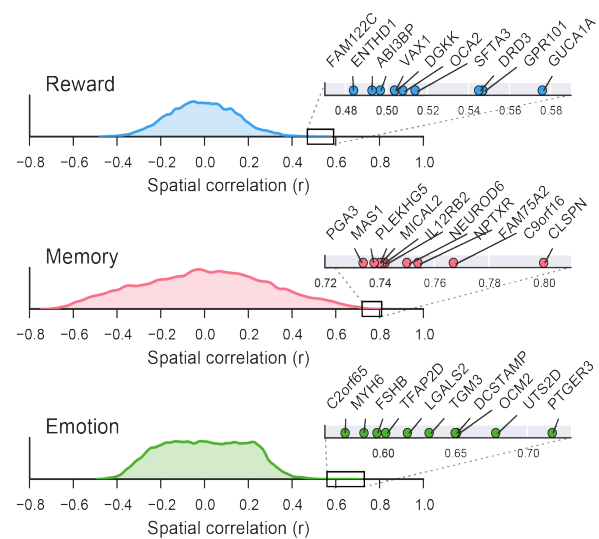


Figure 4. Novel gene-cognition association discovery. Kernel density estimation plots displaying the distribution of spatial correlations with all genes for three sample Neurosynth topics, Reward, Memory and Emotion. Right: zoomed-in view of the top 10 individual gene correlations for each topic.

such as GWAS, and aims to accelerate future mechanistic research by generating novel hypotheses.

Our contention is not, of course, that all—or even most—such associations are likely to accurately reflect a role of specific gene products in human cognition—but rather, that an as-yet undetermined subset of them undoubtedly do. Moreover, as more data become available, the present findings will improve in tandem. While the Allen Human Brain Atlas is a remarkable resource, it is important to remember that it presently contains relatively sparsely sampled data from only six human brains (particularly in cortex as seen in Fig S2c). As the density and quality of the AHBA dataset increases, we anticipate that the sensitivity and specificity of the gene-cognition mappings reported here will also improve—potentially dramatically. Moreover, datasets documenting gene expression changes as a function of age, individual variation, and/or context will only increase the potential for the Neurosynth-Gene approach. In the meantime, to facilitate further development and application of our methods, we have made all of the software, data, and results used to produce these findings publicly available on the web

(<http://github.com/neurosynth/neurosynth-genes>). We also provide interactive, downloadable, whole-brain gene expression and functional activation maps via our Neurosynth web interface (<http://neurosynth.org>; Supplementary Figure 11). Our hope is that geneticists and cognitive neuroscientists will use these new resources for both theory-driven hypothesis testing and bottom-up discovery of a wide range of gene-cognition associations.

Acknowledgements

We would like to thank L. Ruzic, Y Ashar, W. Moore, N.J. Vack, P. Roseboom, J. Oler, and D. Margulies for their helpful consideration of this approach. This work was funded by NIH R01MH096906.

References

1. I. I. Gottesman, T. D. Gould, The endophenotype concept in psychiatry: etymology and strategic intentions, *Am J Psychiatry* **160**, 636–645 (2003).
2. A. Meyer-Lindenberg, D. R. Weinberger, Intermediate phenotypes and genetic mechanisms of psychiatric disorders, *Nat. Rev. Neurosci.* **7**, 818–827 (2006).
3. D. H. Geschwind, G. Konopka, Neuroscience in the era of functional genomics and systems biology, *Nature* **461**, 908–915 (2009).
4. J. P. O'Doherty, Reward representations and reward-related learning in the human brain: insights from neuroimaging, *Curr. Opin. Neurobiol.* **14**, 769–776 (2004).
5. M. Corbetta, G. L. Shulman, Control of goal-directed and stimulus-driven attention in the brain, *Nat. Rev. Neurosci.* **3**, 201–215 (2002).
6. R. Cabeza, P. St Jacques, Functional neuroimaging of autobiographical memory, *Trends in Cognitive Sciences* **11**, 219–227 (2007).
7. P. Khaitovich *et al.*, Regional patterns of gene expression in human and chimpanzee brains, *Genome Res.* **14**, 1462–1473 (2004).
8. M. Hawrylycz *et al.*, Multi-scale correlation structure of gene expression in the brain, *Neural Netw.* **24**, 933–942 (2011).
9. M. E. Phelps, Positron emission tomography provides molecular imaging of biological processes, *Proc. Natl. Acad. Sci. U.S.A.* **97**, 9226–9233 (2000).
10. T. C. Rainbow, W. V. Bleisch, A. Biegton, B. S. McEwen, Quantitative densitometry of neurotransmitter receptors, *J. Neurosci. Methods* **5**, 127–138 (1982).
11. N. D. Volkow *et al.*, PET evaluation of the dopamine system of the human brain, *J. Nucl. Med.* **37**, 1242–1256 (1996).
12. G. Mengod *et al.*, Visualization of dopamine D1, D2 and D3 receptor mRNAs in human and rat brain, *Neurochem. Int.* **20 Suppl**, 33S–43S (1992).
13. B. H. Schott *et al.*, Mesolimbic functional magnetic resonance imaging activations during reward anticipation correlate with reward-related ventral striatal dopamine release, *J. Neurosci.* **28**, 14311–14319 (2008).
14. K. D'Ardenne, S. M. McClure, L. E. Nystrom, J. D. Cohen, BOLD responses reflecting dopaminergic signals in the human ventral tegmental area, *Science* **319**, 1264–1267 (2008).
15. S. Pappata *et al.*, In vivo detection of striatal dopamine release during reward: a PET study with [(11)C]raclopride and a single dynamic scan approach, *Neuroimage* **16**, 1015–1027 (2002).
16. T. Yarkoni, R. A. Poldrack, T. E. Nichols, D. C. Van Essen, T. D. Wager, Large-scale automated synthesis of human functional neuroimaging data, *Nat. Methods* **8**, 665–670 (2011).

17. M. J. Hawrylycz *et al.*, An anatomically comprehensive atlas of the adult human brain transcriptome, *Nature* **489**, 391–399 (2012).
18. L. J. Chang, T. Yarkoni, M. W. Khaw, A. G. Sanfey, Decoding the role of the insula in human cognition: functional parcellation and large-scale reverse inference, *Cereb. Cortex* **23**, 739–749 (2013).
19. R. A. Poldrack *et al.*, Discovering relations between mind, brain, and mental disorders using topic mapping, *PLoS Comput. Biol.* **8**, e1002707 (2012).
20. T. D. Wager, M. A. Lindquist, T. E. Nichols, H. Kober, J. X. Van Snellenberg, Evaluating the consistency and specificity of neuroimaging data using meta-analysis, *Neuroimage* **45**, S210–221 (2009).
21. R. A. Poldrack, Can cognitive processes be inferred from neuroimaging data?, *Trends Cogn. Sci. (Regul. Ed.)* **10**, 59–63 (2006).
22. J. R. Andrews-Hanna, R. Saxe, T. Yarkoni, Contributions of episodic retrieval and mentalizing to autobiographical thought: evidence from functional neuroimaging, resting-state connectivity, and fMRI meta-analyses, *Neuroimage* **91**, 324–335 (2014).
23. S. Ball, T. L. Gilbert, C. C. Overly, The human brain online: an open resource for advancing brain research, *PLoS Biol.* **10**, e1001453 (2012).
24. E. H. Shen, C. C. Overly, A. R. Jones, The Allen Human Brain Atlas: comprehensive gene expression mapping of the human brain, *Trends Neurosci.* **35**, 711–714 (2012).
25. R. A. Wise, P. P. Rompre, Brain dopamine and reward, *Annu Rev Psychol* **40**, 191–225 (1989).
26. I. Kirsch *et al.*, Initial severity and antidepressant benefits: a meta-analysis of data submitted to the Food and Drug Administration, *PLoS Med.* **5**, e45 (2008).
27. J. C. Fournier *et al.*, Antidepressant drug effects and depression severity: a patient-level meta-analysis, *JAMA* **303**, 47–53 (2010).
28. G. Gryglewski, R. Lanzenberger, G. S. Kranz, P. Cumming, Meta-analysis of molecular imaging of serotonin transporters in major depression, *J. Cereb. Blood Flow Metab.* **34**, 1096–1103 (2014).
29. D. Salvemini, T. Doyle, M. Kress, G. Nicol, Therapeutic targeting of the ceramide-to-sphingosine 1-phosphate pathway in pain, *Trends Pharmacol. Sci.* **34**, 110–118 (2013).
30. S. D. Liberles, L. B. Buck, A second class of chemosensory receptors in the olfactory epithelium, *Nature* **442**, 645–650 (2006).
31. N. Hadziselimovic *et al.*, Forgetting is regulated via Musashi-mediated translational control of the Arp2/3 complex, *Cell* **156**, 1153–1166 (2014).
32. I. H. Kim *et al.*, Disruption of Arp2/3 results in asymmetric structural plasticity of dendritic spines and progressive synaptic and behavioral abnormalities, *J. Neurosci.* **33**, 6081–6092 (2013).
33. R. Lamprecht, The actin cytoskeleton in memory formation, *Progress in Neurobiology* **117**, 1–19 (2014).
34. X. Xia *et al.*, Relationship between learning and memory deficits and Arp2 expression in the hippocampus in rats with traumatic brain injury, *World Neurosurg* **78**, 689–696 (2012).
35. H. H. Van Tol *et al.*, Cloning of the gene for a human dopamine D4 receptor with high affinity for the antipsychotic clozapine, *Nature* **350**, 610–614 (1991).
36. A. F. T. Arnsten, B.-M. Li, Neurobiology of executive functions: catecholamine influences on prefrontal cortical functions, *Biol. Psychiatry* **57**, 1377–1384 (2005).

37. G. Burnstock, Purinergic signalling and disorders of the central nervous system, *Nat Rev Drug Discov* **7**, 575–590 (2008).
38. C. J. Wei *et al.*, Selective inactivation of adenosine A(2A) receptors in striatal neurons enhances working memory and reversal learning, *Learn. Mem.* **18**, 459–474 (2011).
39. B. M. Fontinha *et al.*, Adenosine A(2A) receptor modulation of hippocampal CA3-CA1 synapse plasticity during associative learning in behaving mice, *Neuropsychopharmacology* **34**, 1865–1874 (2009).
40. C. Yu, J. Gupta, J.-F. Chen, H. H. Yin, Genetic deletion of A2A adenosine receptors in the striatum selectively impairs habit formation, *J. Neurosci.* **29**, 15100–15103 (2009).
41. J. Gelernter *et al.*, A chromosome 14 risk locus for simple phobia: results from a genomewide linkage scan, *Mol. Psychiatry* **8**, 71–82 (2003).
42. M. Fendt, M. Koch, H. U. Schnitzler, Somatostatin in the pontine reticular formation modulates fear potentiation of the acoustic startle response: an anatomical, electrophysiological, and behavioral study, *J. Neurosci.* **16**, 3097–3103 (1996).
43. J. L. Abelson, R. M. Nesse, A. Vinik, Treatment of panic-like attacks with a long-acting analogue of somatostatin, *J Clin Psychopharmacol* **10**, 128–132 (1990).
44. A. D. Gaudet *et al.*, A role for galectin-1 in the immune response to peripheral nerve injury, *Exp. Neurol.* **220**, 320–327 (2009).
45. F.-T. Liu, G. A. Rabinovich, Galectins: regulators of acute and chronic inflammation, *Ann. N. Y. Acad. Sci.* **1183**, 158–182 (2010).
46. S. C. Starossm *et al.*, Galectin-1 deactivates classically activated microglia and protects from inflammation-induced neurodegeneration, *Immunity* **37**, 249–263 (2012).
47. S. Lefebvre, L. Bürglen, J. Frézal, A. Munnich, J. Melki, The role of the SMN gene in proximal spinal muscular atrophy, *Hum. Mol. Genet.* **7**, 1531–1536 (1998).
48. C. L. Lorson, E. Hahnen, E. J. Androphy, B. Wirth, A single nucleotide in the SMN gene regulates splicing and is responsible for spinal muscular atrophy, *Proc. Natl. Acad. Sci. U.S.A.* **96**, 6307–6311 (1999).
49. M. Feldkötter, V. Schwarzer, R. Wirth, T. F. Wienker, B. Wirth, Quantitative analyses of SMN1 and SMN2 based on real-time lightCycler PCR: fast and highly reliable carrier testing and prediction of severity of spinal muscular atrophy, *Am. J. Hum. Genet.* **70**, 358–368 (2002).
50. P. J. McKinnon, Maintaining genome stability in the nervous system, *Nat. Neurosci.* **16**, 1523–1529 (2013).
51. C. C. S. Chini, J. Chen, Human claspin is required for replication checkpoint control, *J. Biol. Chem.* **278**, 30057–30062 (2003).
52. W. Deng, J. B. Aimone, F. H. Gage, New neurons and new memories: how does adult hippocampal neurogenesis affect learning and memory?, *Nat. Rev. Neurosci.* **11**, 339–350 (2010).
53. F. Doetsch, R. Hen, Young and excitable: the function of new neurons in the adult mammalian brain, *Curr. Opin. Neurobiol.* **15**, 121–128 (2005).

Central amygdala nucleus (Ce) gene expression linked to increased trait-like Ce metabolism and anxious temperament in young primates

Andrew S. Fox^{a,b,c,1}, Jonathan A. Oler^{b,d}, Steven E. Shelton^{b,d}, Steven A. Nanda^d, Richard J. Davidson^{a,b,c,d}, Patrick H. Roseboom^d, and Ned H. Kalin^{a,b,c,d,1}

Departments of ^aPsychology and ^dPsychiatry and ^bHealthEmotions Research Institute, University of Wisconsin, Madison, WI 53719; and ^cWaisman Laboratory for Brain Imaging and Behavior, University of Wisconsin, Madison, WI 53705

Edited by Marcus E. Raichle, Washington University in St. Louis, St. Louis, MO, and approved September 11, 2012 (received for review April 23, 2012)

Children with anxious temperament (AT) are particularly sensitive to new social experiences and have increased risk for developing anxiety and depression. The young rhesus monkey is optimal for studying the origin of human AT because it shares with humans the genetic, neural, and phenotypic underpinnings of complex social and emotional functioning. In vivo imaging in young monkeys demonstrated that central nucleus of the amygdala (Ce) metabolism is relatively stable across development and predicts AT. Transcriptome-wide gene expression, which reflects combined genetic and environmental influences, was assessed within the Ce. Results support a maladaptive neurodevelopmental hypothesis linking decreased amygdala neuroplasticity to early-life dispositional anxiety. For example, high AT individuals had decreased mRNA expression of neurotrophic tyrosine kinase, receptor, type 3 (*NTRK3*). Moreover, variation in Ce *NTRK3* expression was inversely correlated with Ce metabolism and other AT-substrates. These data suggest that altered amygdala neuroplasticity may play a role in the early dispositional risk to develop anxiety and depression.

positron-emission tomography | microarray | brain imaging

The ability to identify brain mechanisms underlying the risk during childhood for developing anxiety and depression is critical for establishing novel early-life interventions aimed at preventing the chronic and debilitating outcomes associated with these common illnesses. To this end, we have optimized a model of anxious temperament (AT), the conserved at-risk phenotype, in young developing rhesus monkeys (1–4). The rhesus monkey is ideal for studying the origin of human AT because these species share the genetic, neural, and phenotypic underpinnings of complex social and emotional functioning (5–10). Importantly, the rhesus developmental model bridges the critical gap between human psychopathology and rodent models, allowing for translation to humans by using *in vivo* imaging measures and translation to rodents by using *ex vivo* molecular methods. Thus, the unique hypotheses that can be generated from the rhesus model are invaluable in guiding both imaging studies in children and mechanistic efforts in rodents.

Of particular relevance to the AT rhesus model is the relatively recent evolutionary divergence between rhesus monkeys and humans (25 million years) compared with rodents and humans (70 million years) (5). This evolutionary closeness is reflected in the species' similarities in social and emotional behaviors. These homologies, instantiated in their conserved genetic and neural systems, underlie the ability of both humans and rhesus monkeys to form and maintain the relationships necessary for living in complex social environments. In this regard, the experience of anxiety has evolved in primates to motivate the formation of long-lasting attachment bonds that serve to increase security and group cohesion. The comparable rearing practices shared by these species (e.g., close mother–infant bonding) promote early social/emotional learning, which serves to adaptively regulate anxiety and promote survival (7).

Although periods of marked anxiety and fear are common during early childhood, most children overcome these anxieties through learning associated with experience and maturation. As they develop, typical children learn to discern real threats from distorted fears and, in concert, effectively regulate their behavior to adaptively cope. However, a subset of children with extreme AT do not develop this capacity, maintaining a stable anxious disposition that confers increased risk for the development of anxiety and mood disorders (11–13). AT begins as early shyness and is later characterized by chronic anxiety, negative affect, and worry (14). AT is also associated with increased activity of stress-sensitive peripheral systems, including increased pituitary–adrenal tone and heightened sympathetic activity (11).

Because early social-emotional learning is critical for the adaptive regulation of anxiety, we have been especially interested in processes demonstrated to underlie learning during development. Furthermore, recent preclinical and clinical research has identified neurotrophic factors (15) and other neuroplastic processes as critical for overcoming adult psychopathology (16–18). Therefore, we hypothesized that altered neurotrophic processes in the young brain would lead to the emergence and maintenance of childhood AT. In particular, we theorize that deficits in the ability to modify the connections and composition of AT's neural substrate could result in a failure to learn how to adaptively regulate anxiety, which can manifest as a tendency to generalize perceptions of threat to neutral stimuli. Because AT can be identified early in life, characterizing the biological factors that promote the maintenance of stable AT can potentially lead to targeted early-life interventions aimed at decreasing the risk for developing psychopathology.

Similar to anxious children, young monkeys with high levels of AT are those that show increased freezing, decreased vocalizations, and increased cortisol when exposed to the no-eye contact condition (NEC) of the human-intruder paradigm, an ethologically relevant mild social threat. Our studies demonstrated that, like human AT, monkey AT is trait-like and heritable (19). Using functional brain imaging in conjunction with *ex vivo* molecular analyses of relevant brain regions, the monkey model allows for the longitudinal study of AT and its underlying neural substrates. With functional brain imaging, we identified the central nucleus of the amygdala (Ce) and anterior hippocampus as components of the neural circuit underlying AT (2, 19).

Author contributions: S.E.S., R.J.D., P.H.R., and N.H.K. designed research; A.S.F., S.E.S., S.A.N., P.H.R., and N.H.K. performed research; A.S.F. contributed new reagents/analytic tools; A.S.F., J.A.O., P.H.R., and N.H.K. analyzed data; and A.S.F., J.A.O., and N.H.K. wrote the paper.

The authors declare no conflict of interest.

This article is a PNAS Direct Submission.

¹To whom correspondence may be addressed. E-mail: asfox@wisc.edu or nkalin@wisc.edu.

This article contains supporting information online at www.pnas.org/lookup/suppl/doi:10.1073/pnas.1206723109/-DCSupplemental.

over, we found that young primates with high AT have increased metabolism in these regions when studied in both stressful and nonstressful contexts (2). These data set the stage for in-depth molecular studies in primates focused on understanding the mechanisms mediating the function of the brain regions underlying AT.

The Ce is of interest because its efferent projections coordinate autonomic, hormonal, behavioral, and emotional responses to stress (20), and Ce lesions in monkeys are sufficient to reduce AT (21). Furthermore, rodent studies demonstrate that direct Ce manipulations markedly alter unconditioned anxiety responses (22), similar to those elicited by novel or potentially threatening situations in children with high AT. The prefrontal cortex and other amygdala nuclei primarily influence fear and anxiety-related responding via the Ce, where intra-Ce microcircuits play a critical role dynamically gating these inputs (23–26). Recent work in rhesus monkeys demonstrates that, unlike most amygdala nuclei, the Ce continues to mature from the first year of life into early adulthood (27). This protracted developmental period suggests that Ce maturation may be particularly susceptible to environmental influences. A causal relation between social group size and dorsal amygdala volume demonstrates the importance of social influences on the primate amygdala (28). These findings are consistent with our data highlighting the importance of environmental contributions to Ce metabolism as it relates to early-life AT (19). For these reasons, we selected the Ce for in depth molecular analyses, with a particular focus on processes within the Ce that underlie learning. Although learning-related research has generally focused on the hippocampus (e.g., refs. 29 and 30) and basal/lateral amygdala regions (31), recent rodent studies highlight the role of plasticity and emotional learning in the Ce (32, 33). In addition to its role in anxiety, the Ce has recently been linked to habit formation (34) and, at a cellular and neurochemical level, it has much in common with the striatum (35), a structure known to mediate the development of long-term ingrained response patterns (36). Although Ce microcircuits are ideally suited to perform the childhood learning that results in adaptive anxiety, when Ce learning is disrupted, it could result in trait-like habitual fear and anxiety responding.

Building on our finding that individual differences in Ce metabolism predict AT, we performed mRNA expression studies in Ce tissue collected from young monkeys repeatedly phenotyped for AT and its associated brain metabolism. This unique, multilevel approach combines the power of functional brain imaging with the potential of gene expression studies to characterize the mRNAs that could underlie the risk for developing anxiety and depression. We hypothesized that high-AT individuals would have alterations in mRNAs within the Ce that reflect the influences of experience on the persistent expression of anxiety. Specifically, we predicted a role for mRNAs encoding molecules with the potential to facilitate habitual anxiety and developmentally appropriate adaptive fear learning. Such alterations are of particular interest, because manipulations of these substrates could result in treatments for high-AT children that would facilitate their ability to modify and adaptively regulate their anxiety.

Accordingly, a subset of 24 animals was selected from 238 rhesus monkeys that were initially characterized for behavior and brain metabolism. The 238 monkeys were injected with [¹⁸F]-fluoro-2-deoxyglucose (FDG) and exposed for 30 min to the NEC condition that elicits the AT phenotype (19). During NEC, a human (“the intruder”) enters the test room and presents her profile to the monkey, avoiding eye contact (1). Following NEC exposure, animals were anesthetized, and high-resolution positron-emission tomography (PET) scans were performed to examine the integrated brain metabolism that occurred during the preceding 30-min NEC exposure. FDG-PET is optimal for simultaneously assessing sustained neural activity and natural behavior in unconstrained individuals because FDG is taken up

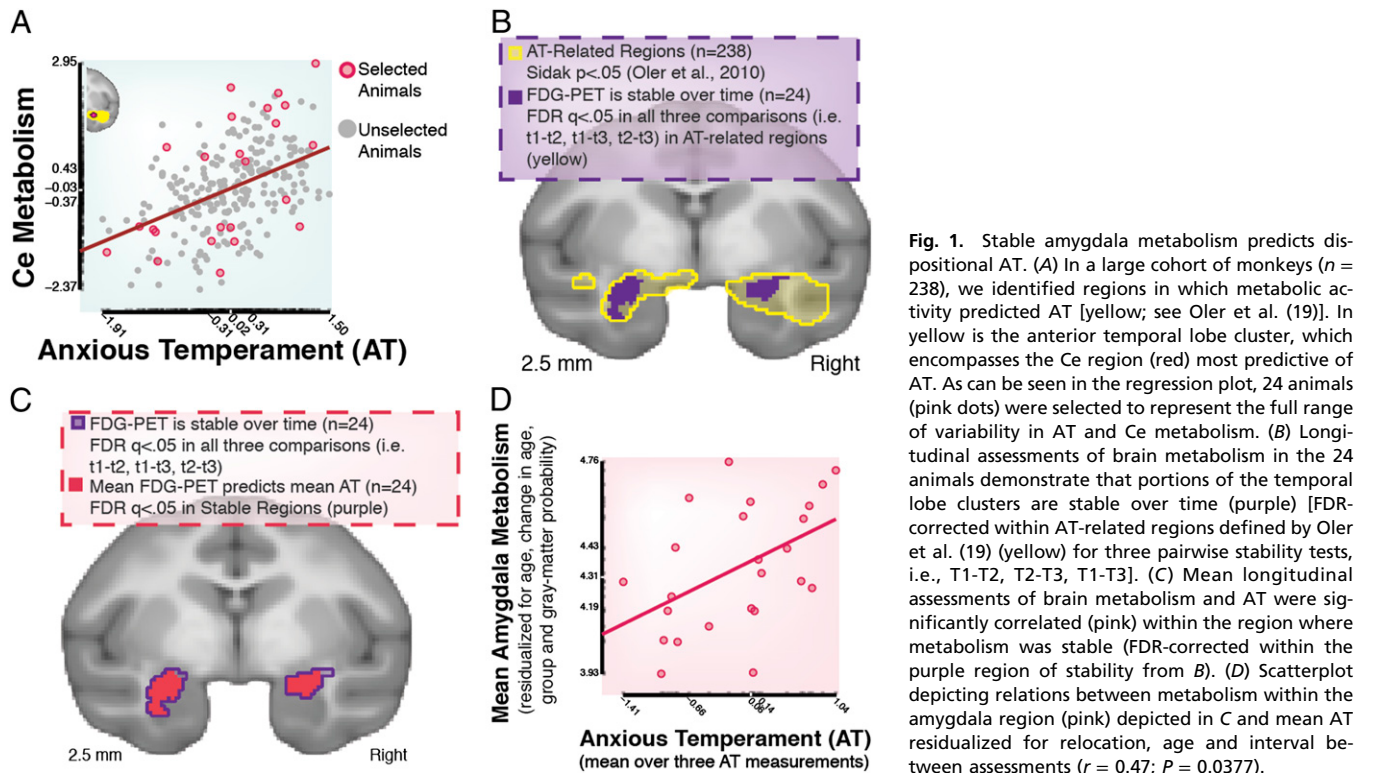
into metabolically active cells over the course of ~30 min and remains trapped for the duration of its ~110-min half-life. This extended assessment of brain metabolism is ideal for studying the neural underpinnings of AT, which are sustained over time.

Results and Discussion

The subset of 24 males underwent further testing to characterize the trait-like components of AT and its neural substrate across development [Fig. 1A; animals noted in pink constituted the subset that was further tested; age at first assessment: mean, 2.1 (range, 0.85–3.5 y); age at last assessment: mean, 3.2 (range, 1.8–4.2)]. The age span of this sample is similar to childhood through early adolescence in humans because 1-y-old monkeys are similar to 3- to 4-y-old children, and male monkeys enter adolescence around 3–4 y of age. The 24 monkeys were phenotyped for brain and behavior on two additional occasions, 6–18 mo after their initial assessment. Between the second and third assessment, half of the animals were relocated every 5 d over a period of 3 wk. Relocation did not have any significant effects on behavior or physiology (*SI Methods*). To examine the stability of AT, we tested the interrelations among the three repeated measurements, controlling for relocation, age, and interval between assessments. Relations among the AT measures were significant [time 1 to time 2: $t = 6.83$, $P < 0.0001$; time 1 to time 3: $t = 3.80$, $P = 0.001$; time 2 to time 3: $t = 5.16$, $P < 0.0001$; accounting for between 44% and 72% of the variance in AT across time points and corresponding to an interclass correlation coefficient ($ICC_{3,1} = 0.72$], confirming AT's relative stability over this developmental period.

We hypothesized that the stability of AT would be reflected by similar consistency in the function of its neural substrates. Therefore, we intercorrelated the three measures of NEC-induced brain metabolism in the regions predictive of AT, controlling for relocation, age, and interval between assessments. AT-predictive regions were defined from our previous study and included bilateral anterior temporal lobe clusters, bilateral occipital lobe clusters, and a midline parietal lobe cluster (19). Results demonstrated relative stability as denoted by significant interrelations among the three NEC-induced metabolism measurements within each of these clusters [corrected for multiple comparisons using false discovery rate (FDR); $q < 0.05$ FDR across maps in AT-related regions, with voxel-wise $ICC_{3,1}$ coefficients ranging from 0.30 to 0.70 (median, 0.57); Fig. 1B and *Table S1*]. Voxels within every cluster we tested, including dorsal and ventral regions of amygdala, anterior portions of hippocampus, superior temporal sulcus (STS), agranular insula, temporal and insular proisocortices, claustrum, visual cortex, and precuneus, demonstrated significantly stable NEC-induced metabolism. These data demonstrate that individual differences in metabolism within the neural circuit underlying AT are relatively stable across juvenile development.

We next examined covariation between the stable components of AT and its neural substrates. For each animal, the stable components of AT and regional brain metabolism were estimated by computing their means across each of the three longitudinal assessments. Mean AT was regressed against mean voxel-wise metabolism in significantly stable AT-related regions, while controlling for relocation, age, the interval between scans, and voxel-wise gray matter probability (GMP). Results demonstrated that mean metabolism in amygdalar regions (including Ce and the basolateral complex), anterior hippocampus, and visual cortex predicted mean AT ($q < 0.05$ FDR in stable AT-related regions; Fig. 1C and D and *Table S2*). To confirm involvement of the Ce within the larger amygdalar cluster we assessed the overlap between this cluster and a map of *in vivo* serotonin transporter binding derived from separate animals (37). Precise localization of the Ce can be determined with this method because this amygdalar nucleus has the highest density of serotonin transporter binding compared with neighboring structures (38) (*SI Methods*). Results confirmed that mean



metabolism in the Ce region predicted mean AT across assessments. This longitudinal assessment of brain and behavior extends prior work characterizing the neural substrates of AT by demonstrating that the trait-like nature of AT is reflected in trait-like metabolism within the Ce and other AT-related brain regions.

To characterize the molecular underpinnings of AT and its neural substrate, animals were killed and brain tissue was collected for assessment of gene expression. Because of our interest in the trait-like nature of AT and its context-independent brain metabolism, we collected brain tissue from animals in their baseline state, 4–5 d following final NEC exposure. In contrast to studies of stimulus-evoked gene expression, this approach allows for optimal characterization of temperament-related transcripts. mRNA was extracted from the Ce region most predictive of AT ($n = 238$; Figs. 1A and 2). mRNA expression levels were assessed using the Affymetrix Rhesus Monkey microarray (SI Methods). Brain samples collected were counterbalanced for hemisphere because bilateral Ce metabolism was associated with AT. To quantify the association between dispositional AT and Ce mRNA levels, mean AT was correlated with mRNA expression levels. Microarray data were analyzed using bioconductor (39) for microarray analysis in R (see SI Methods for details). Microarray data were preprocessed using robust multichip average (RMA) background correction, constant normalized across chips, and summarized across probes using the median-polish technique (40). Resulting gene expression levels were visually inspected using MA plots (Fig. S1). Gene expression was also assessed using Plier background correction and quantile normalization to verify that gene distribution patterns did not arise from specific preprocessing techniques (i.e., Plier and quantile normalization). Robust regression analyses between mean AT- and RMA-determined mRNA levels (controlling for relocation, biopsy hemisphere, and age) were performed on annotated transcripts (<http://www.unmc.edu/rhesusgenechip/>) that had at least moderate expression levels [$>\log_2(100)$]. Covarying for age ensures that significant AT-related transcripts, although assessed during

development, are not reflective of age-related changes. The empirical Bayes method was used to determine levels of significance and the FDR was used to account for multiple comparisons.

Results revealed 139 RMA-determined transcripts that predicted AT (FDR $q < 0.05$, two-tailed; Table S3; to demonstrate these correlations are not attributable to the normalization technique, Table S3 also includes the correlations between AT and Plier background corrected and quantile normalized transcripts). Consistent with the concept that multiple systems underlie stress-related psychopathology, both manual inspection and gene-oncology enrichment analyses revealed that the 139 FDR-corrected AT-related transcripts reflect diverse biological systems (SI Methods and Table S4). Within the Biological Processes ontology, 35 significantly overrepresented terms were identified. Three of these terms are of particular interest in relation to our maladaptive neurodevelopmental hypothesis of AT. These include response to hormone stimulus (GO:0009725) and related terms, positive regulation of axon extension (GO:0045773), and positive regulation of developmental growth (GO:0048639). Of note, the neurotrophic tyrosine kinase, receptor, type 3 (NTRK3) and the leucine-rich repeat protein ISLR2 (Ig superfamily containing leucine-rich repeat 2; also known as Linx) are the only constituents from the FDR corrected list of 139 genes that are represented across all 3 terms. Because multiple comparison correction of AT-related transcripts likely results in false negatives and the possibility that the exclusion of these genes can alter ontology term representation, we also performed gene-oncology enrichment analyses on significantly ($P < 0.05$) uncorrected AT-related genes. Although not identical, the results support the inferences of the FDR-corrected ontology analyses (Table S5). Significantly overrepresented terms included regulation of axon regeneration (GO:0048679) and cell morphogenesis (GO:000902), both of which included NTRK3. Although future research would benefit from exploring other significantly AT-related genes and overrepresented ontology terms, because of our theoretical interest in the mechanisms of Ce-learning during

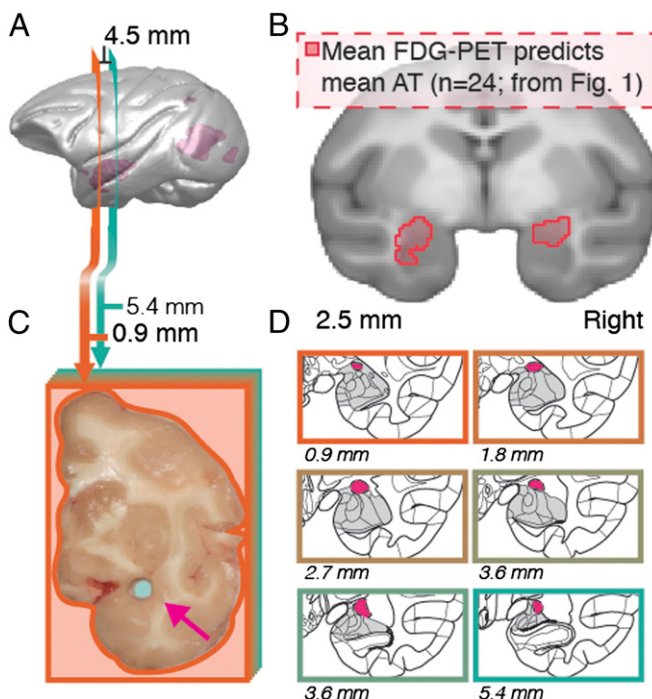


Fig. 2. Stable Ce regions predictive of dispositional AT were used to guide amygdala biopsy. (A–C) Brains from the 24 animals were sectioned into 4.5-mm coronal slabs centered on the functionally defined amygdala region (~0.9 mm [orange] to ~5.4 mm [cyan], posterior to anterior commissure), shown as a 3D rendering (A), a 2D slice through the functionally defined amygdala region (B), and a representative single-subject slab with amygdala biopsy site (magenta arrow) (C). (D) The biopsied region corresponds to the location of Ce (pink), as shown in the series of atlas slices [adapted with permission (69)]. Slices are arranged from anterior (orange) to posterior (cyan).

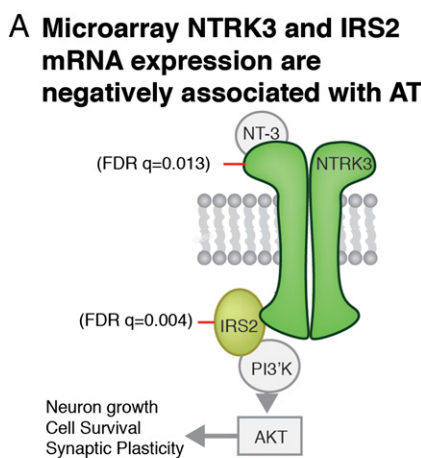
development, we focused our analyses on NTRK3 and related transcripts. Quantitative real-time PCR (qRT-PCR) was performed on select transcripts including NTRK3, IRS2, and ISLR2 (P values, <0.05) to confirm the relations between gene expression and AT.

NTRK3 and insulin receptor substrate 2 (IRS2) are of particular interest because their activation by the endogenous growth

factor neurotrophin-3 (NTF-3) can initiate synaptogenesis and neurogenesis (41, 42) (Fig. 3). The *NTRK3* gene encodes a membrane-bound receptor that phosphorylates intracellular transducers, including IRS2 (43). The downstream influences of IRS2 can manifest via activation of the phosphoinositide 3-kinase/protein kinase B (PI3K/AKT) pathway (44). AKT signaling affects synaptic plasticity, axonal development, amygdala-dependent learning, and behavioral responses to stress (45, 46). Additionally, ISLR2 sits on the cell membrane, aids in the guiding of axons, and can facilitate the activation of trk receptors, including NTRK3 (47, 48). In addition to its involvement in our theoretically motivated focus on neuroplasticity, *NTRK3* genetic variation has been linked to human psychopathology, including childhood-onset mood disorders (49–52), and via its extracellular domain may provide an accessible drug target. Taken together, these findings implicate NTRK3 as a prominent target for future mechanistic studies examining childhood AT.

Using the prospectively acquired trait-like measures of brain metabolism, we investigated the neural systems by which altered Ce NTRK3 expression influences AT. A voxel-wise search, controlling for age, hemisphere of biopsy, relocation, and GMP, was performed to identify AT-related brain regions in which Ce *NTRK3* mRNA levels predicted mean metabolic activity. Results demonstrated significant negative relationships between Ce *NTRK3* expression and glucose metabolism within the right amygdala (including the Ce region) and anterior hippocampus, as well as significant positive relations within visual cortex (Fig. 4; FDR $q < 0.05$ in stable AT-predictive regions; Table S6). Although the left Ce region did not survive multiple comparison correction, the relationship between NTRK3 expression and left Ce metabolism was significant at an uncorrected $P = 0.02$, which was not significantly weaker than the relationship between NTRK3 expression and right Ce metabolism ($t = 0.86$; $P = 0.40$) (53). These primate data combine the use of brain imaging and microarray technology in the same animals and suggest that Ce *NTRK3* is a key molecular mediator of AT via its influences on the neural circuit underlying AT.

To examine the unique relation between Ce NTRK3 expression and AT, we assessed motor cortex NTRK3 mRNA. Results demonstrated that motor cortex *NTRK3* mRNA levels were unrelated to Ce *NTRK3* mRNA levels ($t = 0.09$; $P = 0.928$). Moreover, motor cortex *NTRK3* mRNA levels were not related to AT ($t = 0.24$; $P = 0.812$) nor metabolism in AT-related regions (no



B rt-qPCR NTRK3 mRNA expression predict AT

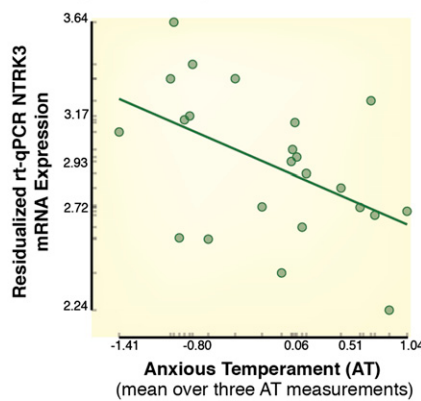


Fig. 3. Ce expression of the neurotrophic receptor NTRK3 predicts AT. (A) Schematic of the pathway for *NTRK3*, a neuroplasticity-associated molecule (green). Microarray data showed that individuals with higher levels of Ce *NTRK3* mRNA expression exhibited lower AT. A similar pattern was found for a downstream target of *NTRK3*, IRS2 (yellow). Other molecules in the *NTRK3* pathway are depicted in gray. (B) qRT-PCR confirmed the negative relationship between Ce *NTRK3* mRNA expression levels and AT, controlling for relocation, biopsy hemisphere, and age ($r = 0.49$; $P = 0.029$).

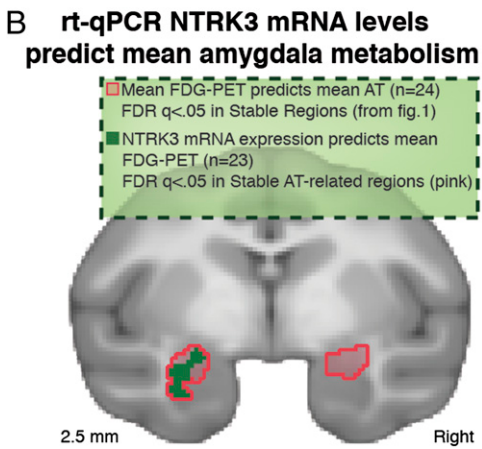
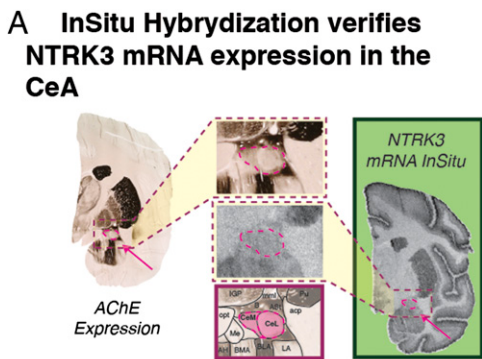


Fig. 4. NTRK3 is expressed in Ce and negatively predicts Ce metabolism. (A) Acetylcholinesterase (AChE) stain (Left) was used to definitively identify Ce in the brain of one subject. In situ hybridization of NTRK3 was performed on an adjacent slice from the same subject (Right). Magnified insets (Center) reveal that the AChE-defined Ce (dashed-pink) expresses NTRK3 mRNA. (B) Individuals showing higher levels of NTRK3 mRNA expression, indexed by qRT-PCR, show reduced Ce metabolism in vivo (green) [FDR-corrected within the stable AT-related region (pink)].

significant results at $FDR\ q < 0.05$). Although motor cortex metabolism was highly predictive of levels of locomotion ($P < 0.05$, Sidak-corrected; *SI Methods* and Table S7), motor cortex NTRK3 mRNA expression was not significantly correlated with either locomotion ($t = -1.31$; $P = 0.190$) or motor cortex metabolism (no significant results at $FDR\ q < 0.05$; *SI Methods*). These findings demonstrate that regional NTRK3 mRNA expression is not a general marker for brain metabolism nor is it a nonspecific reflection of behaviors dependent on the region in which NTRK3 mRNA is assessed (e.g., locomotion for motor cortex). This further underscores the specificity of Ce NTRK3 in relation to AT and highlights the importance of site-specific, differential regulation of the NTRK3 gene.

Our results highlight the role of NTRK3 in AT during development but do not implicate NTRK3 mechanistically. Rather, these findings provide an initial rationale for exploring behavioral or pharmacological interventions aimed at up-regulating regional NTRK3 expression early in the lives of individuals likely to develop anxiety and depressive disorders. Recent studies in rodents demonstrate the feasibility of performing early targeted interventions that have long-term impacts on anxiety and adaptive responses to stress (54–56). For example, neonatal injections of the neuroplasticity-related growth factor fibroblast growth factor 2 (FGF2) altered the developmental trajectory of high-anxious rodents, resulting in decreased adult anxiety (55). Importantly, early-life FGF2 treatment also enhanced adult neurogenesis, which was accompanied by increased hippocampal

expression of NTRK3 (55). Moreover, primate research has demonstrated that neurodevelopmentally relevant gene expression in the amygdala is altered by prolonged maternal separation (57). Taken together, these data are consistent with our demonstration that monkeys with lower levels of AT show greater Ce expression of NTRK3 and further motivate mechanistic research into the role for neurodevelopmentally important transcripts in the development of AT.

Although we focus on NTRK3, it is important to clarify that other genes are also of interest. For example, in addition to its importance in neurotrophic signaling, the involvement of IRS2, which is also critical for insulin signaling, is interesting in its own right. Because of its multiple functions, regulation of IRS2 may be important in the linkages between stress, psychopathology, and the development of associated physiological alterations such as metabolic syndrome and type 2 diabetes. In the periphery, IRS2 regulates insulin sensitivity and in the brain IRS2 impacts multiple functions including reward (58), memory (59, 60), and energy homeostasis (61, 62). Moreover, type 2 diabetes has been associated with amygdala atrophy (63), and bidirectional associations between insulin resistance and affective disorders have been reported (64–66). The possibility that altered IRS2 function may play a role in the associations between insulin-related disorders and alterations in stress-related psychopathology via its effects on the amygdala is intriguing. Of particular interest to stress and AT, alterations in cortisol could be important in modulating IRS2 function because the synthetic glucocorticoid dexamethasone prevents phosphorylation of IRS2 (67, 68).

Recent work demonstrating the ongoing development of the primate Ce suggests this nucleus to be particularly susceptible to environmental influences throughout childhood and adolescence (19, 27). Early in childhood, as young children first extend beyond their parents' reach, they must approach novelty with trepidation. By way of experience and maturation, most children learn to regulate their anxieties and see the world as an opportunity for exploration. This experience-dependent learning results in refined discrimination between threatening and nonthreatening stimuli and likely involves sculpting of intra-Ce connections that dynamically gate the sensory and prefrontal triggers of fear. We hypothesize that decreased capacity for learning and modification within the Ce microcircuit could explain why some children fail to regulate their anxieties and develop an extreme anxious temperament. The findings presented here begin to link specific experience-dependent molecular pathways within the Ce to chronically elevated Ce metabolism and extreme temperamental anxiety. Although there are likely many mediators of AT, these gene expression data are consistent with a maladaptive neurodevelopmental hypothesis as a basis for AT. Future work should aim to extend these data in support of a molecular-neuroscientific rationale for conceptualizing new treatment strategies aimed at normalizing Ce function in vulnerable children before the development of the detrimental behavioral, emotional, and brain sequelae associated with the long-term consequences of chronic anxiety and depression.

Methods

Twenty-four male rhesus monkeys were selected from subjects used by Oler et al. (19) to undergo longitudinal AT and FDG-PET assessments during exposure to potential threat (NEC). Brain tissue was biopsied from the Ce region most predictive of AT, and transcriptome wide RNA expression levels were assessed using Affymetrix GeneChip Rhesus Macaque Genome arrays. All preprocessing and statistical analyses were performed using standard methods. See *SI Methods* for a detailed description of the procedures used.

ACKNOWLEDGMENTS. We thank the staff at the Wisconsin National Primate Center, the Harlow Center for Biological Psychology, the HealthEmotions Research Institute, and The Waisman Laboratory for Brain Imaging and Behavior for facilitating our research. We also thank A. Shackman, A. Alexander, B. Christian, L. Ahlers, A. Converse, T. Oakes, H. Van Valkenberg, K. Myer,

- J. Spears, E. Larson, and D. French for their technical and analytic assistance in running subjects and analyzing data. This work was supported by National Institutes of Health (NIH) Grants MH91550, MH046729, MH081884, MH084051, HD008352, and HD003352; NIH Training Grant MH018931; the Wisconsin National Primate Research Center (through NIH Grants P51OD011106 and P51RR000167); and the HealthEmotions Research Institute.
- Kalin NH, Shelton SE (1989) Defensive behaviors in infant rhesus monkeys: Environmental cues and neurochemical regulation. *Science* 243:1718–1721.
 - Fox AS, Shelton SE, Oakes TR, Davidson RJ, Kalin NH (2008) Trait-like brain activity during adolescence predicts anxious temperament in primates. *PLoS ONE* 3:e2570.
 - Fox AS, et al. (2005) Calling for help is independently modulated by brain systems underlying goal-directed behavior and threat perception. *Proc Natl Acad Sci USA* 102: 4176–4179.
 - Kalin NH, Shelton SE, Fox AS, Oakes TR, Davidson RJ (2005) Brain regions associated with the expression and contextual regulation of anxiety in primates. *Biol Psychiatry* 58:796–804.
 - Gibbs RA, et al.; Rhesus Macaque Genome Sequencing and Analysis Consortium (2007) Evolutionary and biomedical insights from the rhesus macaque genome. *Science* 316:222–234.
 - Kalin NH, Shelton SE (2003) Nonhuman primate models to study anxiety, emotion regulation, and psychopathology. *Ann N Y Acad Sci* 1008:189–200.
 - Harlow HF (1958) The nature of love. *Am Psychol* 13:673–685.
 - Adolphs R (2010) What does the amygdala contribute to social cognition? *Ann N Y Acad Sci* 1191:42–61.
 - Wallis JD (2012) Cross-species studies of orbitofrontal cortex and value-based decision-making. *Nat Neurosci* 15:13–19.
 - Chareyron LJ, Banta Lavenex P, Amaral DG, Lavenex P (2011) Stereological analysis of the rat and monkey amygdala. *J Comp Neurol* 519:3218–3239.
 - Fox NA, Henderson HA, Marshall PJ, Nichols KE, Ghera MM (2005) Behavioral inhibition: Linking biology and behavior within a developmental framework. *Annu Rev Psychol* 56:235–262.
 - Biederman J, et al. (2001) Further evidence of association between behavioral inhibition and social anxiety in children. *Am J Psychiatry* 158:1673–1679.
 - Essex MJ, Klein MH, Slattery MJ, Goldsmith HH, Kalin NH (2010) Early risk factors and developmental pathways to chronic high inhibition and social anxiety disorder in adolescence. *Am J Psychiatry* 167:40–46.
 - Kagan J, Reznick JS, Snidman N (1988) Biological bases of childhood shyness. *Science* 240:167–171.
 - Martinowich K, Manji H, Lu B (2007) New insights into BDNF function in depression and anxiety. *Nat Neurosci* 10:1089–1093.
 - Krystal JH, et al. (2009) Neuroplasticity as a target for the pharmacotherapy of anxiety disorders, mood disorders, and schizophrenia. *Drug Discov Today* 14:690–697.
 - Manji HK, Moore GJ, Rajkowska G, Chen G (2000) Neuroplasticity and cellular resilience in mood disorders. *Mol Psychiatry* 5:578–593.
 - Pittenger C, Duman RS (2008) Stress, depression, and neuroplasticity: A convergence of mechanisms. *Neuropsychopharmacology* 33:88–109.
 - Oler JA, et al. (2010) Amygdalar and hippocampal substrates of anxious temperament differ in their heritability. *Nature* 466:864–868.
 - Davis M, Whalen PJ (2001) The amygdala: Vigilance and emotion. *Mol Psychiatry* 6: 13–34.
 - Kalin NH, Shelton SE, Davidson RJ (2004) The role of the central nucleus of the amygdala in mediating fear and anxiety in the primate. *J Neurosci* 24:5506–5515.
 - Tye KM, et al. (2011) Amygdala circuitry mediating reversible and bidirectional control of anxiety. *Nature* 471:358–362.
 - Ehrlich I, et al. (2009) Amygdala inhibitory circuits and the control of fear memory. *Neuron* 62:757–771.
 - Cicoci S, et al. (2010) Encoding of conditioned fear in central amygdala inhibitory circuits. *Nature* 468:277–282.
 - Haubensak W, et al. (2010) Genetic dissection of an amygdala microcircuit that gates conditioned fear. *Nature* 468:270–276.
 - Pare D, Duvarci S (2012) Amygdala microcircuits mediating fear expression and extinction. *Curr Opin Neurobiol* 22:717–723.
 - Chareyron LJ, Lavenex PB, Amaral DG, Lavenex P (2012) Postnatal development of the amygdala: A stereological study in macaque monkeys. *J Comp Neurol* 520:1965–1984.
 - Sallet J, et al. (2011) Social network size affects neural circuits in macaques. *Science* 334:697–700.
 - Kim JJ, Diamond DM (2002) The stressed hippocampus, synaptic plasticity and lost memories. *Nat Rev Neurosci* 3:453–462.
 - Ming G-L, Song H (2011) Adult neurogenesis in the mammalian brain: Significant answers and significant questions. *Neuron* 70:687–702.
 - Fanselow MS, LeDoux JE (1999) Why we think plasticity underlying Pavlovian fear conditioning occurs in the basolateral amygdala. *Neuron* 23:229–232.
 - Paré D, Quirk GJ, Ledoux JE (2004) New vistas on amygdala networks in conditioned fear. *J Neurophysiol* 92:1–9.
 - Samson RD, Duvarci S, Paré D (2005) Synaptic plasticity in the central nucleus of the amygdala. *Rev Neurosci* 16:287–302.
 - Lingawi NW, Balleine BW (2012) Amygdala central nucleus interacts with dorsolateral striatum to regulate the acquisition of habits. *J Neurosci* 32:1073–1081.
 - Swanson LW, Petrovich GD (1998) What is the amygdala? *Trends Neurosci* 21: 323–331.
 - Packard MG, Knowlton BJ (2002) Learning and memory functions of the Basal Ganglia. *Annu Rev Neurosci* 25:563–593.
 - Christian BT, et al. (2009) Serotonin transporter binding and genotype in the non-human primate brain using [C-11]DASB PET. *Neuroimage* 47:1230–1236.
 - O'Rourke H, Fudge JL (2006) Distribution of serotonin transporter labeled fibers in amygdaloid subregions: Implications for mood disorders. *Biol Psychiatry* 60:479–490.
 - Gentleman RC, et al. (2004) Bioconductor: Open software development for computational biology and bioinformatics. *Genome Biol* 5:R80.
 - Gautier L, Cope L, Bolstad BM, Irizarry RA (2004) affy—analysis of Affymetrix GeneChip data at the probe level. *Bioinformatics* 20:307–315.
 - Lamballe F, Klein R, Barbacid M (1991) trkB, a new member of the trk family of tyrosine protein kinases, is a receptor for neurotrophin-3. *Cell* 66:967–979.
 - Duman CH, Duman RS (2005) Neurobiology and treatment of anxiety: Signal transduction and neural plasticity. *Handb Exp Pharmacol* 169:305–334.
 - Yamada M, et al. (1997) Insulin receptor substrate (IRS)-1 and IRS-2 are tyrosine-phosphorylated and associated with phosphatidylinositol 3-kinase in response to brain-derived neurotrophic factor in cultured cerebral cortical neurons. *J Biol Chem* 272:30334–30339.
 - van der Heide LP, Ramakers GMJ, Smidt MP (2006) Insulin signaling in the central nervous system: Learning to survive. *Prog Neurobiol* 79:205–221.
 - Lin CH, et al. (2001) A role for the PI-3 kinase signaling pathway in fear conditioning and synaptical plasticity in the amygdala. *Neuron* 31:841–851.
 - Ou L-C, Gean P-W (2006) Regulation of amygdala-dependent learning by brain-derived neurotrophic factor is mediated by extracellular signal-regulated kinase and phosphatidylinositol-3-kinase. *Neuropsychopharmacology* 31:287–296.
 - Mandai K, et al. (2009) LIG family receptor tyrosine kinase-associated proteins modulate growth factor signals during neural development. *Neuron* 63:614–627.
 - de Wit J, Hong W, Luo L, Ghosh A (2011) Role of leucine-rich repeat proteins in the development and function of neural circuits. *Annu Rev Cell Dev Biol* 27:697–729.
 - Feng Y, et al.; International Consortium for Childhood-Onset Mood Disorders (2008) Association of the neurotrophic tyrosine kinase receptor 3 (NTRK3) gene and childhood-onset mood disorders. *Am J Psychiatry* 165:610–616.
 - Armeni L, et al. (2002) 5' UTR-region SNP in the NTRK3 gene is associated with panic disorder. *Mol Psychiatry* 7:928–930.
 - Alonso P, et al. (2008) Genetic susceptibility to obsessive-compulsive hoarding: The contribution of neurotrophic tyrosine kinase receptor type 3 gene. *Genes Brain Behav* 7:778–785.
 - Athanasiu L, et al. (2011) Intron 12 in NTRK3 is associated with bipolar disorder. *Psychiatry Res* 185:358–362.
 - Williams EJ (1959) The Comparison of Regression Variables. *J R Stat Soc Series B* 21: 396–399.
 - Zhang T-Y, Parent C, Weaver I, Meaney MJ (2004) Maternal programming of individual differences in defensive responses in the rat. *Ann N Y Acad Sci* 1032:85–103.
 - Turner CA, Clinton SM, Thompson RC, Watson SJ, Jr., Akil H (2011) Fibroblast growth factor-2 (FGF2) augmentation early in life alters hippocampal development and rescues the anxiety phenotype in vulnerable animals. *Proc Natl Acad Sci USA* 108: 8021–8025.
 - Upton KJ, Sullivan RM (2010) Defining age limits of the sensitive period for attachment learning in rat pups. *Dev Psychobiol* 52:453–464.
 - Sabatini MJ, et al. (2007) Amygdala gene expression correlates of social behavior in monkeys experiencing maternal separation. *J Neurosci* 27:3295–3304.
 - Russo SJ, et al. (2007) IRS2-Akt pathway in midbrain dopamine neurons regulates behavioral and cellular responses to opiates. *Nat Neurosci* 10:93–99.
 - Irvine EE, et al. (2011) Insulin receptor substrate 2 is a negative regulator of memory formation. *Learn Mem* 18:375–383.
 - Martin ED, et al. (2012) IRS-2 Deficiency impairs NMDA receptor-dependent long-term potentiation. *Cereb Cortex* 22:1717–1727.
 - White MF (2003) Insulin signaling in health and disease. *Science* 302:1710–1711.
 - Taguchi A, Wartschow LM, White MF (2007) Brain IRS2 signaling coordinates life span and nutrient homeostasis. *Science* 317:369–372.
 - den Heijer T, et al. (2003) Type 2 diabetes and atrophy of medial temporal lobe structures on brain MRI. *Diabetologia* 46:1604–1610.
 - Li C, et al. (2008) Diabetes and anxiety in US adults: Findings from the 2006 Behavioral Risk Factor Surveillance System. *Diabet Med* 25:878–881.
 - Peyrot M, Rubin RR (1997) Levels and risks of depression and anxiety symptomatology among diabetic adults. *Diabetes Care* 20:585–590.
 - Anderson RJ, Freedland KE, Clouse RE, Lustman PJ (2001) The prevalence of comorbid depression in adults with diabetes: A meta-analysis. *Diabetes Care* 24:1069–1078.
 - Caperuto LC, et al. (2006) Distinct regulation of IRS proteins in adipose tissue from obese aged and dexamethasone-treated rats. *Endocrine* 29:391–398.
 - Rojas FA, Hirata AE, Saad MJA (2003) Regulation of insulin receptor substrate-2 tyrosine phosphorylation in animal models of insulin resistance. *Endocrine* 21:115–122.
 - Paxinos G (2009) *The Rhesus Monkey Brain in Stereotaxic Coordinates* (Academic, Amsterdam, Boston, London), 2nd Ed. Copyright Academic Press (2009).

Supporting Information

Fox et al. 10.1073/pnas.1206723109

SI Methods

Subjects: Initial Assessment. Two hundred forty monkeys (*Macaca mulatta*) that were part of a large single-family pedigree were initially assessed using the NEC FDG-PET paradigm. Animals were mother-reared and pair-housed at the Harlow Primate Laboratory and the Wisconsin National Primate Research Center. At the time of initial assessment, the mean age was 2.4 y (range, 0.74–4.2 y). The typical lifespan of a rhesus macaque is ~25 y, and this age range would correspond to a human sample of mostly prepubescent children with some periadolescents. Animal housing and experimental procedures were in accordance with institutional guidelines. For additional details, see Oler et al. (1).

Subjects: Time 2 and Time 3 Assessments. Twenty-four male monkeys from the larger sample were assessed on two additional occasions using the NEC FDG-PET paradigm, for a total of three assessments over 6–18 mo. To ensure sufficient variance in Ce metabolic activity, animals were chosen to reflect the full spectrum of dorsal amygdala metabolism (Fig. 1A). The second and third assessments were separated by 21 d and varied in duration from initial assessment. Animals were 1.82–4.16 y old at second assessment (mean, 3.03; SD, 0.74). Between the second and third assessment half of the animals (6 high and 6 low) were relocated every 5 d. There were no significant effects of relocation on anxious behavior (P values, >0.05) or brain metabolism (q values, >0.05 FDR) in response to the NEC FDG-PET paradigm. All analyses treated brain metabolism and AT as continuous measures because quantile–quantile (QQ) plots revealed no strong deviations from normality.

FDG-PET Acquisition. Animals received i.v. injections of 5–10 mCi of FDG immediately before exposure to the 30-min NEC paradigm (described below), during which FDG-uptake occurred. After the NEC paradigm, subjects were anesthetized with 15 mg/kg ketamine intramuscularly for placement of an endotracheal tube, positioned in a stereotactic head-holder, and given isoflurane gas anesthesia (1–2%) for the duration of the 60-min scanning procedure, during which integrated FDG-uptake from the behavioral paradigm was measured. Scanning was performed using a microPET P4 scanner [Concorde Microsystems (2)] with an approximate resolution of 8 mm³ [2-mm full width half max (FWHM)].

MRI Assessment. Magnetic resonance imaging (MRI) data were acquired after assessments 1 and 2 using a GE Signa 3T scanner (General Electric Medical Systems) with a standard quadrature birdcage headcoil using an axial 3D T1-weighted inversion-recovery fast gradient echo sequence [repetition time (TR): 9.4 ms; echo: 2.1 ms; field of view (FOV): 14 cm; flip: 10°; number of excitations: 2; in-plane: 0.2734 mm; 248 × 1 mm slices (−0.05-mm gap)]. Animals were anesthetized with an intramuscular injection of ketamine (15 mg/kg) before scanning. MRI data were collected within close temporal proximity to the NEC/FDG-PET session.

Serotonin Transporter Binding (DASB). The [¹¹C]DASB-PET methods are detailed elsewhere (3) and are only briefly described here. 3-[¹¹C]-Amino-4-(2-dimethylaminomethylphenylsulfanyl) benzonitrile (DASB) is a high-affinity ligand of serotonin transporter (5-HTT), and the carbon-11 for the radiolabeling was produced with a National Electrostatics 9SDH 6 MeV Van de Graff tandem accelerator. [¹¹C]DASB-PET data were acquired in 34 rhesus monkeys (mean age, 4.4 y; 12 male, 22 female) using a Concorde

microPET P4 scanner (2). The dynamic PET time series were transformed into parametric images with each voxel representing the distribution volume ratio (DVR) serving as an index of receptor binding (4). The cerebellum was used as a reference region, and all voxel values were divided by the average cerebellar DASB binding value. Each subject's DVR image was transformed into standard space based on the corresponding MRI transformation. The group-averaged 5-HTT map was thresholded at 250× background cerebellar binding and used to demarcate the location of the lateral division of the Ce because compared with surrounding regions, the lateral division of the Ce has the highest density of 5-HTT binding (5).

Behavioral Paradigm: NEC Condition. During the NEC condition, FDG uptake occurred and behaviors were unobtrusively monitored. Animals were placed in a test cage and a human intruder entered the room and at a distance of 2.5 m, presenting her profile to the animal. Following 30 min of exposure to the intruder, animals were anesthetized and blood samples were collected. For more information, refer to Kalin and Shelton (6).

Behavioral and Cortisol Assessment. During the NEC condition, freezing was defined as a period of at least 3 s characterized by tense body posture, no vocalizations, and no locomotion except for slow movements of the head. Coo vocalizations were defined as audible calls made by rounding and pursing the lips with an increase and then decrease in frequency and intensity. Locomotion was defined as one or more full movements at any speed in any direction, including such behavior as dropping from ceiling to floor. Cortisol was measured in plasma samples using the Coat-A-Count cortisol RIA (Siemens Medical Solutions Diagnostics).

Creating the AT Composite. The composite measure of AT was calculated in two steps using SPSS (IBM SPSS Data Collection). First, each appropriately transformed measure [$-1 \times$ cooing^{1/2}, cortisol, log_e(freezing)] was residualized to remove variance linearly predicted by age. Note that cooing, which is associated with decreased anxiety in response to the NEC condition, was reversed to match cortisol and freezing, which are associated with increased anxiety. For cortisol, variance predicted by time-of-day was also removed. Second, composite AT was then computed as the mean of the three standardized (Z-transformed) residuals.

Tissue Isolation. After the animal was killed, the brain was removed and placed in a brain block. One hemisphere was cut into 4.5-mm-thick slabs for later biopsying of tissue, and the other hemisphere was cut into 14-mm slabs for subsequent sectioning on a cryostat. The brain slabbing was counterbalanced for hemisphere. Tissue slabs were stored at −80 °C before processing.

Functionally Guided Ce Biopsy. Slabs (4.5 mm) containing the Ce were identified, thawed briefly on wet ice, and placed on an inverted glass Petri dish on top of wet ice. A circular 3-mm punch tool was used to biopsy the region best corresponding to the Ce. Ce regions were identified from the coronal plane as the most dorsal portions of the amygdalar gray matter that were both (i) medial and ventral to the white-matter of the anterior commissure (AC) and (ii) lateral to the medial temporal convexity that houses the amygdalar cortical nuclei and the entorhinal cortex on the surface of the brain. The tissue punches were collected into 1.5-mL microfuge tubes and placed on dry ice. Samples were stored at −80 °C until analysis.

Microarray Gene Expression Assessment. RNA was extracted from each tissue punch using the RNeasy Plus Mini Kit (Qiagen). Labeled cRNA was then prepared using the 3' IVT Express Kit (Affymetrix) and hybridized to Affymetrix GeneChip Rhesus Macaque Genome arrays.

qRT-PCR Gene Expression Assessment. The same RNA used for the gene chip analysis served as template to prepare cDNA using SuperScript Vilo (Life Technologies). Selected genes were confirmed using qRT-PCR with TaqMan probes (Applied Biosystems). Resulting expression values were log-scaled and normalized to levels of *succinate dehydrogenase complex, subunit A, flavoprotein* (*Fp*) (*SDHA*). Two subjects were excluded from these analyses, because of issues regarding RNA yield and quantification.

AChE Assessment. AChE staining was based on a published method (7). Briefly, slides were incubated for 2 h in 0.12% acetyl thiocholine iodide, 0.0072% ethopropazine, 0.075% glycine, 0.05% cupric sulfate, and 0.68% sodium acetate. Following three rinses in water, the slides were immersed in 0.77% sodium sulfide for 30 min and washed three times in water. The stain was then developed for 10 min in 1% silver nitrate protected from light. Following dehydration in ethanol and clearing in xylene, the slides were mounted using DPX mountant.

In Situ NTRK3 Assessment. Ce *NTRK3* expression was confirmed by *in situ* hybridization. To accurately localize Ce, AChE staining was performed on a coronal slice immediately posterior to that used for the *NTRK3* mRNA stain. Ce regions were defined on the AChE stain using the Paxinos atlas (8). The 499-bp rhesus *NTRK3* probe was amplified from rhesus amygdala cDNA using forward (5'-GAATAGAGTCTATGCCCTTGGCAA-3') and reverse (5'-TCTCTGTGGAAACACAACG-3') PCR primers. The sequence was based on the Affymetrix probe set MmugDNA_29582.1.S1_at and was 98% identical to the human *NTRK3* sequence (GenBank accession no. NM_001007156). The PCR product was subcloned into pBluescript II SK(+) (Agilent Technologies) that had been digested with KpnI and SacI (New England Biolabs). The *NTRK3*-pBluescript plasmid was linearized with Acc65I (New England Biolabs) and transcribed and labeled with [α -³⁵S]UTP (Perkin-Elmer) using T3 RNA polymerase with the Riboprobe Combination System (Promega). The labeled probe was purified using ProbeQuant G-50 Micro Columns (GE Healthcare). The slide-mounted brain sections were fixed in 4% paraformaldehyde before being permeabilized with proteinase K. Following acetylation with acetic anhydride and triethanolamine, the tissue was hybridized with the labeled probe overnight at 55 °C. The tissue was treated with RNase A before being washed and exposed to a phosphor screen. Screens were scanned using Typhoon 9410 (GE Healthcare), and the signal was quantified using ImageQuant 5.2 software (GE Healthcare).

FDG-PET Preprocessing. Methods were similar to our prior work (1). Each subject's T1-MRI was manually stripped of extracerebral tissue using SPAMALIZE (<http://brainimaging.waisman.wisc.edu/~oakes/spam>). Skull-stripped images were registered to a 34-brain template in standard space (8, 9) (12-parameter linear) using FLIRT (<http://www.fmrib.ox.ac.uk/fsl/flirt>) and manually verified. Images from the large sample were averaged to create a study-specific, 238-brain template in standard space (8). Skull-stripped images were registered to this template using FNIRT (<http://fsl.fmrib.ox.ac.uk/fsl/fnirt>). Resulting standard-space images were corrected for spatial radiofrequency (RF) inhomogeneities and segmented into gray matter, white matter, and cerebrospinal fluid probabilities using FAST (<http://www.fmrib.ox.ac.uk/fsl/fast4>). To spatially normalize FDG-PET images, we concatenated two transformation matrices: the matrix generated by registering each animal's FDG-PET to its own T1-MRI (six-parameter linear) and

the MRI-to-template matrix described above. The concatenated matrix was applied to the FDG-PET images. FDG-PET image intensities were scaled to the global mean signal across the region defined by their skull-stripped T1-MRI. Scaled FDG-PET images and GMP maps were spatially smoothed (4-mm FWHM). Mean FDG-PET images were created in standard space by taking the voxel-wise mean across FDG-PET assessments.

Microarray Gene Expression Preprocessing. Gene expression data were analyzed using R (<http://cran.r-project.org>) and the bioconductor libraries for microarray analysis [<http://www.bioconductor.org/>; version 2.7 (10)]. Microarray expression values were corrected for background noise using the RMA algorithm, levels of gene expression were normalized across chips with a constant, mismatch probes were ignored, and expression data were summarized across probes using the median-polish technique (11). Gene expression levels were visually inspected using MA plots (Fig. S1). To ensure results were not an artifact of normalization, gene expression was also quantified using Plier background correction and quantile normalization across arrays. Both normalization techniques revealed similar distributions of gene expression across chips. Because AT is likely to be highly polygenic (12), the quantile normalization, which matches overall gene distribution, may be inappropriate. Therefore, the constant normalization method was used in all analyses. Resulting expression estimates for each probe set were filtered using mean expression levels; sub-threshold probe sets [$<\log_2(100)$] were excluded. Genes were annotated using publicly available annotations verified by BLASTing against the human genome by the University of Nebraska Non Human Primate Genomics Center, which developed the Rhesus Monkey microarray chip in collaboration with Affymetrix (<http://www.unmc.edu/rhesusgenechip/>).

FDG-PET Statistical Analyses. Voxel-wise analyses were performed using an adaptation (13) of Fmristat (<http://www.math.mcgill.ca/keith/fmristat/>) (14, 15). Regressions were performed across the whole brain and, when applicable, controlling for age, change in age across assessments, sex, relocation, and voxel-wise GMP. Initial voxel-wise screening for AT-related voxels was reported in Oler et al. (1). Control analyses revealed that results did not substantively change when GMP was omitted from our regressions, confirming the lack of influence of any gray matter differences on the observed relations with metabolic activity.

Identifying regions with stable brain metabolism. To identify stable metabolism in regions predictive of AT, we performed voxel-wise regressions between each pair of longitudinal FDG-PET scans, controlling for age, change in age, relocation, and GMP. Regions surviving FDR correction ($q \leq 0.05$, two-tailed across three maps) within previously identified AT-related regions in each of the three pairwise comparisons [equivalent to logical AND conjunction (16)] were identified as stable. We also computed voxel-wise ICC_{3,1} values to assess test-retest reliability (17). ICC_{3,1} values were computed across the three FDG-PET assessments, controlling for age, change in age, relocation, and GMP. Results are shown in Table S1. It is important to note that significant stability should be interpreted as relative stability rather than invariance.

Identifying stable AT-related regions. Stable components of AT and brain metabolism were computed by averaging across the three assessments. Mean AT was then correlated with mean metabolism within metabolically stable regions (see above), controlling for mean age, relocation, and mean GMP. Maps were thresholded using FDR ($q \leq 0.05$, two-tailed) within stable regions. Results are shown in Table S2.

Identifying locomotion-related regions. Locomotion-related brain regions were identified using the same procedures used for AT but using individual differences in locomotion during the NEC condition as an explanatory variable. A voxel-wise regression was

computed between mean locomotion and the corresponding brain metabolism in the 238 animals described in Oler et al. (1), controlling for age, sex, and GMP. Results were thresholded using the Sidak procedure. This revealed reliable associations between locomotion and metabolic activity in motor cortex (**Table S7**)

Microarray Gene Expression Statistical Analyses. The primary analysis of interest was the relationship between mean AT across the three assessments and individual differences in gene expression levels. Microarray analyses were performed using robust regression. Robust regression attenuates the influence of high-leverage outliers, minimizing the likelihood that a small number of observations exerted disproportionate effects on the β estimate. Regression analyses were performed between mean AT and all probe sets that were abundant [$>\log_2(100)$] and annotated. Statistical significance was assessed using an empirical Bayes method (18) and corrected for multiple comparisons using FDR ($q \leq 0.05$, two-tailed). Results revealed 148 probe-sets representing 139 genes, which are shown in **Table S3**. To ensure that results were not simply reflecting the normalization procedure, the same statistical analyses were performed on quantile and Plier normalized data. Results from Plier background-corrected and quantile-normalized gene-AT analyses are reported in **Table S3** for each gene that was significant using RMA background correction and constant normalization. Probe sets that were confirmed with PCR were further validated by BLAST probe sets against the rhesus monkey genome.

To identify sets of genes that were overrepresented in our list of 139 significant genes, we performed gene set enrichment analyses on gene ontologies using weighted correlation network analysis (WGCNA) and GOTools packages in R. We examined the number of significant (FDR $q < 0.05$) genes in each term within the HomoSapien ontology database (**Table S4**). This was per-

formed on each term within each of the three gene ontologies in the gene ontology database (Molecular Function, Cellular Component, and Biological Processes) by computing Fisher's exact test on a table with genes falling into the four bins of a Significant (Yes/No) by In-Term (Yes/No) cross-tabulation. This test is equivalent to a one-tailed hypergeometric test. Additionally, to ensure that our inferences were not influenced by the false negatives resulting from our stringent multiple comparison correction, we performed the same ontology enrichment analyses for the set of genes that predicted AT at a significant ($P < 0.05$) uncorrected threshold (**Table S5**).

qRT-PCR Gene Expression Statistical Analyses. qRT-PCR-measured gene expression levels were regressed against AT using the same methods applied to the microarray data (see above).

Assessing the relationship between gene expression and stable AT-related metabolism. Voxel-wise regressions were performed between qRT-PCR-measured Ce *NTRK3* gene expression levels and mean FDG-PET across three assessments, controlling for mean age, relocation, and mean GMP. Resulting maps were thresholded using FDR ($q \leq 0.05$, two-tailed) in stable AT-related regions. Results are shown in **Table S6**. Similar analyses were performed for qRT-PCR-measured motor cortex *NTRK3* gene expression levels and mean FDG-PET in AT-related regions. Results demonstrated no significant effects.

Assessing the relationship between gene expression and locomotion-related metabolism. Voxel-wise regression were performed between qRT-PCR-measured motor cortex *NTRK3* gene expression levels and mean FDG-PET across the three assessments controlling for mean age, relocation, and mean GMP. Resulting maps were corrected for multiple comparisons using FDR ($q \leq 0.05$, two-tailed) in stable locomotion-related regions described above. This analysis revealed no significant results.

1. Oler JA, et al. (2010) Amygdalar and hippocampal substrates of anxious temperament differ in their heritability. *Nature* 466:864–868.
2. Tai C, et al. (2001) Performance evaluation of the microPET P4: A PET system dedicated to animal imaging. *Phys Med Biol* 46:1845–1862.
3. Christian BT, et al. (2009) Serotonin transporter binding and genotype in the nonhuman primate brain using [C-11]DASB PET. *Neuroimage* 47:1230–1236.
4. Innis RB, et al. (2007) Consensus nomenclature for in vivo imaging of reversibly binding radioligands. *J Cereb Blood Flow Metab* 27:1533–1539.
5. O'Rourke H, Fudge JL (2006) Distribution of serotonin transporter labeled fibers in amygdaloid subregions: Implications for mood disorders. *Biol Psychiatry* 60: 479–490.
6. Kalin NH, Shelton SE (1989) Defensive behaviors in infant rhesus monkeys: Environmental cues and neurochemical regulation. *Science* 243:1718–1721.
7. Lim MM, Hammock EAD, Young LJ (2004) A method for acetylcholinesterase staining of brain sections previously processed for receptor autoradiography. *Biotech Histochem* 79:11–16.
8. Paxinos G (2009) *The Rhesus Monkey Brain in Stereotaxic Coordinates* (Academic, Amsterdam, Boston, London), 2nd Ed.
9. Fox AS, Shelton SE, Oakes TR, Davidson RJ, Kalin NH (2008) Trait-like brain activity during adolescence predicts anxious temperament in primates. *PLoS ONE* 3:e2570.
10. Gentleman RC, et al. (2004) Bioconductor: Open software development for computational biology and bioinformatics. *Genome Biol* 5:R80.
11. Gautier L, Cope L, Bolstad BM, Irizarry RA (2004) affy—analysis of Affymetrix GeneChip data at the probe level. *Bioinformatics* 20:307–315.
12. Flint J (2001) Psychiatric genetics: A frightful chromosome. *Curr Biol* 11:R907–R909.
13. Oakes TR, et al. (2007) Integrating VBM into the General Linear Model with voxelwise anatomical covariates. *Neuroimage* 34:500–508.
14. Friston KJ, et al. (1995) Analysis of fMRI time-series revisited. *Neuroimage* 2:45–53.
15. Worsley KJ, Poline JB, Friston KJ, Evans AC (1997) Characterizing the response of PET and fMRI data using multivariate linear models. *Neuroimage* 6:305–319.
16. Nichols T, Brett M, Andersson J, Wager T, Poline J-B (2005) Valid conjunction inference with the minimum statistic. *Neuroimage* 25:653–660.
17. Shrout PE, Fleiss JL (1979) Intraclass correlations: Uses in assessing rater reliability. *Psychol Bull* 86:420–428.
18. Smyth GK (2004) Linear models and empirical bayes methods for assessing differential expression in microarray experiments. *Stat Appl Genet Mol Biol* 3:Article3.

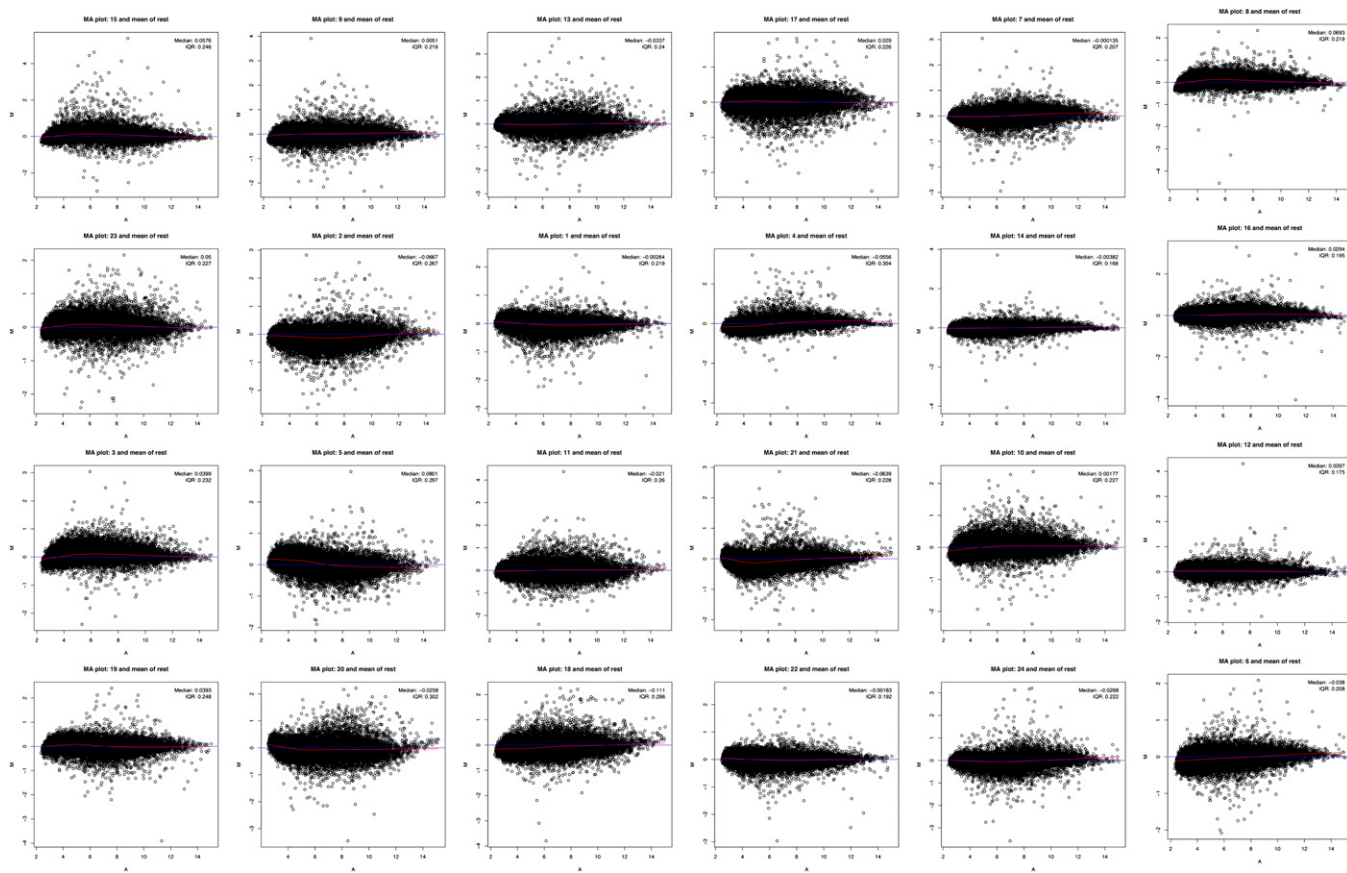


Fig. S1. Limited nonlinear distortion demonstrated using MA plots showing the relationship between the average of each chip and the mean of the other chips (A) and the difference between that chip and the mean of the other chips (M). The chips are ordered by AT from left to right and top to bottom, with the lowest AT subject in the upper-left corner and the highest AT subject in the lower-right corner.

Other Supporting Information Files

- [Table S1 \(XLSX\)](#)
- [Table S2 \(XLSX\)](#)
- [Table S3 \(XLSX\)](#)
- [Table S4 \(XLSX\)](#)
- [Table S5 \(XLSX\)](#)
- [Table S6 \(XLSX\)](#)
- [Table S7 \(XLSX\)](#)

A Translational Neuroscience Approach to Understanding the Development of Social Anxiety Disorder and Its Pathophysiology

Andrew S. Fox, Ph.D.

Ned H. Kalin, M.D.

This review brings together recent research from molecular, neural circuit, animal model, and human studies to help understand the neurodevelopmental mechanisms underlying social anxiety disorder. Social anxiety disorder is common and debilitating, and it often leads to further psychopathology. Numerous studies have demonstrated that extremely behaviorally inhibited and temperamentally anxious young children are at marked risk of developing social anxiety disorder. Recent work in human and nonhuman primates has identified a distributed brain network that underlies early-life anxiety including the central nucleus of the amygdala, the anterior hippocampus, and the orbitofrontal cortex. Studies in nonhuman primates have demonstrated that alterations in this

circuit are trait-like in that they are stable over time and across contexts. Notably, the components of this circuit are differentially influenced by heritable and environmental factors, and specific lesion studies have demonstrated a causal role for multiple components of the circuit. Molecular studies in rodents and primates point to disrupted neurodevelopmental and neuroplastic processes within critical components of the early-life dispositional anxiety neural circuit. The possibility of identifying an early-life at-risk phenotype, along with an understanding of its neurobiology, provides an unusual opportunity to conceptualize novel preventive intervention strategies aimed at reducing the suffering of anxious children and preventing them from developing further psychopathology.

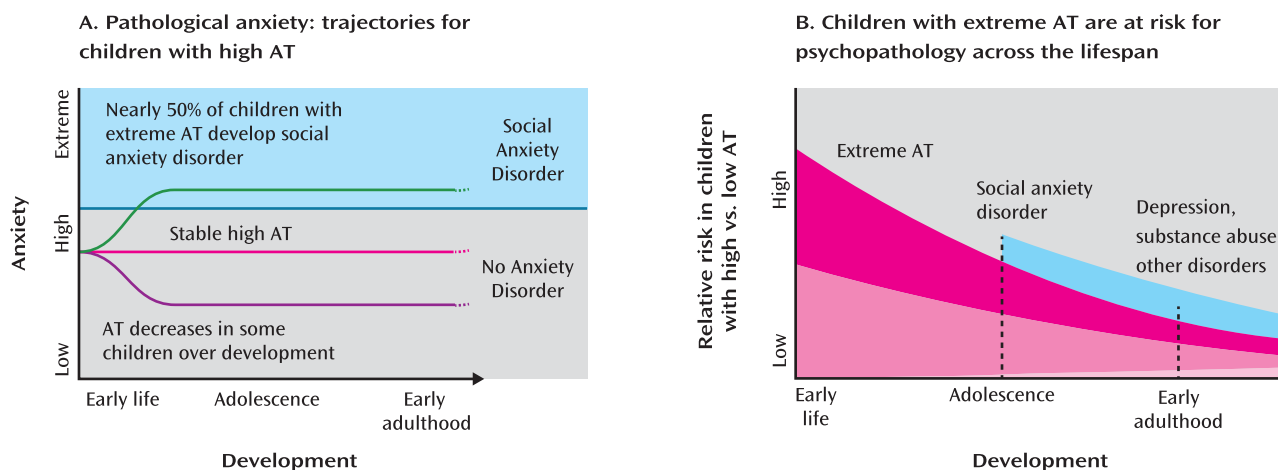
Am J Psychiatry Fox et al.; AiA:1–12

Social anxiety disorder is highly prevalent and debilitating (1), with an estimated prevalence of about 18% (2, 3). The disorder is characterized by marked fearfulness and anxiety in social or performance situations, frequently resulting in avoidance and significant disability. In addition to suffering with social anxiety disorder, afflicted individuals often develop comorbid depressive and substance use disorders (1). Data suggest that social anxiety disorder is ~20%–40% heritable, with environmental factors accounting for the remaining variability (4). Although social anxiety disorder is commonly diagnosed during adolescence, a period during which teenagers attempt to adjust to social change, it can start before adolescence, and its antecedents often manifest early in life (5, 6). Accumulating evidence suggests that a behaviorally inhibited or temperamentally anxious disposition during childhood can lead to the development of social anxiety disorder (5, 7). This at-risk phenotype is characterized by heightened, but nonpathological, levels of anxiety and may constitute a prodromal phenotype for social anxiety disorder. Although this phenotype is moderately stable over the course of development, it does not consistently predict the development of social anxiety disorder, nor is it invariant. This suggests that early-life interventions targeting highly anxious children have the potential to prevent

the development of full-blown social anxiety disorder and its common comorbidities.

In this review, we take a cross-species approach to examine the behavior, neural circuits, and molecular systems that underlie the risk of developing social anxiety disorder. We discuss the biological basis of temperamental anxiety using data from humans and rodents, but we focus on insights gleaned from our studies of nonhuman primates. Rhesus monkeys are ideal for studying mechanisms underlying human development because, given their relatively recent evolutionary divergence from humans, the organization and function of the neural systems relevant to human anxiety, including the amygdala and prefrontal cortex, are conserved (8, 9). Rhesus monkeys and humans also share similar complex social environments that rely on parent-child bonding and peer relationships. These early relationships can both encourage and discourage the adaptive social and emotional learning that helps regulate anxiety and promote survival. Our aim is to understand how inborn and environmental influences converge on the specific biological systems that underlie extreme temperamental anxiety and the risks it confers. It is our hope that understanding the mechanisms modulating these biological substrates will guide the development of novel early-life behavioral and pharmacological interventions

FIGURE 1. Trajectories of Pathological Anxiety and Risk of Psychopathology for Children With Early-Life Anxious Temperament (AT)^a



^a Extreme AT exists on a continuum with social anxiety disorder (panel A), and many children with high levels of AT go on to experience disabling anxiety. Nearly 50% of children with extreme AT eventually develop social anxiety disorder, while in other children levels of AT remain stable or diminish with experience and maturation (7). During childhood and adolescence (panel B), children with extreme AT are most likely to develop social anxiety disorder, but throughout life individuals with extreme AT remain at a higher risk of developing other disorders that typically become manifest later in life, such as major depressive disorder and substance use disorders (1, 13, 22).

that will provide effective treatment for children at risk of suffering from social anxiety disorder and related disorders.

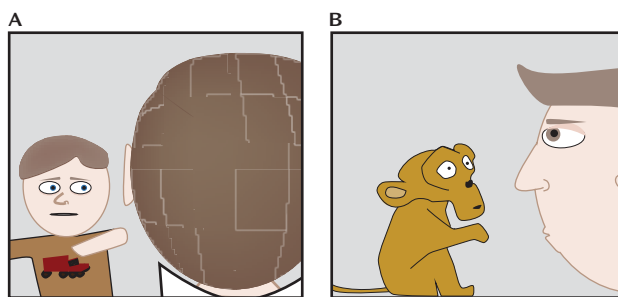
The earliest manifestations of adaptive anxiety-related responses to potential threat occur during infancy and childhood; during infancy, they are characterized by increased excitability, and later, by behavioral inhibition. Behavioral inhibition occurs in response to novelty and potential threat and is associated with autonomic and pituitary-adrenal activation. Childhood behavioral inhibition is thought to manifest during the second year of life, around the time that a child emerges from the normative stage of stranger anxiety and is developing the ability to behaviorally cope with threat (10, 11). Extreme behavioral inhibition, which has received considerable attention from the pioneering work of Jerome Kagan (12), often manifests as excessive shyness and extremely reserved and avoidant behavior in social situations.

Several prospective longitudinal studies have found that extreme behavioral inhibition is associated with increased odds of developing anxiety and depressive disorders (13–18). A recent meta-analysis (7) suggested that early-life behavioral inhibition is the single greatest predictor of the development of social anxiety disorder, as nearly 50% of highly behaviorally inhibited children go on to develop social anxiety disorder (Figure 1A). Although behavioral inhibition fluctuates throughout childhood, studies suggest that individuals with stable levels of high behavioral inhibition have the greatest risk of developing social anxiety disorder (15, 19–21). Several prospective and retrospective self-report studies have implicated childhood behavioral inhibition as a risk factor for depressive disorders (22–24), and children of mothers with anxiety or depressive disorders tend to exhibit elevated levels of behavioral inhibition (25–27). Estimates of

the heritability of behavioral inhibition are consistent with the estimates of ~20%–40% for the heritability of anxiety disorders and anxiety-related neuroticism (4, 28, 29). Many anxiety disorders, including those likely to develop later in highly behaviorally inhibited children, demonstrate partial shared heritability with each other (4, 30, 31). These studies suggest that extreme behavioral inhibition is an early phenotype that confers risk for the development of a broad range of stress-related psychopathology (32–35) (Figure 1B).

To further understand the biology of extreme early anxiety, our group has extensively validated a developmental rhesus monkey model. To assess behavioral inhibition, our initial studies developed the no-eye-contact (NEC) condition of the human intruder paradigm, in which the duration of freezing behavior, analogous to behavioral inhibition, was assessed in response to the uncertain threat of a human intruder looking away and presenting only his or her profile, being careful to make no eye contact with the monkey (Figure 2) (36). The NEC context can last for 30 minutes, during which the human intruder remains motionless, continuously presenting his or her profile throughout the entire test period. Our extensive studies examining various fear- and anxiety-related contexts have demonstrated that the NEC context specifically and reliably elicits freezing. In contrast, direct eye contact by the human intruder often elicits an overt aggressive response from the monkey. Freezing responses are evolutionarily conserved across diverse species, functioning to help the organism remain undetected in the presence of a potential predator (37). Freezing is often accompanied by reduced coo vocalizations. Although rhesus monkey coo vocalizations are affiliative and can be used to recruit support from conspecifics, they can also attract predators. Thus, the reduction in coo calling during the NEC context is

FIGURE 2. Measurement of Anxious Temperament (AT) in Human Children and Young Monkeys by Exposing Them to Potentially Threatening Contexts^a



A staring stranger elicits behavioral inhibition in children with extreme AT.

A human intruder making no eye contact elicits increased freezing in monkeys with extreme AT.

^a In panel A, children confronted with a stranger or novel situation respond with varying degrees of behavioral inhibition and physiological activation. In panel B, during the no-eye-contact (NEC) context, an unfamiliar human intruder stands approximately 2.5 m from the monkey and remains still while looking away and presenting his or her profile to the monkey, making sure to make no eye contact. This potentially threatening NEC context specifically elicits robust behavioral inhibition and physiological activation. In contrast, other contexts, such as when a human intruder stares at the monkey, more robustly elicit fight-or-flight responses (36). Depending on the experiment, the NEC context can last 10–30 minutes. The human intruder remains motionless, continuing to present his or her profile throughout the entire test period.

adaptive, as in the presence of a potential predator the value of remaining undetected is a survival imperative. The NEC context also induces physiological changes, such as increased cortisol levels and right-frontal EEG asymmetry (38, 39). Moreover, similar to symptoms of anxiety in humans, behavioral inhibition in monkeys can be decreased with administration of the GABA-enhancing anxiolytic agent diazepam (36).

To extend the assessment of behavioral inhibition, we developed the concept of anxious temperament (AT) to more completely reflect an individual's dispositional physiological and behavioral responses to potential threat. In the monkey model, this composite AT measure is an average of standardized levels of NEC-context-induced freezing, coo vocalization reductions, and NEC-induced cortisol levels. More broadly, in relation to humans, we use the term AT to define the temperamental predisposition to display behavioral inhibition (increased freezing and decreased vocalizations) along with increased physiological reactivity (increased levels of the stress hormone cortisol) when exposed to novelty, unfamiliar individuals, or other potentially threatening situations. Compared with behavioral inhibition alone, we believe that the composite AT measure better estimates the at-risk human phenotype (40).

Although there are no diagnostic criteria for mental disorders in nonhuman primates, data suggest that monkeys with high AT are functionally impaired. Anecdotally, the veterinary records from one extremely high AT monkey in our colony revealed significant stress-related symptoms,

including hair loss, chronic diarrhea, and extreme fearfulness (e.g., refusal to take treats, retreating to the back of the cage, and excessive "crying"). We also characterized AT during the NEC context in a large free-ranging colony of monkeys on the island of Cayo Santiago. Naturalistic observations of these animals revealed that high AT, tested in a field-improvised laboratory, was associated with elevated social inhibition (unpublished data). Specifically, high AT predicted fewer conspecific approaches ($r_s = -0.44, 0.007$) when animals were free ranging, and high-AT animals maintained larger distances between themselves and their peers ($r_s = -0.31, p = 0.03$). At the most extreme, some of the highest AT animals were never observed to approach their peers, while during the same period their low-AT counterparts approached their peers upwards of 50 times. These data add to the relevance of the extreme-AT monkey model as it relates to the dysfunction experienced by extremely anxious children. Further supporting the homology between human and monkey AT is our demonstration that individual differences in AT are relatively stable across development and that AT is ~20%–40% heritable (41, 42). Like human children, some high-AT monkeys exhibit a reduction in their AT levels as they mature, providing a unique opportunity for future studies to prospectively characterize brain mechanisms underlying recovery and resilience.

Brain Regions Associated With AT

In an initial functional MRI (fMRI) study, Schwartz et al. examined young adults who during their second year of life had been characterized as inhibited or uninhibited (43). Strikingly, the results demonstrated that inhibited individuals had increased amygdala activation in response to novel neutral faces approximately 20 years after the original assessment. More recently, researchers demonstrated increased novelty-related amygdala activation in inhibited males approximately 18 years after being characterized as highly reactive at 4 months of age (44). Similarly, young adolescents (~12.5 years old) who were inhibited during childhood had increased amygdala activation when instructed to rate their emotional responses to fearful faces (45). Extending these studies in prospectively characterized children, Blackford et al. (46–51) studied young adults who self-reported current and past behavioral inhibition. These studies provide additional evidence that amygdala activation is associated with an inhibited temperament, and they extend previous findings by implicating specific processes within the amygdala. Specifically, Blackford et al. demonstrated that highly inhibited young adults show faster amygdala response (46), prolonged and exaggerated amygdala reactivity (47, 48), decreased amygdala habituation (49), and increased amygdala volume (50). In addition to elucidating the role of the amygdala, Blackford et al. have begun to extend the set of regions associated with behavioral inhibition to include the hippocampus (49), the lateral and

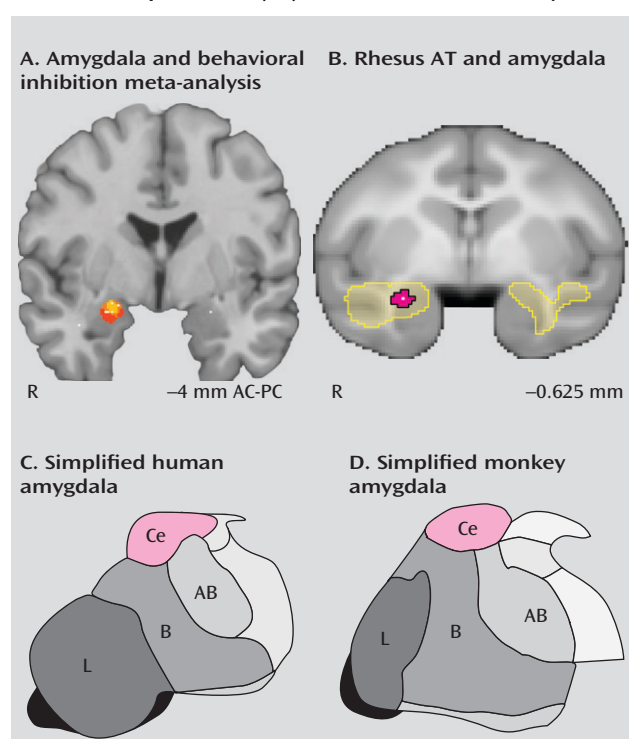
medial orbitofrontal cortex (47, 48), and the insular cortex (48), as well as altered behavioral inhibition-related connectivity between these regions and the amygdala (51).

In neuroimaging studies of behavioral inhibition, the amygdala regions associated with behavioral inhibition are in the dorsal amygdala (Figure 3A). The dorsal amygdala is anatomically distinct from the more ventrally located quasi-cortical basal and lateral amygdalar nuclei. The central nucleus of the amygdala, which is located within the dorsal amygdala region, is primarily composed of striatal-like GABA-ergic neurons and is considered to be the primary output structure of the amygdala complex (53). In imaging studies, the precise localization of dorsal amygdala activations should be considered tentative, given the relatively large spatial confidence intervals associated with fMRI, particularly in studies examining relatively small groups of individuals (i.e., less than 50). Nevertheless, these studies suggest that the central nucleus may be important for instantiating the increased emotional reactivity characteristic of high-AT individuals.

fMRI studies in healthy individuals experiencing fear and anxiety have consistently identified an underlying neural circuit that includes the amygdala, the hippocampus, the prefrontal cortex, and the insula. Moreover, adults with anxiety disorders (e.g., social and specific phobia) show increased activation in these same regions (54). Interestingly, novel social stimuli, such as emotional faces and eye whites, are sufficient to activate the amygdala (55). Consistent with the continuity between dispositional anxiety and anxiety disorders, children with generalized anxiety disorder also show increased amygdala activation (56). In addition to activation in the amygdala, children with generalized anxiety disorder demonstrate increased activation in prefrontal cortical area 47 near the anterior limb of the insula and increased amygdala-mid-insula functional coupling (56).

To further examine the temperamental nature of anxiety-related brain metabolism, we examined young rhesus monkeys (1–4 years old, corresponding approximately to ages 3–12 years in humans) by phenotyping them for AT and performing [¹⁸F]fluorodeoxyglucose positron emission tomography (FDG-PET). Because the FDG-PET human intruder paradigm allows for the simultaneous assessment of brain metabolism and AT, this model can provide insights into the neural substrates underlying AT. As previously described, AT was assessed by combining the NEC-context-induced decreased spontaneous “coo” vocalizations (thought to reflect “calls for help”), increased freezing (or behavioral inhibition), and increased stress-induced cortisol levels (36, 40). Our initial studies demonstrated that the components of AT are associated with metabolism in the extended amygdala, including the central nucleus of the amygdala and the bed nucleus of the stria terminalis (Figure 3B), as well as the hippocampus, the anterior temporal lobe, and the brainstem periaqueductal gray matter (57, 58). The extended amygdala comprises the central nucleus of the amygdala, the bed nucleus of the stria terminalis,

FIGURE 3. Dorsal Amygdala Activation Predicts Variation in Anxious Temperament (AT) in Humans and Monkeys^a



^a From seven published reports examining the role of the amygdala in individuals with a history of childhood behavioral inhibition, we performed a two-dimensional activation likelihood meta-analysis of the location of activation peaks in the dorsal/ventral and medial/lateral dimensions. As shown in panel A, after dilating each peak with a 4-mm² sphere, we found that six of the eight amygdala peaks overlapped (yellow) in the dorsal amygdala region (four of the peaks extended into the region shown in red) (AC-PC=anterior commissure-posterior commissure). In panel B, [¹⁸F]fluorodeoxyglucose positron emission tomography of 238 rhesus monkeys (41) revealed that metabolism within the anterior temporal lobe predicted AT (yellow). Similar to the human studies, the peak of this region was located in the dorsal amygdala (the peak is shown in white and the 95% spatial confidence interval in red). In both humans (panel C) and monkeys (panel D), the peak activations correspond to the location of the central nucleus of the amygdala (52). Ce=central nucleus; AB=accessory basal nucleus; B=basal nucleus; L=lateral nucleus.

and other forebrain structures that play an important role in the initiation of fear and maintenance of anxiety. Moreover, we found that our composite AT measure predicted significantly more variance in amygdala metabolism than any of the components that comprise AT (40, 59). Later studies examining FDG-PET in relation to AT during the NEC context in more than 200 young rhesus monkeys revealed that metabolism in anterior temporal lobe structures, including the central nucleus of the amygdala, the anterior hippocampus, and the anterior temporal pole, robustly predicted AT (41). These findings are consistent with human research in highly behaviorally inhibited individuals and in patients with anxiety disorders in that they provide evidence for the involvement of anterior temporal systems in the at-risk phenotype.

The fMRI and FDG-PET studies discussed above have been limited to studying brain activity in potentially stressful contexts—in the MRI scanner (60) and in the NEC context. To further elucidate the temperamental nature of brain metabolism, we extended these studies to examine brain activity during nonstressful conditions. Specifically, we performed FDG-PET scans on animals that were each exposed to two different stressful conditions (NEC and separation from cagemate into a test cage), and two different nonstressful conditions (alone in the home cage without cagemate and life as usual in the home cage with cagemate). Trait-like positive correlations between individual differences in AT and metabolism in the amygdala, hippocampus, anterior temporal pole, and periaqueductal gray matter were found in each condition regardless of the level of stress (40). Additionally, we examined the stability of AT's neural substrates across time by assessing AT and FDG-PET in 24 animals that were exposed to the NEC context three times over 6–18 months. The results demonstrated interindividual stability over time in brain metabolism within AT-related regions (61). Additionally, the mean metabolism across the three observations predicted the individual's mean AT (61). These data indicate that context-independent and temporally stable neural substrates underlie the trait-like nature of AT. These findings provide insight into AT, as they suggest that the neural substrates of AT are present even when no behavioral manifestations are apparent.

While our definition of AT is fairly circumscribed, there remains substantial variability in how AT presents. This variability is similar to the symptom heterogeneity observed within anxiety and affective diagnostic categories. For example, some monkeys display substantial freezing behavior while maintaining average levels of cortisol and emitting a normative number of coo calls. In contrast, other monkeys have high levels of cortisol relative to their behavioral responses. Studies in rodents by the Blanchards and others examining threat responses have suggested that while the activation of different physiological and behavioral responses can adaptively work together, they may also have different adaptive functions (37). This raises the intriguing possibility that animals expressing different anxiety response profiles have tendencies to activate common neural circuits that can, through their effects on specific neural substrates, bias physiology and behavior toward different adaptive responses. In examining the neural substrates underlying AT's components, we found both common and specific brain regions that underlie the phenotype's heterogeneity (59). The common brain regions included the central nucleus of the amygdala and anterior hippocampal regions, in which metabolism was independently associated with variation in freezing, cooing, and cortisol levels. This finding suggests that regardless of their “symptomatic” presentation, individuals with high levels of AT have increased metabolism in these brain regions. We also identified regional metabolism that was specific to each component of AT. For example,

metabolism in the mid-hippocampus was uniquely associated with cortisol levels, as compared with freezing or coo vocalizations. Together these findings demonstrate that AT has both common and presentation-specific neural substrates and highlight the opportunity for understanding neural substrates that cut across phenotypic heterogeneity.

To understand how different brain systems relate to the heritability of AT, we used our large sample of brain imaging data from a multigenerational family pedigree to perform whole-brain heritability analyses. This was the first study to examine the heritability of brain metabolism across the entire brain. We were surprised to find differential heritability within AT's neural substrates. Our results demonstrated significant heritability of anterior hippocampal metabolism, but no significant heritability of amygdalar central nucleus metabolism (41). These findings call into question the view that it is solely amygdala-altering genes that are responsible for the intergenerational transmission of anxiety. Rather, our findings suggest that AT-related genes are more likely to exert their influence by altering function in other components of the AT-related circuit. Moreover, the lack of heritability within the central nucleus of the amygdala implies that this region may be more likely to mediate the environmental influences known to modulate AT, such as parenting, behavior modeling, and exposure to stress.

Causal Brain Regions and AT

Studies have been performed in patients with varying degrees of amygdala damage (62–64). Consistent with functional imaging findings, a rare patient with bilateral damage to her entire amygdala was shown not to experience psychological discomfort in response to invasions of her personal space (65), did not have normative distrust of strangers (66, 67), and did not report normal fearfulness (68)—all features associated with decreased AT. This work supports the role of an amygdala-centered network in adaptive fear and anxiety as well as in anxiety disorders.

Targeted lesion studies in nonhuman primates reveal a causal role for dorsal amygdala regions in AT. Specific amygdala lesions decrease one's reticence to act in potentially threatening situations and alter stress-induced cortisol release (69–71). Amygdala lesions also decrease anxiety in novel social situations, consistent with its role in social anxiety (72, 73). Our studies employing specific neurotoxic lesions of the central nucleus of the amygdala (74) demonstrated decreased freezing behavior and increased spontaneous coo vocalizations, two core components of AT. Although the central nucleus lesions did not directly affect cortisol, they reduced plasma concentrations of ACTH and CSF concentrations of corticotropin-releasing hormone, the two key upstream mediators of cortisol release.

Targeted lesion studies in primates have also assessed the causal influences of the hippocampus and orbitofrontal cortex on components of AT. Both of these regions have direct connections to the amygdala and are thought to play regulatory roles and provide contextual/regulatory information to the amygdala (Figure 4). Of particular interest is the finding that orbitofrontal cortex aspiration lesions decrease freezing behavior and cortisol levels (70, 71, 75). By combining the lesion strategy with FDG-PET imaging, we found that the effects of orbitofrontal cortex lesions on AT could be explained by orbitofrontal cortex-induced changes in the extended amygdala (i.e., the bed nucleus of the stria terminalis), a region we previously found to be associated with AT (76). Because orbitofrontal cortex aspiration lesions can also disrupt axons passing through this region, it is possible that the effects of these lesions are not due to orbitofrontal cortex damage per se, but rather result from damage to fibers originating in other prefrontal cortical regions. Consistent with this possibility, our recent fMRI study (77) found that increased metabolism of the central nucleus of the amygdala and AT are associated with decreased central nucleus-dorsolateral prefrontal cortical intrinsic connectivity. In contrast to the effects of lesions of the orbitofrontal cortex and central nucleus, the evidence for hippocampal lesions affecting primate AT is mixed (69, 70). Together, these data suggest that the central nucleus of the amygdala, the orbitofrontal cortex, and possibly the hippocampus may each causally influence AT, emphasizing the contribution of multiple regions to dispositional anxiety.

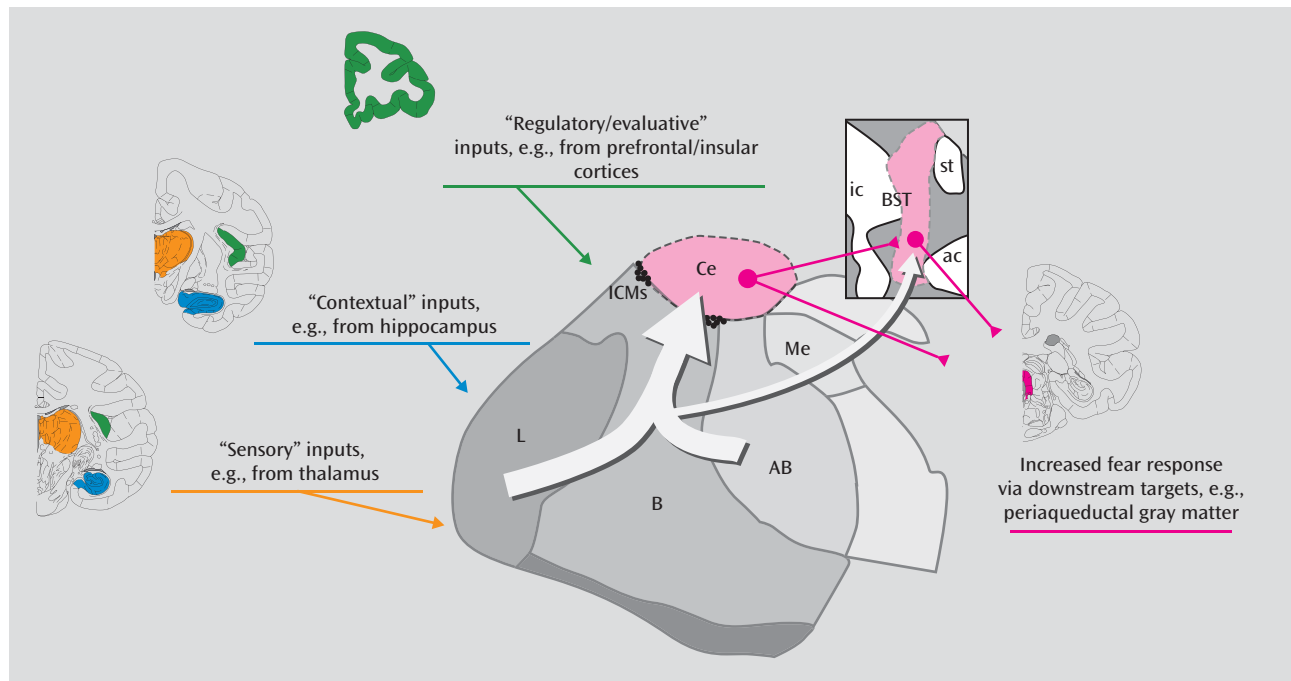
Lesion studies in rodents, although not assessing AT specifically, have demonstrated a causal role for many AT-related regions in unconditioned anxiety behaviors. In particular, rodent studies of unconditioned anxiety have causally implicated the amygdala (78), the ventral hippocampus (similar to the anterior hippocampus in primates) (79, 80), and the extended amygdala, including both the central nucleus of the amygdala and the bed nucleus of the stria terminalis (78, 81). In both rodents and primates, the central nucleus of the amygdala and the bed nucleus of the stria terminalis project to the downstream structures necessary for initiating specific behavioral and physiological aspects of the fear response (Figure 4). Elegant rodent studies have demonstrated dissociable roles for the central nucleus of the amygdala and the bed nucleus of the stria terminalis, such that the central nucleus is required for processing immediate and imminent threats, whereas the bed nucleus of the stria terminalis is required for responding to prolonged and more distant threats (82). More recently, targeted optogenetic functional manipulations of specific projections and detailed anatomical studies have begun to elucidate projection- and cell-specific function within AT-related circuits. For example, some basolateral amygdala neurons provide excitatory input to the hippocampus and the central nucleus of the amygdala, which can initiate unconditioned fear- and anxiety-related

behaviors (83, 84). Moreover, specific subregions and cell types within the central nucleus of the amygdala and the bed nucleus of the stria terminalis have been demonstrated to mediate specific phenotypic expressions of anxiety (85, 86). This suggests that selective alterations in the extended amygdala could give rise to the phenotypic heterogeneity observed in high-AT primates and humans with anxiety disorders. The rodent studies complement the human and nonhuman primate studies, strengthening support for the central nucleus of the amygdala in unconditioned anxiety and drawing attention to other components of the extended amygdala.

Molecular Processes Underlying AT

To develop ideal interventions aimed at preventing the long-term negative consequences of early-life AT, it is important to understand the molecular alterations occurring within the AT neural circuit. Genetic studies indicate that either extremely rare critical polymorphisms or many polymorphisms with small additive effects influence anxiety. Moreover, the influence of parents can have effects on anxiety via alterations in DNA methylation and other epigenetic phenomena that, in the case of methylation, can be passed down as alterations in parental methylation profiles and modified by parental behavior (87–89). Because mRNA levels reflect the confluence of genetic and environmental effects, we believe that examining gene expression within the neural substrates of AT can provide important clues. Because genetic methylation and expression profiles vary by tissue, region, and time, animal models are critical for developing a better understanding of the molecular alterations that underlie the altered brain function occurring in early-life AT.

Because the strongest evidence linking brain alterations to AT points to the central nucleus of the amygdala, we examined individual differences in central nucleus gene expression in relation to AT (61, 90). We performed prospective longitudinal brain imaging with behavioral and physiological assessments on 24 rhesus monkeys prior to measuring central nucleus gene expression. Altered gene expression occurred in some prominent anxiety-related neurochemical systems—neuropeptide Y and serotonin systems—such that individuals with high levels of *NPY1R* or *5HT2C* gene expression in the central nucleus demonstrated lower levels of AT. AT was also negatively associated with alterations in neurodevelopmental systems within neurotrophic and cellular adhesion pathways (Figure 5). In particular, we observed a negative correlation between AT and the expression of neurotrophic receptor kinase 3 (*NTRK3*, also known as *trkc*) as well as its downstream partners, insulin receptor substrate 2 (*IRS2*) and ribosomal protein S6 kinase, 90kDa, polypeptide 3 (*RPS6KA3*, also known as *RSK2*). These genes are involved in growth factor membrane signaling (*NTRK3*), intracellular signaling (*IRS2*), and nuclear activation (*RPS6KA3*).

FIGURE 4. Simplified Amygdala-Centric Model of the Brain Systems That Contribute to Monkey Anxious Temperament (AT)^a

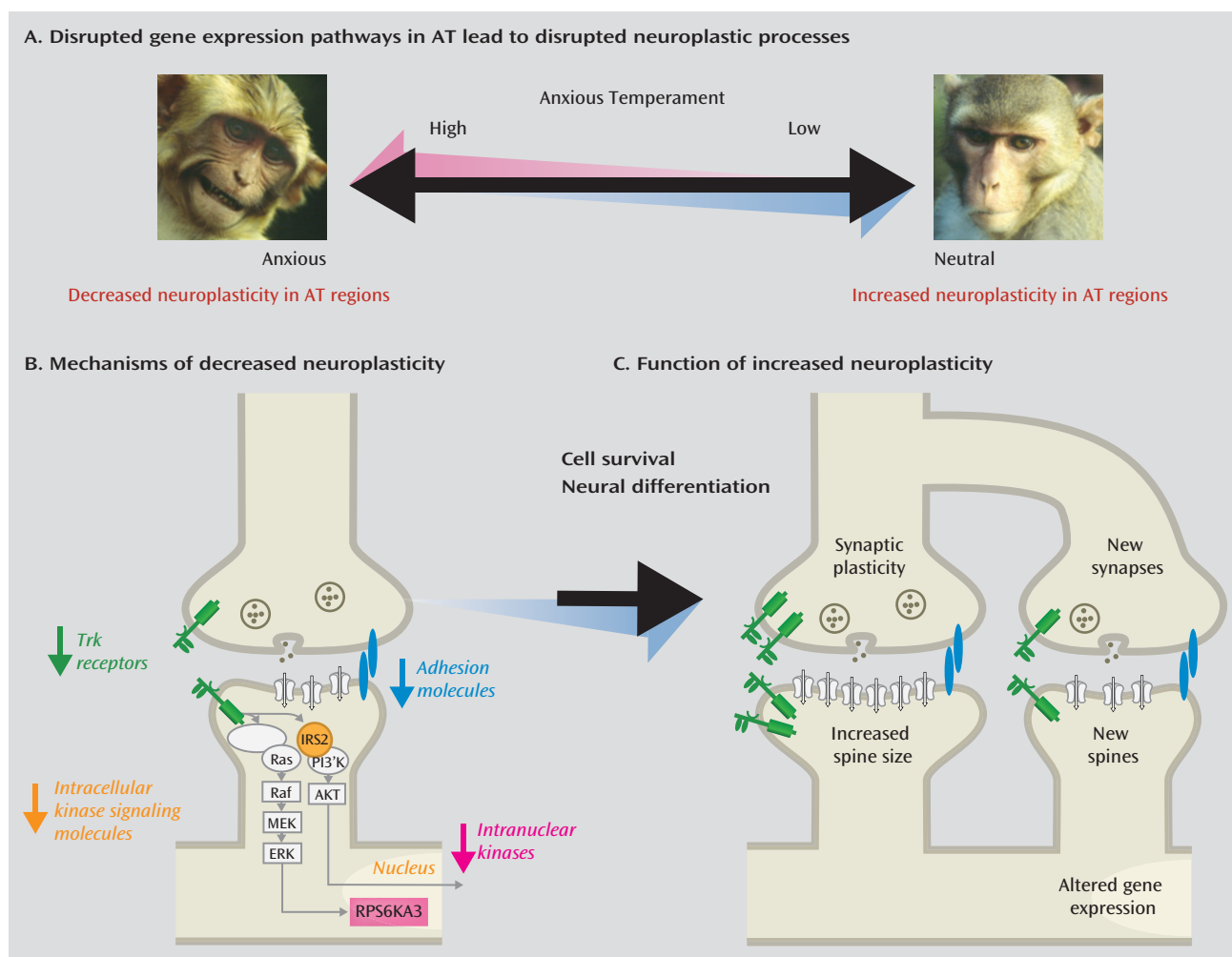
^a Although the full extent of AT's neural substrates remains unknown, neuroimaging work is beginning to identify regions that are more active in individuals with extreme AT, and lesion work suggests that at least some of these regions are causally involved in the genesis of AT. The most compelling evidence exists for the amygdala, which is a critical component of AT's neural substrates and is the focus of extensive research that implicates it in fear- and anxiety-related processing. Here we present a simplified diagram of the monkey amygdala and how it fits into the larger set of brain systems that influence AT. The amygdala receives input from AT-related regulatory/evaluative (green), contextual (blue), and sensory (orange) neural systems, each of which is distributed throughout the brain. In general, amygdala information flows from the more ventral basal regions toward the central nucleus of the amygdala and the bed nucleus of the stria terminalis, which, via their projections to brainstem and hypothalamic structures (pink), initiate fear- and anxiety-related physiological and behavioral responses. All images are shown on slices adapted from reference 52. Ce=central nucleus; AB=accessory basal nucleus; B=basal nucleus; L=lateral nucleus; Me=medial nucleus; ICMs=intercalated masses; BST=bed nucleus of stria terminalis; ic=internal capsule; st=stria terminalis; ac=anterior commissure.

(Figure 5B), all of which contribute to synaptic plasticity and development (Figure 5C). Importantly, individual differences in expression levels of *NTRK3* in the central nucleus of the amygdala predicted trait-like central nucleus metabolism. *NTRK3* is a growth-factor receptor that when activated can initiate widespread changes in cell growth and plasticity, similar to those seen after injection of *BDNF*, which binds to *NTRK2* (also known as *TrkB*). In relation to potential epigenetic mechanisms associated with AT, we observed that high-AT individuals had decreased levels of *GADD45B* (growth arrest and DNA-damage-inducible, beta) in the central nucleus of the amygdala. *GADD45B* is known to be involved in plasticity and neurogenesis through activity-dependent methylation of growth factors and thus may be relevant to the observed decreases in levels of *NTRK3* and its downstream partners (91). Other nonhuman primate studies of early-life stress have also implicated neurodevelopmental pathways (92, 93). Interestingly, recent research in squirrel monkeys demonstrated that coping in response to mild stress increases hippocampal neurogenesis and identified neurogenesis-related hippocampal gene expression in growth-related pathways that included *NTRK3* (92).

Akil et al. have found similar results in relation to anxiety and depression (94). Studies of gene expression in the frontal cortex of patients with major depressive disorder identified decreased expression of fibroblast growth factor 2 (*FGF2*) (95). Much like activation of *NTRK3*, activation of *FGF2* can increase neurogenesis and synaptic plasticity. *FGF2* was also down-regulated in rodents bred to be behaviorally inhibited (96). Excitingly, a single injection of *FGF2* into the behaviorally inhibited rodents during the first days of life, prior to formation of the blood-brain barrier, was sufficient to decrease behavioral inhibition (97). Follow-up study of these rodents revealed increased hippocampal neurogenesis and increased expression of neuroplasticity-related genes, including *NTRK3*, in relevant brain regions (97). These data implicate the FGF family as important for the development of anxiety during early life and further support plasticity-related interventions aimed at decreasing AT (94).

Researchers investigating the serotonin system in rodents have suggested that similar neuroplasticity-related mechanisms underlie anxiety and the efficacy of selective serotonin reuptake inhibitors (SSRIs). SSRIs are effective in treating anxiety disorders but often take weeks to fully work, suggesting an indirect mechanism. Stress impairs, whereas SSRIs increase hippocampal neurogenesis (98, 99),

FIGURE 5. Mechanisms of Decreased Neuroplasticity Mechanisms in the Maintenance of Early-Life Anxious Temperament (AT)^a



^a Research suggests that anxious individuals have decreased neurodevelopmental- and neuroplasticity-related gene activation in brain regions underlying AT, such as the central nucleus of the amygdala and the hippocampus (panel A). Within these regions (panel B), genes that encode adhesion molecules (e.g., EPHB4), trk receptors (e.g., NTRK3), intracellular kinase signaling molecules (e.g., IRS2), and intranuclear kinases (e.g., RPS6KA3) are inversely associated with individual differences in AT. These specific genes function to increase neuroplasticity (panel C) through their influences on synaptic plasticity, increasing spine size and creating new synapses, new spines, and new neurons.

and preventing hippocampal neurogenesis via irradiation blocks the effects of SSRIs (99, 100). Recent studies have suggested that immature hippocampal neurons, in part, mediate the effects of SSRIs by enhancing the ability to discriminate complex threat-relevant information (101, 102). Interestingly, the effects of SSRIs on neurogenesis seem to be mediated by the BDNF receptor, NTRK2 (i.e., TrkB). These data further support the role of tyrosine kinase pathways, as well as neuroplasticity, in relation to anxiety.

Research and Treatment Implications

Social anxiety disorder is common and debilitating. Lifelong social anxiety disorder often leads to further psychopathology, including mood and substance use

disorders. Because it is possible to identify children at risk for social anxiety disorder early in life, the field has an unusual opportunity to conceptualize novel preventive intervention strategies. Treatments for social anxiety disorder are not completely effective, and no treatments exist for children with extreme AT, the forerunner of social anxiety disorder. While some children with extreme AT overcome their anxiety, early interventions promise to increase the number of children who grow up to be psychopathology free (19, 21).

Evolutionarily conserved anxiety-related phenotypes have facilitated cross-species translational research. Studies of the neural circuits of social anxiety disorder and nonhuman primate AT implicate the dorsal amygdala, the anterior hippocampus, brainstem regions, and the orbitofrontal cortex. The homology between rhesus AT,

childhood dispositional anxiety, and social anxiety disorder provides a framework for the valid use of nonhuman primates in new treatment development.

Alterations in brain function associated with AT are stable over time and are context independent. In contrast, the symptoms associated with AT and social anxiety disorder are elicited by specific cues and contexts associated with potential threat. These findings provide a conceptual basis for new treatments directed at changing the stable altered neural tendencies of individuals affected by AT and social anxiety disorder. Attempting to modify one's trait-like brain function has the potential advantage of targeting mechanisms that may result in relapse and failure to respond. Lesions to different components of AT's neural circuit diminish but fail to completely normalize AT. Thus, treatments targeting multiple AT-related brain regions are likely to be most successful in treating social anxiety disorder and preventing its development. Our research provides insights into which brain regions should be targeted. We identified anxiety-general regions that underlie anxiety regardless of how it is expressed and phenotype-specific regions that are uniquely involved in a particular expression of anxiety, such as freezing. Therefore, fully effective treatments will need to target anxiety-general regions as well as response-specific regions as they relate to the diverse presentations of individuals with AT and social anxiety disorder. The data demonstrate that the intergenerational transmission of anxiety is mediated by a widely distributed set of brain regions with large variation in the extent to which altered metabolism in these regions is heritable. This raises the possibility that optimal neural treatment targets could vary depending on one's family history of anxiety. As treatments become more neuroscientifically focused, it is likely that neural measures reflecting treatment-related changes in AT's neural circuits will be useful predictors of long-term treatment outcomes.

Characterizing the molecular alterations in brain regions associated with anxiety and AT has begun to identify novel treatment targets. Numerous rodent studies have focused on the hippocampus, where plasticity and neurogenesis have been associated with lower anxiety. Our group initially focused on the central nucleus of the amygdala for molecular analyses because the central nucleus is a core and causal component of AT's stable neural substrate. Finding a reduction in neuroplasticity-related genes that are associated with increased central nucleus metabolism and AT led us to speculate that extreme early-life AT may result from a diminished ability to modify intra-central nucleus circuits. Studies of amygdala development in nonhuman primates have demonstrated that the central nucleus undergoes protracted development (103), which seems to parallel the developmental course for children's increased tendency to react by freezing to uncertainty and novelty (i.e., normative stranger anxiety). Thus, plasticity within this network is likely to be critical for the capacity to emerge from this period of heightened childhood fearfulness. We further hypothesize that the

maturational ability to overcome or "unlearn" normative childhood fears relies on neuroplasticity mechanisms within AT's neural substrates. Although the work described above specifically implicates *NTRK3*, *FGF2*, and other plasticity-related targets in relation to anxiety, we believe that the study results reflect involvement of broader neuroplasticity-related systems. Based on these results, it is likely that treatments that specifically increase neuroplasticity within the central nucleus and other components of AT's neural substrates will be most effective in modulating early-life AT and preventing the development of social anxiety disorder. Neuroplasticity mechanisms in the hippocampus have been well studied and linked to antidepressant effects (99, 100). Because of the central role of the central nucleus of the amygdala in AT, studies elucidating central nucleus-specific neuroplasticity molecular pathways will be important in conceptualizing novel treatments.

We have made the case for developing early interventions that are aimed at preventing high-AT children from developing anxiety disorders. Because AT emerges during a period when the brain is rapidly changing, treatments aimed at altering mechanisms underlying aberrant brain development are likely to have the potential for long-term changes in anxiety trajectories. Animal studies provide evidence for many ways to influence neuroplasticity that are relevant to treatment, such as exercise, SSRIs, and brain electrical stimulation. The building of synapses, neurons, and the resulting refinement of brain networks is a complex process involving many diverse molecules. Future work should focus on behavioral, pharmacological, and neuromodulatory strategies aimed at modulating diverse neuroplasticity-related molecules within specific components of AT's neural substrates, such as the central nucleus of the amygdala and the anterior hippocampus.

In summary, research relevant to AT and the development of social anxiety disorder has revealed a number of important insights that can be helpful in formulating neuroscientifically based early-life interventions: 1) children with extreme AT are at high risk of developing further psychopathology, especially social anxiety disorder; 2) the neural circuits that underlie social anxiety disorder and human temperamental anxiety are similar to those implicated in monkeys with extreme AT; 3) the neural circuits that underlie AT are trait-like; 4) heterogeneous presentations of AT are associated with activity in both shared and phenotype-specific neural substrates; 5) environment and heritability differentially influence components of AT's neural circuit; and 6) preliminary evidence points to altered neuroplasticity-related gene expression in the genesis of AT. It is our hope that this review will help focus research efforts on early interventions that are designed to not only reduce the suffering of anxious children but also to prevent them from developing further psychopathology.

Received April 4, 2014; revision received June 6, 2014; accepted June 16, 2014 (doi: 10.1176/appi.ajp.2014.14040449). From the Departments of Psychiatry and Psychology, the HealthEmotions Research Institute, and the Waisman Center for Brain Imaging and Behavior, University of Wisconsin, Madison. Address correspondence to Dr. Kalin (nkalin@wisc.edu).

Dr. Fox reports no financial relationships with commercial interests. Dr. Kalin has served on scientific advisory boards for Corcept Therapeutics, Neuronetics, CeNeRx BioPharma, and Skyland Trail; is a stockholder with equity options in Corcept Therapeutics and CeNeRx BioPharma; owned Promoter Neurosciences; and holds patents for promoter sequences for corticotropin-releasing factor CRF2alpha and a method of identifying agents that alter the activity of the promoter sequences, promoter sequences for urocortin II and the use thereof, and promoter sequences for corticotropin-releasing factor binding protein and the use thereof.

Supported by NIH Intramural Research Program and extramural grants R21MH91550, R01MH81884, R01MH46729, P50MH84051, MH100031, R21MH09258, the HealthEmotions Research Institute, and Meriter Hospital.

The authors thank Jonathan A. Oler, Alexander J. Shackman, Do P.M. Tromp, Richard J. Davidson, Brad Postle, Wen Li, and Rick Jenison for their comments on early versions of the manuscript. They thank Steven E. Shelton, Helen VanValkenberg, Marissa Riedel, and the staff at the Harlow Center for Biological Psychology, the HealthEmotions Research Institute, the Waisman Center, the Waisman Laboratory for Brain Imaging and Behavior, and the Wisconsin National Primate Center.

References

1. Stein MB, Stein DJ: Social anxiety disorder. *Lancet* 2008; 371: 1115–1125
2. Kessler RC, Chiu WT, Demler O, Merikangas KR, Walters EE: Prevalence, severity, and comorbidity of 12-month DSM-IV disorders in the National Comorbidity Survey Replication. *Arch Gen Psychiatry* 2005; 62:617–627
3. Kessler RC, Berglund P, Demler O, Jin R, Merikangas KR, Walters EE: Lifetime prevalence and age-of-onset distributions of DSM-IV disorders in the National Comorbidity Survey Replication. *Arch Gen Psychiatry* 2005; 62:593–602
4. Hettema JM, Neale MC, Kendler KS: A review and meta-analysis of the genetic epidemiology of anxiety disorders. *Am J Psychiatry* 2001; 158:1568–1578
5. Fox NA, Henderson HA, Marshall PJ, Nichols KE, Ghera MM: Behavioral inhibition: linking biology and behavior within a developmental framework. *Annu Rev Psychol* 2005; 56:235–262
6. Kessler RC, Ruscio AM, Shear K, Wittchen H-U: Epidemiology of anxiety disorders. *Curr Top Behav Neurosci* 2010; 2:21–35
7. Clauss JA, Blackford JU: Behavioral inhibition and risk for developing social anxiety disorder: a meta-analytic study. *J Am Acad Child Adolesc Psychiatry* 2012; 51:1066–1075.e1
8. Rhesus Macaque Genome Sequencing and Analysis Consortium et al: Evolutionary and biomedical insights from the rhesus macaque genome. *Science* 2007; 316:222–234
9. Wallis JD: Cross-species studies of orbitofrontal cortex and value-based decision-making. *Nat Neurosci* 2012; 15:13–19
10. Scarr S, Salapatek P: Patterns of fear development during infancy. *Merrill-Palmer Quarterly* 1970; 16:53–90
11. Schaffer HR: The onset of fear of strangers and the incongruity hypothesis. *J Child Psychol Psychiatry* 1966; 7:95–106
12. Kagan J, Reznick JS, Snidman N: Biological bases of childhood shyness. *Science* 1988; 240:167–171
13. Biederman J, Hirshfeld-Becker DR, Rosenbaum JF, Hérot C, Friedman D, Snidman N, Kagan J, Faraone SV: Further evidence of association between behavioral inhibition and social anxiety in children. *Am J Psychiatry* 2001; 158:1673–1679
14. Chronis-Tuscano A, Degnan KA, Pine DS, Perez-Edgar K, Henderson HA, Diaz Y, Raggi VL, Fox NA: Stable early maternal report of behavioral inhibition predicts lifetime social anxiety disorder in adolescence. *J Am Acad Child Adolesc Psychiatry* 2009; 48:928–935
15. Essex MJ, Klein MH, Slattery MJ, Goldsmith HH, Kalin NH: Early risk factors and developmental pathways to chronic high inhibition and social anxiety disorder in adolescence. *Am J Psychiatry* 2010; 167:40–46
16. Hirshfeld-Becker DR, Biederman J, Henin A, Faraone SV, Davis S, Harrington K, Rosenbaum JF: Behavioral inhibition in preschool children at risk is a specific predictor of middle childhood social anxiety: a five-year follow-up. *J Dev Behav Pediatr* 2007; 28:225–233
17. Prior M, Smart D, Sanson A, Oberklaid F: Does shy-inhibited temperament in childhood lead to anxiety problems in adolescence? *J Am Acad Child Adolesc Psychiatry* 2000; 39:461–468
18. Schwartz CE, Snidman N, Kagan J: Adolescent social anxiety as an outcome of inhibited temperament in childhood. *J Am Acad Child Adolesc Psychiatry* 1999; 38:1008–1015
19. Fox NA, Henderson HA, Rubin KH, Calkins SD, Schmidt LA: Continuity and discontinuity of behavioral inhibition and exuberance: psychophysiological and behavioral influences across the first four years of life. *Child Dev* 2001; 72:1–21
20. Hirshfeld DR, Rosenbaum JF, Biederman J, Bolduc EA, Faraone SV, Snidman N, Reznick JS, Kagan J: Stable behavioral inhibition and its association with anxiety disorder. *J Am Acad Child Adolesc Psychiatry* 1992; 31:103–111
21. Pfeifer M, Goldsmith HH, Davidson RJ, Rickman M: Continuity and change in inhibited and uninhibited children. *Child Dev* 2002; 73:1474–1485
22. Beesdo K, Bittner A, Pine DS, Stein MB, Höfle M, Lieb R, Wittchen H-U: Incidence of social anxiety disorder and the consistent risk for secondary depression in the first three decades of life. *Arch Gen Psychiatry* 2007; 64:903–912
23. Caspi A, Moffitt TE, Newman DL, Silva PA: Behavioral observations at age 3 years predict adult psychiatric disorders: longitudinal evidence from a birth cohort. *Arch Gen Psychiatry* 1996; 53:1033–1039
24. Gladstone GL, Parker GB: Is behavioral inhibition a risk factor for depression? *J Affect Disord* 2006; 95:85–94
25. Battaglia M, Bajo S, Strambi LF, Brambilla F, Castronovo C, Vanni G, Bellodi L: Physiological and behavioral responses to minor stressors in offspring of patients with panic disorder. *J Psychiatr Res* 1997; 31:365–376
26. Rosenbaum JF, Biederman J, Gersten M, Hirshfeld DR, Meminger SR, Herman JB, Kagan J, Reznick JS, Snidman N: Behavioral inhibition in children of parents with panic disorder and agoraphobia: a controlled study. *Arch Gen Psychiatry* 1988; 45:463–470
27. Rosenbaum JF, Biederman J, Hirshfeld-Becker DR, Kagan J, Snidman N, Friedman D, Nineberg A, Gallery DJ, Faraone SV: A controlled study of behavioral inhibition in children of parents with panic disorder and depression. *Am J Psychiatry* 2000; 157:2002–2010
28. Jardine R, Martin NG, Henderson AS: Genetic covariation between neuroticism and the symptoms of anxiety and depression. *Genet Epidemiol* 1984; 1:89–107
29. Martin N, Goodwin G, Fairburn C, Wilson R, Allison D, Cardon LR, Flint J: A population-based study of personality in 34,000 sib-pairs. *Twin Res* 2000; 3:310–315
30. Olvera RL, Bearden CE, Velligan DI, Almasy L, Carless MA, Curran JE, Williamson DE, Duggirala R, Blangero J, Glahn DC: Common genetic influences on depression, alcohol, and substance use disorders in Mexican-American families. *Am J Med Genet B Neuropsychiatr Genet* 2011; 156B:561–568
31. Tambs K, Czajkowski N, Roysamb E, Neale MC, Reichborn-Kjennerud T, Aggen SH, Harris JR, Ørstavik RE, Kendler KS: Structure of genetic and environmental risk factors for dimensional representations of DSM-IV anxiety disorders. *Br J Psychiatry* 2009; 195:301–307

32. Dilalla LF, Kagan J, Reznick JS: Genetic etiology of behavioral inhibition among 2-year-old children. *Infant Behav Dev* 1994; 17:405–412
33. Goldsmith HH, Gottesman II: Origins of variation in behavioral style: a longitudinal study of temperament in young twins. *Child Dev* 1981; 52:91–103
34. Plomin R, Dunn J (eds): *The Study of Temperament: Changes, Continuities, and Challenges*. Hillsdale, NJ, Lawrence Erlbaum Associates, 1986
35. Robinson JL, Kagan J, Reznick JS, Corley R: The heritability of inhibited and uninhibited behavior: a twin study. *Dev Psychol* 1992; 28:1030–1037
36. Kalin NH, Shelton SE: Defensive behaviors in infant rhesus monkeys: environmental cues and neurochemical regulation. *Science* 1989; 243:1718–1721
37. Blanchard DC, Blanchard RJ: Defensive behaviors, fear, and anxiety, in *Handbook of Behavioral Neuroscience*, vol 17, *Handbook of Anxiety and Fear*. Edited by Blanchard RJ, Blanchard DC, Griebel G, Nutt D. New York, Elsevier, 2008, pp 63–79 (<http://www.sciencedirect.com/science/article/pii/S1569733907000057>)
38. Davidson RJ, Kalin NH, Shelton SE: Lateralized response to diazepam predicts temperamental style in rhesus monkeys. *Behav Neurosci* 1993; 107:1106–1110
39. Kalin NH, Shelton SE, Rickman M, Davidson RJ: Individual differences in freezing and cortisol in infant and mother rhesus monkeys. *Behav Neurosci* 1998; 112:251–254
40. Fox AS, Shelton SE, Oakes TR, Davidson RJ, Kalin NH: Trait-like brain activity during adolescence predicts anxious temperament in primates. *PLoS ONE* 2008; 3:e2570
41. Oler JA, Fox AS, Shelton SE, Rogers J, Dyer TD, Davidson RJ, Shelledy W, Oakes TR, Blangero J, Kalin NH: Amygdalar and hippocampal substrates of anxious temperament differ in their heritability. *Nature* 2010; 466:864–868
42. Rogers J, Shelton SE, Shelledy W, Garcia R, Kalin NH: Genetic influences on behavioral inhibition and anxiety in juvenile rhesus macaques. *Genes Brain Behav* 2008; 7:463–469
43. Schwartz CE, Wright CI, Shin LM, Kagan J, Rauch SL: Inhibited and uninhibited infants “grown up”: adult amygdalar response to novelty. *Science* 2003; 300:1952–1953
44. Schwartz CE, Kunwar PS, Greve DN, Kagan J, Snidman NC, Bloch RB: A phenotype of early infancy predicts reactivity of the amygdala in male adults. *Mol Psychiatry* 2012; 17:1042–1050
45. Pérez-Edgar K, Roberson-Nay R, Hardin MG, Poeth K, Guyer AE, Nelson EE, McClure EB, Henderson HA, Fox NA, Pine DS, Ernst M: Attention alters neural responses to evocative faces in behaviorally inhibited adolescents. *Neuroimage* 2007; 35:1538–1546
46. Blackford JU, Avery SN, Shelton RC, Zald DH: Amygdala temporal dynamics: temperamental differences in the timing of amygdala response to familiar and novel faces. *BMC Neurosci* 2009; 10:145
47. Clauss JA, Cowan RL, Blackford JU: Expectation and temperament moderate amygdala and dorsal anterior cingulate cortex responses to fear faces. *Cogn Affect Behav Neurosci* 2011; 11:13–21
48. Blackford JU, Avery SN, Cowan RL, Shelton RC, Zald DH: Sustained amygdala response to both novel and newly familiar faces characterizes inhibited temperament. *Soc Cogn Affect Neurosci* 2011; 6:621–629
49. Blackford JU, Allen AH, Cowan RL, Avery SN: Amygdala and hippocampus fail to habituate to faces in individuals with an inhibited temperament. *Soc Cogn Affect Neurosci* 2013; 8:143–150
50. Clauss JA, Seay AL, Vanderklok RM, Avery SN, Cao A, Cowan RL, Benningfield MM, Blackford JU: Structural and functional bases of inhibited temperament. *Soc Cogn Affect Neurosci* (Epub ahead of print, March 11, 2014)
51. Blackford JU, Clauss JA, Avery SN, Cowan RL, Benningfield MM, VanDerKlok RM: Amygdala-cingulate intrinsic connectivity is associated with degree of social inhibition. *Biol Psychol* 2014; 99:15–25
52. Paxinos G: *The Rhesus Monkey Brain in Stereotaxic Coordinates*, 2nd ed. Boston, Academic Press, 2009
53. Swanson LW, Petrovich GD: What is the amygdala? *Trends Neurosci* 1998; 21:323–331
54. Etkin A, Wager TD: Functional neuroimaging of anxiety: a meta-analysis of emotional processing in PTSD, social anxiety disorder, and specific phobia. *Am J Psychiatry* 2007; 164:1476–1488
55. Whalen PJ, Kagan J, Cook RG, Davis FC, Kim H, Polis S, McLaren DG, Somerville LH, McLean AA, Maxwell JS, Johnstone T: Human amygdala responsivity to masked fearful eye whites. *Science* 2004; 306:2061
56. McClure EB, Monk CS, Nelson EE, Parrish JM, Adler A, Blair RJR, Fromm S, Charney DS, Leibenluft E, Ernst M, Pine DS: Abnormal attention modulation of fear circuit function in pediatric generalized anxiety disorder. *Arch Gen Psychiatry* 2007; 64:97–106
57. Fox AS, Oakes TR, Shelton SE, Converse AK, Davidson RJ, Kalin NH: Calling for help is independently modulated by brain systems underlying goal-directed behavior and threat perception. *Proc Natl Acad Sci USA* 2005; 102:4176–4179
58. Kalin NH, Shelton SE, Fox AS, Oakes TR, Davidson RJ: Brain regions associated with the expression and contextual regulation of anxiety in primates. *Biol Psychiatry* 2005; 58:796–804
59. Shackman AJ, Fox AS, Oler JA, Shelton SE, Davidson RJ, Kalin NH: Neural mechanisms underlying heterogeneity in the presentation of anxious temperament. *Proc Natl Acad Sci USA* 2013; 110:6145–6150
60. Eatough EM, Shirtcliff EA, Hanson JL, Pollak SD: Hormonal reactivity to MRI scanning in adolescents. *Psychoneuroendocrinology* 2009; 34:1242–1246
61. Fox AS, Oler JA, Shelton SE, Nanda SA, Davidson RJ, Roseboom PH, Kalin NH: Central amygdala nucleus (Ce) gene expression linked to increased trait-like Ce metabolism and anxious temperament in young primates. *Proc Natl Acad Sci USA* 2012; 109:18108–18113
62. Adolphs R: The biology of fear. *Curr Biol* 2013; 23:R79–R93
63. Terburg D, Morgan BE, Montoya ER, Hooge IT, Thornton HB, Hariri AR, Panksepp J, Stein DJ, van Honk J: Hypervigilance for fear after basolateral amygdala damage in humans. *Transl Psychiatr* 2012; 2:e115
64. van Honk J, Eisenegger C, Terburg D, Stein DJ, Morgan B: Generous economic investments after basolateral amygdala damage. *Proc Natl Acad Sci USA* 2013; 110:2506–2510
65. Kennedy DP, Glässcher J, Tyszka JM, Adolphs R: Personal space regulation by the human amygdala. *Nat Neurosci* 2009; 12: 1226–1227
66. Adolphs R, Tranel D, Damasio AR: The human amygdala in social judgment. *Nature* 1998; 393:470–474
67. Tranel D, Gullickson G, Koch M, Adolphs R: Altered experience of emotion following bilateral amygdala damage. *Cogn Neuropsychiatry* 2006; 11:219–232
68. Feinstein JS, Adolphs R, Damasio A, Tranel D: The human amygdala and the induction and experience of fear. *Curr Biol* 2011; 21:34–38
69. Chudasama Y, Izquierdo A, Murray EA: Distinct contributions of the amygdala and hippocampus to fear expression. *Eur J Neurosci* 2009; 30:2327–2337
70. Machado CJ, Bachevalier J: Behavioral and hormonal reactivity to threat: effects of selective amygdala, hippocampal, or orbital frontal lesions in monkeys. *Psychoneuroendocrinology* 2008; 33:926–941
71. Murray EA, Izquierdo A: Orbitofrontal cortex and amygdala contributions to affect and action in primates. *Ann N Y Acad Sci* 2007; 1121:273–296
72. Emery NJ, Capitanio JP, Mason WA, Machado CJ, Mendoza SP, Amaral DG: The effects of bilateral lesions of the amygdala on dyadic social interactions in rhesus monkeys (*Macaca mulatta*). *Behav Neurosci* 2001; 115:515–544

73. Machado CJ, Emery NJ, Capitanio JP, Mason WA, Mendoza SP, Amaral DG: Bilateral neurotoxic amygdala lesions in rhesus monkeys (*Macaca mulatta*): consistent pattern of behavior across different social contexts. *Behav Neurosci* 2008; 122:251–266
74. Kalin NH, Shelton SE, Davidson RJ: The role of the central nucleus of the amygdala in mediating fear and anxiety in the primate. *J Neurosci* 2004; 24:5506–5515
75. Kalin NH, Shelton SE, Davidson RJ: Role of the primate orbitofrontal cortex in mediating anxious temperament. *Biol Psychiatry* 2007; 62:1134–1139
76. Fox AS, Shelton SE, Oakes TR, Converse AK, Davidson RJ, Kalin NH: Orbitofrontal cortex lesions alter anxiety-related activity in the primate bed nucleus of stria terminalis. *J Neurosci* 2010; 30:7023–7027
77. Birn RM, Shackman AJ, Oler JA, Williams LE, McFarlin DR, Rogers GM, Shelton SE, Alexander AL, Pine DS, Slattery MJ, Davidson RJ, Fox AS, Kalin NH: Evolutionarily conserved prefrontal–amygdala dysfunction in early-life anxiety. *Mol Psychiatry* (Epub ahead of print, May 27, 2014)
78. Davis M, Whalen PJ: The amygdala: vigilance and emotion. *Mol Psychiatry* 2001; 6:13–34
79. Fanselow MS, Dong H-W: Are the dorsal and ventral hippocampus functionally distinct structures? *Neuron* 2010; 65:7–19
80. Kjelstrup KG, Tuveson FA, Steffenach H-A, Murison R, Moser EI, Moser M-B: Reduced fear expression after lesions of the ventral hippocampus. *Proc Natl Acad Sci USA* 2002; 99:10825–10830
81. Walker DL, Toufexis DJ, Davis M: Role of the bed nucleus of the stria terminalis versus the amygdala in fear, stress, and anxiety. *Eur J Pharmacol* 2003; 463:199–216
82. Davis M, Walker DL, Miles L, Grillon C: Phasic vs sustained fear in rats and humans: role of the extended amygdala in fear vs anxiety. *Neuropsychopharmacology* 2010; 35:105–135
83. Tye KM, Prakash R, Kim S-Y, Fenno LE, Grosenick L, Zarabi H, Thompson KR, Gradinaru V, Ramakrishnan C, Deisseroth K: Amygdala circuitry mediating reversible and bidirectional control of anxiety. *Nature* 2011; 471:358–362
84. Felix-Ortiz AC, Beyeler A, Seo C, Leppla CA, Wildes CP, Tye KM: BLA to vHPC inputs modulate anxiety-related behaviors. *Neuron* 2013; 79:658–664
85. Kim S-Y, Adhikari A, Lee SY, Marshel JH, Kim CK, Mallory CS, Lo M, Pak S, Mattis J, Lim BK, Malenka RC, Warden MR, Neve R, Tye KM, Deisseroth K: Diverging neural pathways assemble a behavioural state from separable features in anxiety. *Nature* 2013; 496:219–223
86. Viviani D, Charlet A, van den Burg E, Robinet C, Hurni N, Abatis M, Magara F, Stoop R: Oxytocin selectively gates fear responses through distinct outputs from the central amygdala. *Science* 2011; 333:104–107
87. Dias BG, Ressler KJ: Parental olfactory experience influences behavior and neural structure in subsequent generations. *Nat Neurosci* 2014; 17:89–96
88. Zhang T-Y, Parent C, Weaver I, Meaney MJ: Maternal programming of individual differences in defensive responses in the rat. *Ann N Y Acad Sci* 2004; 1032:85–103
89. Zhang TY, Labonté B, Wen XL, Turecki G, Meaney MJ: Epigenetic mechanisms for the early environmental regulation of hippocampal glucocorticoid receptor gene expression in rodents and humans. *Neuropsychopharmacology* 2013; 38: 111–123
90. Roseboom PH, Nanda SA, Fox AS, Oler JA, Shackman AJ, Shelton SE, Davidson RJ, Kalin NH: Neuropeptide Y receptor gene expression in the primate amygdala predicts anxious temperament and brain metabolism. *Biol Psychiatry* (Epub ahead of print, Nov 13, 2013)
91. Ma DK, Jang M-H, Guo JU, Kitabatake Y, Chang M-L, Pow-Anpongkul N, Flavell RA, Lu B, Ming G-L, Song H: Neuronal activity-induced Gadd45b promotes epigenetic DNA demethylation and adult neurogenesis. *Science* 2009; 323: 1074–1077
92. Lyons DM, Buckmaster PS, Lee AG, Wu C, Mitra R, Duffey LM, Buckmaster CL, Her S, Patel PD, Schatzberg AF: Stress coping stimulates hippocampal neurogenesis in adult monkeys. *Proc Natl Acad Sci USA* 2010; 107:14823–14827
93. Sabatini MJ, Ebert P, Lewis DA, Levitt P, Cameron JL, Mirnics K: Amygdala gene expression correlates of social behavior in monkeys experiencing maternal separation. *J Neurosci* 2007; 27:3295–3304
94. Turner CA, Watson SJ, Akil H: The fibroblast growth factor family: neuromodulation of affective behavior. *Neuron* 2012; 76:160–174
95. Evans SJ, Choudary PV, Neal CR, Li JZ, Vawter MP, Tomita H, Lopez JF, Thompson RC, Meng F, Stead JD, Walsh DM, Myers RM, Bunney WE, Watson SJ, Jones EG, Akil H: Dysregulation of the fibroblast growth factor system in major depression. *Proc Natl Acad Sci USA* 2004; 101:15506–15511
96. Perez JA, Clinton SM, Turner CA, Watson SJ, Akil H: A new role for FGF2 as an endogenous inhibitor of anxiety. *J Neurosci* 2009; 29:6379–6387
97. Turner CA, Clinton SM, Thompson RC, Watson SJ Jr, Akil H: Fibroblast growth factor-2 (FGF2) augmentation early in life alters hippocampal development and rescues the anxiety phenotype in vulnerable animals. *Proc Natl Acad Sci USA* 2011; 108:8021–8025
98. Perera TD, Coplan JD, Lisanby SH, Lipira CM, Arif M, Carpio C, Spitzer G, Santarelli L, Scharf B, Hen R, Rosoklija G, Sackeim HA, Dwork AJ: Antidepressant-induced neurogenesis in the hippocampus of adult nonhuman primates. *J Neurosci* 2007; 27:4894–4901
99. Sahay A, Hen R: Adult hippocampal neurogenesis in depression. *Nat Neurosci* 2007; 10:1110–1115
100. Santarelli L, Saxe M, Gross C, Surget A, Battaglia F, Dulawa S, Weissstaub N, Lee J, Duman R, Arancio O, Belzung C, Hen R: Requirement of hippocampal neurogenesis for the behavioral effects of antidepressants. *Science* 2003; 301:805–809
101. Aimone JB, Deng W, Gage FH: Resolving new memories: a critical look at the dentate gyrus, adult neurogenesis, and pattern separation. *Neuron* 2011; 70:589–596
102. Sahay A, Wilson DA, Hen R: Pattern separation: a common function for new neurons in hippocampus and olfactory bulb. *Neuron* 2011; 70:582–588
103. Chareyron LJ, Banta Lavenex P, Amaral DG, Lavenex P: Stereological analysis of the rat and monkey amygdala. *J Comp Neurol* 2011; 519:3218–3239

Overexpressing corticotropin-releasing hormone (CRH) in the primate amygdala increases anxious temperament and alters its neural circuit

Ned H Kalin^{1,2,4}, Andrew S Fox¹, Rothem Kovner^{1,2}, Marissa K Riedel¹, Eva M Fekete¹, Patrick H Roseboom^{1,2}, Do P M Tromp^{1,2}, Benjamin P Grabow³, Miles E Olsen³, Ethan K Brodsky^{3,5}, Andrew L Alexander^{1,3,5}, Marina E Emborg^{2,3,4}, Walter F Block^{3,5}, Julie L Fudge⁶ and Jonathan A Oler¹

¹ Department of Psychiatry, ² Neuroscience Training Program, ³ Department of Medical Physics, University of Wisconsin, Madison, WI; ⁴ Wisconsin National Primate Research Center, Madison, WI; ⁵ inseRT MRI, Inc.; ⁶ Departments of Neurobiology and Anatomy, and Psychiatry, University of Rochester Medical Center.

Corresponding Author:

Jonathan A Oler, PhD
University of Wisconsin School of Medicine and Public Health
Department of Psychiatry
6001 Research Park Boulevard
Madison, WI 53719
e-mail: oler@wisc.edu

Number of words in abstract: 237

Number of words in text: 4094

Number of tables: 1

Number of figure: 8

Number of supplemental materials: 1 (including methods, results, 2 figures and 7 tables)

ABSTRACT

Background: Nonhuman primate models are critical for understanding mechanisms underlying human psychopathology. We established a non-human primate model of anxious temperament (AT) for studying the early-life risk to develop anxiety and depression. Studies have identified the central nucleus of the amygdala (Ce) as an essential component of AT's neural substrates. Corticotropin-releasing hormone (CRH) is expressed in the Ce, has a role in stress, and is linked to psychopathology. Here, in young rhesus monkeys, we combined viral vector technology with assessments of anxiety and multimodal neuroimaging to understand the consequences of chronically increased CRH in the Ce-region.

Methods: Using real-time intraoperative MRI-guided convection-enhanced delivery, 5 monkeys received bilateral dorsal amygdala Ce-region infusions of adeno-associated virus serotype 2 (AAV2) containing the CRH construct. Their cage-mates served as unoperated controls. AT, regional brain metabolism, "resting" fMRI, and diffusion tensor imaging (DTI) were assessed before and two months after viral infusions.

Results: Dorsal amygdala CRH overexpression significantly increased AT and metabolism within the dorsal amygdala. Additionally, we observed changes in metabolism in other AT-related regions, as well as in measures of functional and structural connectivity.

Conclusion: This study provides a translational roadmap that is important for understanding human psychopathology by combining molecular manipulations used in rodents with behavioral phenotyping and multimodal neuroimaging measures used in humans. The results indicate that chronic CRH overexpression in primates not only increases AT, but also affects metabolism and connectivity within components of AT's neural circuitry.

INTRODUCTION

Nonhuman primate models are critical for understanding mechanisms underlying the development and expression of human psychopathology (1, 2). This is supported by the remarkable correspondence between nonhuman and human primates in brain structure and function that underlies their similarities in behavior, rearing methods, psychosocial development, and cognition (2, 3). The imperative to identify new molecular treatment targets to treat psychiatric disorders (4, 5), along with the evolutionary linkage between nonhuman and human primates, provides a compelling rationale to develop techniques in nonhuman primates that can alter the function of candidate genes in a targeted brain-region selective manner. Furthermore, the ability to use multimodal imaging methods to understand the impact of region-specific molecular manipulations in a relevant primate model allows for understanding the mechanisms associated with altered neural circuits in psychiatric illnesses.

To date, our nonhuman primate studies have focused on establishing a model for investigating mechanisms underlying the development of extreme early life anxiety (2, 6-15). First, we developed and standardized the no eye contact condition of the human intruder paradigm (NEC) to assess individual trait-like differences in anxiety-related behavior in response to potential threat (16). This trait-like disposition, termed anxious temperament (AT), is a prominent childhood risk factor for the later development of anxiety disorders, depression, and comorbid substance abuse (17-21). With our nonhuman primate model, we identified the altered neural circuitry that underlies the development of AT and found that it is similar to that observed in humans with anxiety disorders (3, 8, 10, 22). This neural systems level information provides the critical

groundwork for directly testing regionally specific molecular hypotheses potentially important in the pathophysiology of AT.

When extreme, AT or its major behavioral component, *behavioral inhibition*, markedly increase a child's risk for the later development of stress-related psychopathology (17-19, 23). By combining measures of threat-related behavioral inhibition (increased freezing and decreased vocalizations) and pituitary-adrenal activation (threat-induced cortisol), along with ^{18}F -fluoro-deoxyglucose positron emission tomography (FDG-PET) in rhesus monkeys, we characterized a nonhuman primate developmental model of AT (6, 14). Although the AT neural circuit is distributed across prefrontal, limbic, and brain-stem regions, neuroimaging studies in monkeys and humans point to the dorsal amygdala, a region containing the central nucleus of the amygdala (Ce), as a fundamental component of the circuit (8, 10, 11) (see **Figure 1**). The Ce is of particular interest because it is the major outflow region of the amygdala with its downstream projections mediating the hypothalamic and brain-stem contributions to the stress response (24, 25). The Ce is causally involved in mediating AT as neurotoxic lesions of the rhesus monkey dorsal amygdala, which encompassed the Ce, decreased the expression of behavioral inhibition and pituitary-adrenal activity (26).

The Ce is predominantly composed of GABAergic neurons that also contain numerous modulatory neuropeptides and receptors (27). Within the Ce there is expression of corticotropin-releasing hormone (CRH; **Figure 1**), its two receptors, and its binding protein (28-31). CRH containing neurons in the paraventricular nucleus of the hypothalamus (PVN) play a prominent role in mediating the stress-related pituitary-

adrenal response. Interestingly, extra-hypothalamic brain CRH neurons, including those in the Ce, can be regulated differently (32) and are important in coordinating the autonomic, emotional, behavioral and cognitive components of the stress response (33, 34). Rodent studies have demonstrated that stress increases the expression of CRH in the PVN and Ce (35), whereas corticosterone administration decreases expression of CRH in the PVN while concomitantly increasing the expression of Ce CRH (32). In addition to its role in modulating adaptive stress responses, overactivity of the CRH system is hypothesized to be an important pathophysiological mediator of symptoms associated with anxiety and depressive disorders (36). Recent reports suggest that structural variation of genes in the CRH family may contribute to the expression and pathophysiology of human depression and anxiety disorders (37-41), as well as to extreme monkey AT and its associated altered brain metabolism (42).

In addition to the translational value of nonhuman primate models, it is important to emphasize that primates significantly differ from rodents in the distribution and organization of brain CRH systems (31). Rodent studies have used transgenic, viral vector and other neuronal modulatory strategies to model CRH molecular alterations hypothesized to underlie stress-related psychopathology (43-48). However, these mechanistic studies have not been translated to primate species. Therefore, using a viral vector gene delivery strategy to chronically increase the expression of CRH in the dorsal amygdala of young rhesus monkeys, we aimed to identify the role of amygdala CRH systems in the expression of primate anxiety.

Here, we demonstrate that regional chronic overexpression of a putative anxiogenic neuropeptide results in increased anxiety-like behaviors along with anxiety-

related changes in primate brain function. Using a viral vector infused with convection-enhanced delivery and guided by real-time intraoperative MRI (RT-IMRI), we aimed to chronically overexpress CRH in the Ce-region of the amygdala. This approach was combined with multimodal functional and structural brain imaging to test the hypothesis that increased dorsal amygdala CRH would increase AT, as well as glucose metabolism in the Ce. To allow for new insights into how increased amygdala CRH may influence brain-wide neural alterations underlying stress-related psychopathology, we also examined the impact of chronic dorsal amygdala CRH overexpression on functional and structural connectivity with other relevant brain regions. This study provides a framework for further development of preclinical nonhuman primate strategies to evaluate novel, region-specific molecular targets for the treatment of human psychopathology.

Insert Figure 1 here

METHODS AND MATERIALS

Overall study design:

Behavioral measures of AT and glucose-based measures of brain metabolism (FDG-PET) were assessed during NEC before surgery and again approximately 2 months later in 5 CRH-overexpressing monkeys, and at similar intervals in their 5 matched unoperated controls. Additionally, MRI measures of structural connectivity with diffusion

tensor imaging (DTI) and functional intrinsic connectivity with 'resting' fMRI, were acquired before and after surgery. Paired-sample t-tests were used to test for group differences in post-pre measures that resulted from CRH overexpression (i.e., CRH group _(post-pre) – Control group _(post-pre)).

The surgeries were performed using RT-IMRI guidance to localize the target. To estimate the dispersion of AAV2-CRH we infused the viral vector concurrently with the MR visible marker Gadobenate dimeglumine (Gd, MultiHance, Bracco Diagnostics). To characterize the pattern of CRH expression, animals were euthanized approximately one year after surgery and immunohistochemical staining for CRH was performed.

Note that space limitations do not allow for a complete description of the methods in the body of the paper and much of the methodological detail concerning the surgery and brain imaging analyses (FDG-PET, fMRI, and DTI) can be found in the supplemental information that accompanies this paper.

Subjects:

First, two cynomolgus monkeys (*Macaca fascicularis*) were used in pilot studies to: 1) demonstrate the effectiveness of the AAV2-CRH virus to direct CRH overexpression *in vivo* and 2) to visual endogenous CRH expression in the Ce (see **supplemental information**). Next, ten young male rhesus monkeys (*Macaca mulatta*; 1.76-2.63 years old, 2.77-5.25 kg) were used in the CRH overexpression experiment. Five animals received bilateral infusions (2 infusions per hemisphere) of AAV2-CRH into the dorsal amygdala Ce region. The other 5 non-operated control animals were age-matched and pair-housed with each of their corresponding transfected monkeys. Animals were

housed and cared for at the Harlow Center for Biological Psychology and the Wisconsin National Primate Research Center on a 12-h light/dark cycle, in a temperature and humidity controlled vivarium. For all imaging and surgical procedures, the animals were fasted overnight. The experiments were performed according to the federal guidelines of animal use and care (49) and with approval of UW-Madison IACUC committees.

Characterizing Anxious Temperament (AT):

AT was characterized using the NEC condition of the human intruder paradigm. In this paradigm the monkey is placed in a test cage and a potentially threatening human intruder stands ~2.5 meters away, presenting his or her profile to the monkey while making no eye contact for 30 minutes. In contrast to being alone or exposed to a human intruder staring at the monkey, the NEC context reliably elicits freezing behavior and reductions in coo vocalizations (16). Blood samples were taken immediately after NEC-exposure to measure plasma cortisol levels, and a composite measure of AT (6, 14) was computed as the combination of standardized freezing, cooing and cortisol measures (see **supplemental information** for further detail).

Measuring brain glucose metabolism during NEC:

NEC assessment always coincided with the administration of FDG followed by PET. This technique results in FDG-PET scans that represent the integrated brain metabolism throughout the 30-minute NEC exposure. FDG-PET images were transformed to standard space, intensity-normalized to facilitate cross-subject

comparisons, and smoothed to account for individual differences in brain anatomy and registration (see **supplemental information** for further detail).

Insert Figure 2 here

Real-Time Intraoperative MRI (RT-IMRI):

Placement of the MRI-compatible trajectory guide bases followed previously reported methods (see (50, 51) for details) modified for Ce targeting. The intraoperative targeting was performed using a platform for real-time MR-guided prospective stereotaxy (52) that was initially developed by the University of Wisconsin (53-56). A detailed description of the RT-IMRI methods can be found in the **supplemental information**. Briefly, using a pre-surgical MRI, a target point in the Ce was determined and a trajectory was planned to define the location of skull entry (**Figure 2A**). On the day of the surgery, after craniotomy, intraoperative MRI guidance of the catheter was performed using a pivot point-based MRI compatible external trajectory guide (NavigusTM brain port, Medtronic Inc., Minneapolis, MN, see **Figure 2B**). The RT-IMRI platform allows the user to align the brain port to orient catheters with real-time feedback in an interactive manner (**Figure 2C**). Once the brain port was determined to be on target, the catheter was advanced to its final position (**Figure 2D**), the stylet was retracted, and the infusion began. To facilitate *in vivo* MRI visualization of the infusion, the viral vector infusate contained Gd (**Figure 2E**). The rhesus Ce is approximately 5

mm long in the A-P plane, and approximately 1-2 mm in the D-V and M-L planes. To cover as much of the Ce as possible while minimizing treatment to surrounding regions, two 12 μ l infusions were performed per hemisphere (one anterior Ce target, one posterior Ce target), for a total of 24 μ l per hemisphere. After each infusion the catheter was removed, and after all infusions were complete the animal was transported back to the surgical suite and the craniotomies were closed.

Assessing CRH overexpression

Approximately 1 year after AAV2 infusions the animals were euthanized. The brains were extracted and fixed overnight in 4% paraformaldehyde, cryoprotected, and then sectioned at 40 μ m. CRH immunoreactivity was assessed as described in the **supplemental information**. 1:12 sections through the brain were immunostained for CRH. Adjacent coronal brain sections were processed for acetylcholinesterase (AChE), a cholinergic marker that facilitates anatomical identification of amygdala nuclei and subnuclei (57).

For each animal, the distribution of CRH-positive cells was charted through the rostrocaudal extent of the Ce region using camera lucida techniques. Sections were initially drawn under brightfield illumination at 1.6x, to include labeled cells and landmarks such as blood vessels and fiber tracks. The distribution of labeled cells was then confirmed under 10x brightfield illumination. Adjacent AChE-stained sections were then viewed under darkfield illumination, using landmarks in the charted sections for alignment. This permitted overlay of AChE-determined boundaries of amygdala nuclei and subnuclei for each section. Finally, paper maps were digitized using a drawing

tablet in conjunction with the program Adobe Illustrator CS2 (Adobe Systems, San Jose, CA).

To compare the relative distribution of labeled cells resulting from viral-mediated CRH expression and/or endogenous CRH expression across animals, we overlaid individual maps from each animal upon one another in transparent layers, matching rostrocaudal levels as closely as possible. Labeled cells for each pair of animals was color-coded to assist in the analysis.

RESULTS

Characterization of CRH overexpression:

Post mortem immunocytochemical analyses demonstrated marked overexpression of CRH in the dorsal amygdala region of the experimental animals compared to the levels of endogenous CRH in the control animals.

Insert Figure 3 here

The RT-IMRI Gd infusion scan from each animal was compared to the animal's pattern of CRH overexpression defined by immunocytochemistry (**Figure 3**). We found that across all transfected animals the extent and location of the infusions as determined by RT-IMRI matched the areas of CRH overexpression determined with

immunocytochemistry (compare **Figures 4A and 5**). This demonstrates the ability to use *in vivo* imaging methods to estimate the extent of infusion as well as AAV2-CRH transfection. As can be seen in **Figure 4A**, in all experimental animals CRH overexpression was evident in the dorsal amygdala including regions of the lateral and medial divisions of the Ce as well as in surrounding areas such as the dorsal regions of the accessory basal nucleus, the magnocellular region of the basal nucleus, the amygdala striatal transition zone, and portions of the ventral putamen (see **Table 1**).

Insert Figures 4 and 5 here

Effects of CRH overexpression on AT and brain metabolism:

As predicted, compared to controls the CRH overexpressing animals demonstrated a significant increase in AT [CRH group _(post-pre) – Control group _(post-pre)] ($p < .05$, one-tailed, **Figure 6**). It is noteworthy that CRH concentrations in cerebrospinal fluid (CSF) did not significantly differ between experimental and control animals (see **supplemental information** for methods). Corresponding analyses of FDG-PET data revealed that CRH overexpression also resulted in significant increases in dorsal amygdala metabolism ($p < .01$, uncorrected, **Figure 7A**). Additional whole-brain voxelwise analyses revealed that the CRH overexpression animals had significantly greater increases in metabolism in orbitofrontal/anterior insular cortices (OPro/AI), and hippocampus ($p < .01$, two-tailed, uncorrected; **Figure 7A** and **supplemental Table 1**). It is important to underscore that these regions have been implicated as part of the AT

network as well as in human anxiety disorders. To identify regions across both control and experimental animals in which post-pre changes in AT were predicted by changes in metabolism, we looked within brain regions that demonstrated an effect of CRH overexpression **Figure 7B**, yellow outline). This analysis revealed that, regardless of treatment condition, changes in AT from the pre- to post-surgical assessment were predicted by individual differences in metabolic increases in regions of the dorsal amygdala, OPro/AI, and hippocampus (red, $p < .05$, two-tailed, uncorrected, **Figure 7B** and **supplemental Table 2**). These findings suggest that the effects of dorsal amygdala CRH overexpression on increasing AT involve activation of this distributed neural circuit.

Insert Figures 6 and 7 here

Effects of CRH overexpression on functional connectivity and white matter integrity

The fMRI data demonstrated that chronic CRH overexpression altered resting functional connectivity. The dorsal amygdala seed region for the functional connectivity analyses was determined by the overlap of the infusion area detected with Gd (see yellow region in **Figure 5**) with that of the metabolic region that was affected by CRH overexpression (see yellow region in **Figure 7A, right**). Results demonstrated that CRH overexpression altered functional connectivity such that connectivity with the right dorsal amygdala seed in various regions differed between groups ($p < .01$, two-tailed, uncorrected, see

Supplemental Table 3). Of note, increased connectivity was found between right dorsal amygdala and regions encompassing bilateral portions of OPro/AI.

Insert Figure 8 here

Analyses of the DTI data were performed to examine effects of long-term CRH overexpression on white matter microstructure. Voxelwise analyses were performed on measures of diffusivity and fractional anisotropy (FA). Investigation of mean diffusivity (MD), axial diffusivity (AD) and radial diffusivity (RD) demonstrated significant alterations in various regions (see **Supplemental Tables 4-6**). Of particular interest, CRH overexpression in the dorsal amygdala was associated with significant increases in MD, AD and RD in a region of the brain that overlaps with the extended amygdala/bed nucleus of the stria terminalis ($p < 0.005$, two-tailed, uncorrected). Such an increase in MD, AD and RD can be indicative of decreased density of microstructure, but can also be explained by increased levels of CSF. Since this region is proximal to the ventricles this possibility should be considered.

Analysis of FA, an overall indicator of white matter integrity, demonstrated that dorsal amygdala-CRH overexpression resulted in decreased FA in various regions including portions of the medial/midline thalamus ($p < 0.005$, two-tailed, uncorrected, **Figure 8A and Supplemental Table 7**). This region of medial thalamus encompasses the ventral edge of the medial dorsal thalamus, portions of the central medial and paracentral thalamic nuclei, as well as the magnocellular division of the ventral anterior thalamic nucleus. Fiber tractography enabled an investigation of the connectivity of this

region with the rest of the brain. Tractography was seeded in the region of significant FA change in the thalamus and demonstrated that this specific region of the medial/midline thalamus is structurally connected to medial-temporal lobe and PFC regions (**Figure 8B-C**).

Discussion

In this study, we validated methods combining RT-IMRI with convection-enhanced delivery to reliably locate and accurately infuse AAV2-CRH into the primate Ce region. This demonstrates the feasibility of translating rodent mechanistic studies that directly manipulate gene function in the brain to primates, and implicates overactive brain CRH systems in the pathophysiology of excessive primate anxiety. These findings further point to the dorsal amygdala, Ce region, as a key site involved in determining individual differences in dispositional anxiety and the phenotype that represents the risk to develop stress-related psychopathology. This study is the first to use viral vector strategies in non-human primates to directly manipulate CRH molecular systems hypothesized to be involved in human psychiatric disorders. Our primate model provides a unique opportunity to assess the effects of gene manipulation on primate behavior in conjunction with the same *in vivo* measures of brain function and structure that are used to assess human neuropsychiatric patients.

While much of the mechanistic work focused on the role of CRH in anxiety and fear has been performed in rodents, a few studies have been done in primates. Because of the similarities in brain function and structure, behavior, and social functioning between non-human primates and humans, rhesus monkeys provide an

important and valuable model for studying human psychopathology. The marked difference in distribution of brain CRH receptors between rodents and primates further supports the use of primates for studies of stress-related psychopathology. For example, primates have both CRH R1 and CRH R2 in the Ce whereas the rodent Ce is only populated with CRH R1 (31, 58). Early rodent studies site-specifically administering CRH or CRH antagonists established a key role for the amygdala, including the Ce, as being important in mediating the effects of CRH on anxiety and fear responses (59-65). Other studies suggest that within the rodent Ce, it is likely that CRH acts via activation of CRH R1 (66-68). Additionally, mouse transgenic and knockout studies manipulating expression of CRH or CRHR1 demonstrated an important role for CRH systems in mediating adaptive and maladaptive behavioral and physiological responses to stress (for review see (69)).

Our early work in rhesus monkeys is consistent with results from the rodent studies. For example, we demonstrated that intraventricularly administered CRH increased anxiety when administered at low doses and at higher doses resulted in depressive-like behaviors (70). Because of the wide distribution of CRH receptors throughout the brain (31, 58, 71, 72), it is likely that these effects were mediated by activation of CRH receptors in diverse brain regions – a finding that is supported by brain-wide metabolic brain changes seen following very high doses of intraventricular CRH (73). In another study, we also reported a relation between CSF levels of CRH and threat-induced behavioral inhibition (74), however this finding has not been replicated (unpublished data). It is important to note that some, but not all, human studies demonstrate increased CSF CRH concentrations associated with depression and/or

suicide (75) and *post mortem* analyses of suicide victims have revealed increased activity in brain CRH systems (76-80). Neurotoxic lesion studies in primates demonstrated that Ce lesions not only reduced anxiety but also decreased concentrations of CSF CRH (26). Thus, in the Ce lesion study, the reduction in anxiety could be accounted for by the global reduction in CSF CRH. In the current study, in which we use a viral vector strategy to overexpress CRH in the dorsal amygdala region, anxiety and brain function were affected in the absence of a detectable increase in CSF CRH levels. Taken together, these findings suggest that while CRH can have profound impacts throughout the brain, the Ce is a site that is critically involved in mediating these effects.

Recent viral vector studies in rodents have implicated the chronic overexpression of Ce CRH in inducing anxiety- and depression-related behaviors (44, 46, 47, 81, 82). In general, but not always, overexpression of Ce CRH is reported to affect physiological parameters such as the startle response and HPA activity (46, 47, 81, 82). Our current findings in nonhuman primates are consistent as we demonstrate that overexpression of CRH increases AT.

With the functional and structural brain imaging measures used in our study, we were able to extend the rodent studies by examining the impact of chronically increased dorsal amygdala CRH on brain metabolism, as well as functional and structural connectivity. These analyses provide potential insights into mechanisms underlying the neural circuit alterations associated with human anxiety and other stress-related psychopathologies. Our data are the first to demonstrate that an overactive amygdala CRH system has local effects on brain metabolic activity as well as on other

components of the neural circuit associated with anxiety and AT. Specifically, we found that CRH overexpression resulted in increased metabolism in posterior regions of the orbitofrontal cortex (OPro), anterior insula (AI) regions, and hippocampus. These effects cannot be definitively attributed to Ce CRH overexpression as the areas of overexpression encompassed Ce and other neighboring regions, and we also found evidence that in some cases the virus was anterogradely and/or retrogradely transported to other brain regions monosynaptically connected to the site of infusion.

In the present study, we also found that dorsal amygdala CRH overexpression increased functional connectivity between this area and the OPro/AI region of posterior orbital cortex. The findings regarding the OPro/AI region may be particularly relevant as this region of the prefrontal cortex is highly connected with the amygdala (83). We recently demonstrated in a sample of 592 young rhesus monkeys that NEC-related glucose metabolism in the OPro/AI region (along with the bed nucleus of the stria terminalis (BST) and the periaqueductal gray (PAG)) correlated with AT and was heritable (10). Importantly, brain metabolism in these regions was also genetically correlated with AT, which implies the involvement of similar genes in mediating AT and altered brain function in OPro/AI, BST, and PAG.

Perhaps even more interesting are the structural brain changes that were associated with long-term increased CRH overexpression. Using measures of white matter integrity we found evidence for decreases in FA in the medial thalamus encompassing portions of the central medial thalamic nucleus, paracentral thalamic nucleus, and the magnocellular division of the ventral anterior thalamic nucleus. Primate studies demonstrate that these regions contain CRH-immunoreactive cell bodies and

fibers as well as relatively high densities of CRH R1 (31, 84, 85). It is therefore possible that overexpression of CRH in the dorsal amygdala could lead to increased activation of medial thalamic CRH R1. Our tractography methods demonstrated that white matter fibers link the thalamic region of significant FA change with other components of the neural network important in the expression and regulation of anxiety. This is consistent with *ex vivo* tract tracing studies in macaques that demonstrate projections from the dorsal amygdala to midline thalamic nuclei (86, 87). Also, medial thalamic nuclei are reciprocally connected to posterior orbitofrontal cortex that includes the OPro/AI (88). Thus, the medial/midline thalamus may link dorsal amygdala CRH to metabolic changes in the OPro/AI.

Early excitement relevant to developing new treatments for human anxiety and depression resulted from numerous mechanistic studies, mostly performed in rodents, directly manipulating brain CRH systems (for reviews see (89, 90)). Although findings from these studies failed to be translated to positive outcomes in human CRH antagonist clinical trials (91-93), our current findings suggest that continued pursuit of mechanisms directed at altering Ce CRH function in primates might be useful in providing insights into optimizing CRH-altering treatments for human disorders.

Our study also underscores the potential for gene delivery in primate models to elucidate the mechanisms of regional gene-expression on distributed brain function, as well as to explore novel treatment strategies for refractory psychiatric illnesses. Taken together these results indicate that chronically increased dorsal amygdala CRH expression influences AT, metabolic activity within AT's neural substrates, as well as long-range functional connectivity and white-matter microstructure. This work, aimed at

understanding the effects of increased CRH in the dorsal amygdala, will help motivate the design of novel interventions to prevent the development of anxiety disorders and other stress-related psychopathology.

Acknowledgements

We thank the personnel of the Harlow Center for Biological Psychology, the HealthEmotions Research Institute, the Waisman Laboratory for Brain Imaging and Behavior, the Wisconsin National Primate Research Center, the Wisconsin Institutes for Medical Research, K. Brunner, A. Shackman, M. Jesson, L. Williams, D. McFarlin, D. Hsu, S. Shelton, N. Alcock, and especially H. Van Valkenberg. This work was supported by the National Institutes of Health grants R01-MH046729 to NHK, R01-MH63291 to JLF, R24-OD019803 to MEE, R43-CA177205 to ALA and WFB, and P51-OD011106 (Wisconsin National Primate Research Center, University of Wisconsin-Madison). Preliminary versions of this work were presented in poster form at the 2014 Society for Neuroscience meeting in Washington, D.C., and at the 2015 Society of Biological Psychiatry meeting in Toronto, Ontario.

Financial Disclosures

Drs. Alexander, Block and Brodsky are part owners of inseRT MRI, Inc., which provided technology that was used for navigation and monitoring of the infusion experiments. Dr. Kalin is a stockholder and on the advisory board of Corcept Therapeutics. Dr. Fox, Ms. Kovner, Ms. Riedel, Dr. Fekete, Dr. Roseboom, Ms. Tromp, Mr. Grabow, Mr. Olsen, Dr. Emborg, Dr. Fudge and Dr. Oler reported no biomedical financial interests or potential conflicts of interest.

Table and Figure Legends

Figure 1. Endogenous CRH expression in the AT-related Ce-region. (A) Using FDG-PET imaging, we found that metabolism within the Ce predicted individual differences in AT in young rhesus monkeys (*reprinted with permission* (8)). (B) The Ce region was defined by its overlap (purple) with serotonin transporter ligand binding determined with PET imaging (blue). (C) The serotonin transporter binding characterized by PET mirrors its neuroanatomical distribution observed with immunohistochemical methods (*reprinted with permission* (94)). (D) Within this critical primate Ce region (adapted from (95) we found (E) a moderate amount of endogenous CRH immunoreactivity (green) located in neurons, as defined by the overlap with NeuN expression (blue).

Figure 2. Real-time intraoperative MRI guided targeting and infusion monitoring.

(A) Prior to surgery a structural MRI was obtained to visualize the target and plan the trajectory. (B) A pivot point-based MRI compatible external trajectory guide was mounted on the skull (*reprinted with permission* (50)). (C) Precise targeting was performed by imaging a plane orthogonal to the long axis of the external trajectory guide, as if it were visualized by a camera from above. The inset boxes represent the plane in which the trajectory guide (white dot) is visualized and aligned in relation to the target injection point (red dot). (D) The depth of the catheter is advanced to approximately 2 mm above the target. Another MRI was acquired to make precise measurements between the catheter tip and the target prior to advancing the catheter to

its final position. (E) Immediately after the AAV2-CRH / gadolinium infusion was complete, a final MRI was acquired to verify the infusion delivery region.

Figure 3. *In vivo* estimation and *post mortem* verification of dorsal amygdala CRH overexpression

(A) The gadolinium clouds in the dorsal amygdala, Ce region, during and immediately following AAV2-CRH delivery provided an estimate of the location and extent of the infusions. (B) Camera lucida drawings of CRH expression from *post mortem* tissue reflected the extent of viral infusion as estimated from the intraoperative gadolinium signal. Gray regions in B represent neuropil staining and the black dots represent CRH overexpressing cells. (C) Acetylcholinesterase (AChE) staining defined the boundaries of the amygdalar nuclei. Note the relative absence of AChE staining in the CeL. (D) Adjacent sections were used for CRH immunohistochemistry demonstrating marked overexpression in the dorsal amygdala, Ce region.

Figure 4. Quantification of dorsal amygdala CRH expression. (A) *Post mortem* analyses demonstrated overexpression of CRH in the dorsal amygdala and surrounding regions in the experimental animals, compared to (B) the levels of endogenous CRH observed in the cage-mate control animals (top = anterior, bottom = posterior). Each pair of animals is represented by a different color in the composite image, and each dot represents a CRH expressing cell body. Note that endogenous CRH expression levels in controls were found in the most posterior regions of the Ce (only the left hemisphere

is presented), and were substantially lower than that induced by AAV2-CRH transfection. Abbreviations: AAA, anterior amygdaloid area; ABmc, accessory basal nucleus, magnocellular subdivision; AC, anterior commissure; Astr, amygdalostriatal transition zone; Bmc, basal nucleus, magnocellular subdivision; CeLcn, central nucleus, lateral central subdivision; CeLpc, central nucleus, lateral paracapsular subdivision; CeM, central nucleus, medial subdivision; H, hippocampus; L, lateral nucleus; M, medial nucleus; nbm, nucleus basalis of Meynert; P, putamen; V, ventricle.

Figure 5. Quantification of gadolinium diffusion extent and cross-subject overlap.

Based on the intraoperative gadolinium images, we estimated the infusion extent in standard MRI space. This provides a link to the *post mortem* CRH expression data (compare to Figure 4A), and allows for an estimation of the across-subject overlap of CRH expression. The overlap of the gadolinium injection clouds across all 5 experimental animals demonstrates the replicability of the MRI-guided targeting procedure. The colors represent the number of animals with gadolinium signal at each voxel. Note the bilateral overlap across all experimental animals within the Ce-region (yellow). R = right.

Figure 6. CRH overexpressing animals demonstrated a significant increase in Anxious Temperament (AT). Compared to their matched controls, the CRH overexpressing animals demonstrated increased post-surgical levels of AT (mean ± S.E.M). Significance was determined using a paired-samples t-test comparing dorsal

amygdala CRH animals and their cage-mate controls [CRH group _(post-pre) – Control group _(post-pre)] ($p < .05$, one-tailed; see inset and methods for details).

Figure 7. CRH overexpressing animals demonstrated significant increases in brain metabolism. (A) Compared to their matched controls, the CRH overexpressing animals demonstrated increased post-pre change in metabolism within the dorsal amygdala, orbitofrontal/insular cortex (OPro/AI), and hippocampus (yellow, $p < 0.01$, two-tailed uncorrected; and see **Supplementary Table 1**). All of these regions have been implicated in Anxious Temperament (AT). (B) Within regions that were affected by CRH overexpression (yellow outline), we identified areas in which the post-pre change in metabolism correlated with the post-pre change in AT (red; $p < 0.05$, one-tailed uncorrected). Across all 10 animals, changes in AT were associated with changes in brain metabolism in the dorsal amygdala and in bilateral regions of the posterior orbitofrontal/insular cortex (OPro/AI). R = right.

Figure 8. Diffusion tensor imaging demonstrated altered thalamic structural integrity as assessed with FA. (A) Whole-brain voxelwise analyses indicated CRH-induced reductions in FA in a region overlapping with the medial dorsal/midline thalamus [CRH group _(post-pre) – Control group _(post-pre)] ($p < 0.005$, uncorrected). R = right. (B & C) Deterministic tractography, seeded in the thalamic region of significant FA change, is visualized on coronal MRIs that are rotated to view fiber connectivity projected along the A-P plane. This demonstrates that the seed region is connected to the prefrontal cortex, and medial temporal lobe.

Table 1

CASE	CeLcn/pc	CeM	Bmc	ABmc	Astr	ventral putamen
CRH-1	++	++	++	+++++	+++++	+++
CRH-2	++	+	+++++	++++	+++++	+++++
CRH-3	+++	+	+++++	+	+++++	+++++
CRH-4	+++	++	+	+++++	+++++	+
CRH-5	+++	+++	+++++	+++++	++++	+++++
CON-1	+					
CON-2	+					
CON-3	+					
CON-4	+					
CON-5	+					

Table 1. Relative density of CRH-labeled cells in both hemispheres, summing across all rostrocaudal levels. Abbreviations: ABmc, accessory basal nucleus, magnocellular subdivision; Astr, amygdalostriatal transition zone; Bmc, basal nucleus, magnocellular subdivision; CeLcn/pc, central nucleus, lateral central subdivision/paracapsular subdivision; CeM, central nucleus, medial subdivision.

References

1. Nelson EE, Winslow JT (2009): Non-human primates: model animals for developmental psychopathology. *Neuropsychopharmacology*. 34:90-105.
2. Kalin NH, Shelton SE (2003): Nonhuman primate models to study anxiety, emotion regulation, and psychopathology. *Ann N Y Acad Sci*. 1008:189-200.
3. Fox AS, Kalin NH (2014): A Translational Neuroscience Approach to Understanding the Development of Social Anxiety Disorder and Its Pathophysiology. *The American journal of psychiatry*.
4. Insel TR (2012): Next-generation treatments for mental disorders. *Sci Transl Med*. 4:155ps119.
5. Hyman SE (2014): The unconscionable gap between what we know and what we do. *Sci Transl Med*. 6:253cm259.
6. Fox AS, Shelton SE, Oakes TR, Davidson RJ, Kalin NH (2008): Trait-like brain activity during adolescence predicts anxious temperament in primates. *PLoS ONE*. 3:e2570.
7. Kalin NH, Shelton SE, Fox AS, Oakes TR, Davidson RJ (2005): Brain regions associated with the expression and contextual regulation of anxiety in primates. *Biol Psychiatry*. 58:796-804.
8. Oler JA, Fox AS, Shelton SE, Rogers J, Dyer TD, Davidson RJ, et al. (2010): Amygdalar and hippocampal substrates of anxious temperament differ in their heritability. *Nature*. 466:864-868.
9. Alisch RS, Chopra P, Fox AS, Chen K, White AT, Roseboom PH, et al. (2014): Differentially methylated plasticity genes in the amygdala of young primates are linked to anxious temperament, an at risk phenotype for anxiety and depressive disorders. *J Neurosci*. 34:15548-15556.
10. Fox AS, Oler JA, Shackman AJ, Shelton SE, Raveendran M, McKay DR, et al. (2015): Intergenerational neural mediators of early-life anxious temperament. *Proc Natl Acad Sci U S A*. 112:9118-9122.
11. Fox AS, Oler JA, Shelton SE, Nanda SA, Davidson RJ, Roseboom PH, et al. (2012): Central amygdala nucleus (Ce) gene expression linked to increased trait-like Ce metabolism and anxious temperament in young primates. *Proc Natl Acad Sci U S A*. 109:18108-18113.
12. Oler JA, Fox AS, Shelton SE, Christian BT, Murali D, Oakes TR, et al. (2009): Serotonin transporter availability in the amygdala and bed nucleus of the stria terminalis

- predicts anxious temperament and brain glucose metabolic activity. *J Neurosci*. 29:9961-9966.
13. Roseboom PH, Nanda SA, Fox AS, Oler JA, Shackman AJ, Shelton SE, et al. (2014): Neuropeptide Y receptor gene expression in the primate amygdala predicts anxious temperament and brain metabolism. *Biol Psychiatry*. 76:850-857.
 14. Shackman AJ, Fox AS, Oler JA, Shelton SE, Davidson RJ, Kalin NH (2013): Neural mechanisms underlying heterogeneity in the presentation of anxious temperament. *Proceedings of the National Academy of Sciences of the United States of America*. 110:6145-6150.
 15. Fox AS, Oakes TR, Shelton SE, Converse AK, Davidson RJ, Kalin NH (2005): Calling for help is independently modulated by brain systems underlying goal-directed behavior and threat perception. *Proc Natl Acad Sci U S A*. 102:4176-4179.
 16. Kalin NH, Shelton SE (1989): Defensive behaviors in infant rhesus monkeys: environmental cues and neurochemical regulation. *Science*. 243:1718-1721.
 17. Fox NA, Henderson HA, Marshall PJ, Nichols KE, Ghera MM (2005): Behavioral inhibition: linking biology and behavior within a developmental framework. *Annual review of psychology*. 56:235-262.
 18. Clauss JA, Blackford JU (2012): Behavioral inhibition and risk for developing social anxiety disorder: a meta-analytic study. *J Am Acad Child Adolesc Psychiatry*. 51:1066-1075 e1061.
 19. Gladstone GL, Parker GB (2006): Is behavioral inhibition a risk factor for depression? *J Affect Disord*. 95:85-94.
 20. Beesdo K, Bittner A, Pine DS, Stein MB, Hofler M, Lieb R, et al. (2007): Incidence of social anxiety disorder and the consistent risk for secondary depression in the first three decades of life. *Arch Gen Psychiatry*. 64:903-912.
 21. Caspi A, Moffitt TE, Newman DL, Silva PA (1996): Behavioral observations at age 3 years predict adult psychiatric disorders. Longitudinal evidence from a birth cohort. *Arch Gen Psychiatry*. 53:1033-1039.
 22. Birn RM, Shackman AJ, Oler JA, Williams LE, McFarlin DR, Rogers GM, et al. (2014): Evolutionarily conserved prefrontal-amyg达尔 dysfunction in early-life anxiety. *Mol Psychiatry*. 19:915-922.
 23. Essex MJ, Klein MH, Slattery MJ, Goldsmith HH, Kalin NH (2010): Early risk factors and developmental pathways to chronic high inhibition and social anxiety disorder in adolescence. *The American journal of psychiatry*. 167:40-46.

24. Davis M, Whalen PJ (2001): The amygdala: vigilance and emotion. *Mol Psychiatry*. 6:13-34.
25. Janak PH, Tye KM (2015): From circuits to behaviour in the amygdala. *Nature*. 517:284-292.
26. Kalin NH, Shelton SE, Davidson RJ (2004): The role of the central nucleus of the amygdala in mediating fear and anxiety in the primate. *J Neurosci*. 24:5506-5515.
27. Swanson LW, Petrovich GD (1998): What is the amygdala? *Trends Neurosci*. 21:323-331.
28. Potter E, Behan DP, Linton EA, Lowry PJ, Sawchenko PE, Vale WW (1992): The central distribution of corticotropin-releasing factor (CRF)-binding protein predicts multiple sites and modes of interaction with CRF. *Proc Natl Acad Sci U S A*. 89:4192-4196.
29. Potter E, Sutton S, Donaldson C, Chen R, Perrin M, Lewis K, et al. (1994): Distribution of corticotropin-releasing factor receptor mRNA expression in the rat brain and pituitary. *Proc Natl Acad Sci U S A*. 91:8777-8781.
30. Swanson LW, Sawchenko PE, Rivier J, Vale WW (1983): Organization of ovine corticotropin-releasing factor immunoreactive cells and fibers in the rat brain: an immunohistochemical study. *Neuroendocrinology*. 36:165-186.
31. Sanchez MM, Young LJ, Plotsky PM, Insel TR (1999): Autoradiographic and in situ hybridization localization of corticotropin-releasing factor 1 and 2 receptors in nonhuman primate brain. *J Comp Neurol*. 408:365-377.
32. Schukkin J, Gold PW, McEwen BS (1998): Induction of corticotropin-releasing hormone gene expression by glucocorticoids: implication for understanding the states of fear and anxiety and allostatic load. *Psychoneuroendocrinology*. 23:219-243.
33. Owens MJ, Nemeroff CB (1991): Physiology and pharmacology of corticotropin-releasing factor. *Pharmacol Rev*. 43:425-472.
34. Takahashi LK (2001): Role of CRF(1) and CRF(2) receptors in fear and anxiety. *Neurosci Biobehav Rev*. 25:627-636.
35. Hsu DT, Chen FL, Takahashi LK, Kalin NH (1998): Rapid stress-induced elevations in corticotropin-releasing hormone mRNA in rat central amygdala nucleus and hypothalamic paraventricular nucleus: an in situ hybridization analysis. *Brain Res*. 788:305-310.
36. Arborelius L, Owens MJ, Plotsky PM, Nemeroff CB (1999): The role of corticotropin-releasing factor in depression and anxiety disorders. *J Endocrinol*. 160:1-12.

37. Hsu DT, Mickey BJ, Langenecker SA, Heitzeg MM, Love TM, Wang H, et al. (2012): Variation in the corticotropin-releasing hormone receptor 1 (CRHR1) gene influences fMRI signal responses during emotional stimulus processing. *J Neurosci*. 32:3253-3260.
38. Binder EB, Nemeroff CB (2010): The CRF system, stress, depression and anxiety-insights from human genetic studies. *Mol Psychiatry*. 15:574-588.
39. Binder EB, Owens MJ, Liu W, Deveau TC, Rush AJ, Trivedi MH, et al. (2010): Association of polymorphisms in genes regulating the corticotropin-releasing factor system with antidepressant treatment response. *Archives of general psychiatry*. 67:369-379.
40. Smoller JW, Rosenbaum JF, Biederman J, Kennedy J, Dai D, Racette SR, et al. (2003): Association of a genetic marker at the corticotropin-releasing hormone locus with behavioral inhibition. *Biol Psychiatry*. 54:1376-1381.
41. Smoller JW, Yamaki LH, Fagerness JA, Biederman J, Racette S, Laird NM, et al. (2005): The corticotropin-releasing hormone gene and behavioral inhibition in children at risk for panic disorder. *Biol Psychiatry*. 57:1485-1492.
42. Rogers J, Raveendran M, Fawcett GL, Fox AS, Shelton SE, Oler JA, et al. (2013): CRHR1 genotypes, neural circuits and the diathesis for anxiety and depression. *Mol Psychiatry*. 18:700-707.
43. Pleil KE, Rinker JA, Lowery-Gionta EG, Mazzone CM, McCall NM, Kendra AM, et al. (2015): NPY signaling inhibits extended amygdala CRF neurons to suppress binge alcohol drinking. *Nat Neurosci*. 18:545-552.
44. Li XF, Hu MH, Li SY, Geach C, Hikima A, Rose S, et al. (2014): Overexpression of corticotropin releasing factor in the central nucleus of the amygdala advances puberty and disrupts reproductive cycles in female rats. *Endocrinology*. 155:3934-3944.
45. Toth M, Gresack JE, Bangasser DA, Plona Z, Valentino RJ, Flandreau EI, et al. (2014): Forebrain-specific CRF overproduction during development is sufficient to induce enduring anxiety and startle abnormalities in adult mice. *Neuropsychopharmacology*. 39:1409-1419.
46. Regev L, Neufeld-Cohen A, Tsoory M, Kuperman Y, Getselter D, Gil S, et al. (2011): Prolonged and site-specific over-expression of corticotropin-releasing factor reveals differential roles for extended amygdala nuclei in emotional regulation. *Mol Psychiatry*. 16:714-728.
47. Keen-Rhinehart E, Michopoulos V, Toufexis DJ, Martin EI, Nair H, Ressler KJ, et al. (2009): Continuous expression of corticotropin-releasing factor in the central

- nucleus of the amygdala emulates the dysregulation of the stress and reproductive axes. *Mol Psychiatry*. 14:37-50.
48. Sink KS, Walker DL, Freeman SM, Flandreau EI, Ressler KJ, Davis M (2013): Effects of continuously enhanced corticotropin releasing factor expression within the bed nucleus of the stria terminalis on conditioned and unconditioned anxiety. *Mol Psychiatry*. 18:308-319.
49. Clark JD, Gebhart GF, Gonder JC, Keeling ME, Kohn DF (1997): Special Report: The 1996 Guide for the Care and Use of Laboratory Animals. *ILAR J*. 38:41-48.
50. Emborg ME, Joers V, Fisher R, Brunner K, Carter V, Ross C, et al. (2010): Intraoperative intracerebral MRI-guided navigation for accurate targeting in nonhuman primates. *Cell transplantation*. 19:1587-1597.
51. Emborg ME, Hurley SA, Joers V, Tromp do PM, Swanson CR, Ohshima-Hosoyama S, et al. (2014): Titer and product affect the distribution of gene expression after intraputaminal convection-enhanced delivery. *Stereotact Funct Neurosurg*. 92:182-194.
52. Truwit CL, Liu H (2001): Prospective stereotaxy: a novel method of trajectory alignment using real-time image guidance. *Journal of magnetic resonance imaging : JMRI*. 13:452-457.
53. Brodsky EK, Block WF, Alexander AL, Emborg ME, Ross CD, Sillay KA (2011): Intraoperative device targeting using real-time MRI. *Biomedical Sciences and Engineering Conference (BSEC), 2011*, pp 1-4.
54. Grabow B, Block W, Alexander AL, Hurley S, CD R, Sillay K, et al. (2012): Extensible real-time MRI platform for intraoperative targeting and monitoring. *ISMRM Nineteenth Annual Scientific Meeting and Exhibition, poster presentation #1585*. Melbourne, Australia.
55. Grabow BP, Oler JA, Riedel M, Fekete EM, Kovner R, brodsky EK, et al. (2014): Alteration of Molecular Neurochemistry: MRI-guided Delivery of Viral Vectors to the Primate Amygdala. *ISMRM Twenty-First Annual Scientific Meeting and Exhibition, oral presentation #672*. Milan, Italy.
56. Brady ML, Raghavan R, Block W, Grabow B, Ross C, Kubota K, et al. (2015): The Relation between Catheter Occlusion and Backflow during Intraparenchymal Cerebral Infusions. *Stereotact Funct Neurosurg*. 93:102-109.
57. Amaral DG, Bassett JL (1989): Cholinergic innervation of the monkey amygdala: An immunohistochemical analysis with antisera to choline acetyltransferase. *J Comp Neurol*. 281:337-361.

58. Van Pett K, Viau V, Bittencourt JC, Chan RK, Li HY, Arias C, et al. (2000): Distribution of mRNAs encoding CRF receptors in brain and pituitary of rat and mouse. *J Comp Neurol.* 428:191-212.
59. Liang KC, Lee EHY (1988): Intra-Amygdala Injections of Corticotropin Releasing Factor Facilitate Inhibitory Avoidance Learning and Reduce Exploratory Behavior in Rats. *Psychopharmacology.* 96:232-236.
60. Sajdyk TJ, Schober DA, Gehlert DR, Shekhar A (1999): Role of corticotropin-releasing factor and urocortin within the basolateral amygdala of rats in anxiety and panic responses. *Behav Brain Res.* 100:207-215.
61. Tazi A, Dantzer R, LeMoal M, Rivier J, Vale W, Koob GF (1987): Corticotropin-Releasing factor Antagonist Blocks Stress-Induced Fighting in Rats. *Regulatory peptides.* 18:37-42.
62. Heinrichs SC, Pich EM, Miczek KA, Britton KT, Koob GF (1992): Corticotropin-Releasing Factor Antagonist Reduces Emotionality in Socially Defeated Rats Via Direct Neurotropin Action. *Brain Research.* 581:190-197.
63. Rainnie DG, Bergeron R, Sajdyk TJ, Patil M, Gehlert DR, Shekhar A (2004): Corticotrophin releasing factor-induced synaptic plasticity in the amygdala translates stress into emotional disorders. *J Neurosci.* 24:3471-3479.
64. Sajdyk TJ, Gehlert DR (2000): Astressin, a corticotropin releasing factor antagonist, reverses the anxiogenic effects of urocortin when administered into the basolateral amygdala. *Brain Res.* 877:226-234.
65. Jochman KA, Newman SM, Kalin NH, Bakshi VP (2005): Corticotropin-releasing factor-1 receptors in the basolateral amygdala mediate stress-induced anorexia. *Behav Neurosci.* 119:1448-1458.
66. Koob GF, Heinrichs SC (1999): A role for corticotropin releasing factor and urocortin in behavioral responses to stressors. *Brain Res.* 848:141-152.
67. Justice NJ, Yuan ZF, Sawchenko PE, Vale W (2008): Type 1 corticotropin-releasing factor receptor expression reported in BAC transgenic mice: implications for reconciling ligand-receptor mismatch in the central corticotropin-releasing factor system. *J Comp Neurol.* 511:479-496.
68. Swiergiel AH, Takahashi LK, Kalin NH (1993): Attenuation of stress-induced behavior by antagonism of corticotropin- releasing factor receptors in the central amygdala in the rat. *Brain Res.* 623:229-234.
69. Bakshi VP, Kalin NH (2000): Corticotropin-releasing hormone and animal models of anxiety: gene- environment interactions. *Biol Psychiatry.* 48:1175-1198.

70. Kalin NH, Shelton SE, Kraemer GW, McKinney WT (1983): Corticotropin-releasing factor administered intraventricularly to rhesus monkeys. *Peptides*. 4:217-220.
71. Chalmers DT, Lovenberg TW, De Souza EB (1995): Localization of novel corticotropin-releasing factor receptor (CRF2) mRNA expression to specific subcortical nuclei in rat brain: comparison with CRF1 receptor mRNA expression. *J Neurosci*. 15:6340-6350.
72. Rominger DH, Rominger CM, Fitzgerald LW, Grzanna R, Largent BL, Zaczek R (1998): Characterization of [¹²⁵I]sauvagine binding to CRH2 receptors: membrane homogenate and autoradiographic studies. *J Pharmacol Exp Ther*. 286:459-468.
73. Strome EM, Wheler GH, Higley JD, Loriaux DL, Suomi SJ, Doudet DJ (2002): Intracerebroventricular corticotropin-releasing factor increases limbic glucose metabolism and has social context-dependent behavioral effects in nonhuman primates. *Proc Natl Acad Sci U S A*. 99:15749-15754.
74. Kalin NH, Shelton SE, Davidson RJ (2000): Cerebrospinal fluid corticotropin-releasing hormone levels are elevated in monkeys with patterns of brain activity associated with fearful temperament. *Biol Psychiatry*. 47:579-585.
75. Nemeroff CB, Widerlov E, Bissette G, Walleus H, Karlsson I, Eklund K, et al. (1984): Elevated concentrations of CSF corticotropin-releasing factor-like immunoreactivity in depressed patients. *Science*. 226:1342-1344.
76. Austin MC, Janosky JE, Murphy HA (2003): Increased corticotropin-releasing hormone immunoreactivity in monoamine-containing pontine nuclei of depressed suicide men. *Mol Psychiatry*. 8:324-332.
77. Hiroi N, Wong ML, Licinio J, Park C, Young M, Gold PW, et al. (2001): Expression of corticotropin releasing hormone receptors type I and type II mRNA in suicide victims and controls. *Mol Psychiatry*. 6:540-546.
78. Merali Z, Du L, Hrdina P, Palkovits M, Faludi G, Poulter MO, et al. (2004): Dysregulation in the suicide brain: mRNA expression of corticotropin-releasing hormone receptors and GABA(A) receptor subunits in frontal cortical brain region. *J Neurosci*. 24:1478-1485.
79. Merali Z, Kent P, Du L, Hrdina P, Palkovits M, Faludi G, et al. (2006): Corticotropin-releasing hormone, arginine vasopressin, gastrin-releasing peptide, and neuromedin B alterations in stress-relevant brain regions of suicides and control subjects. *Biol Psychiatry*. 59:594-602.
80. Raadsheer FC, van Heerikhuize JJ, Lucassen PJ, Hoogendoijk WJ, Tilders FJ, Swaab DF (1995): Corticotropin-releasing hormone mRNA levels in the paraventricular

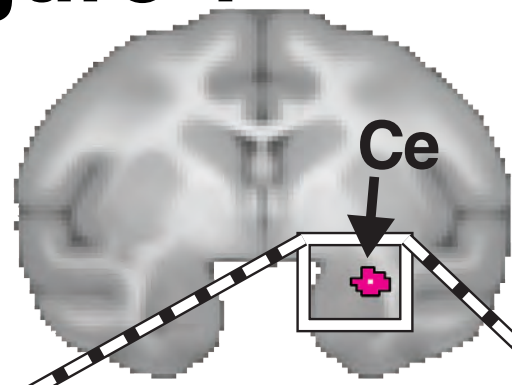
nucleus of patients with Alzheimer's disease and depression. *The American journal of psychiatry*. 152:1372-1376.

81. Flandreau EI, Ressler KJ, Owens MJ, Nemeroff CB (2012): Chronic overexpression of corticotropin-releasing factor from the central amygdala produces HPA axis hyperactivity and behavioral anxiety associated with gene-expression changes in the hippocampus and paraventricular nucleus of the hypothalamus. *Psychoneuroendocrinology*. 37:27-38.
82. Regev L, Tsoory M, Gil S, Chen A (2012): Site-specific genetic manipulation of amygdala corticotropin-releasing factor reveals its imperative role in mediating behavioral response to challenge. *Biol Psychiatry*. 71:317-326.
83. Ghashghaei HT, Hilgetag CC, Barbas H (2007): Sequence of information processing for emotions based on the anatomic dialogue between prefrontal cortex and amygdala. *Neuroimage*. 34:905-923.
84. Kostich WA, Grzanna R, Lu NZ, Largent BL (2004): Immunohistochemical visualization of corticotropin-releasing factor type 1 (CRF1) receptors in monkey brain. *J Comp Neurol*. 478:111-125.
85. Foote SL, Cha CI (1988): Distribution of corticotropin-releasing-factor-like immunoreactivity in brainstem of two monkey species (*Saimiri sciureus* and *Macaca fascicularis*): an immunohistochemical study. *J Comp Neurol*. 276:239-264.
86. Amaral DG, Price JL, Pitkänen A, Carmichael ST (1992): Anatomical organization of the primate amygdaloid complex. In: Aggleton JP, editor. *The Amygdala: Neurobiological Aspects of Emotion, Memory, and mental Dysfunction*. New York: Wiley-Liss, pp 1-66.
87. Price JL, Amaral DG (1981): An autoradiographic study of the projections of the central nucleus of the monkey amygdala. *J Neurosci*. 1:1242-1259.
88. Ray JP, Price JL (1993): The organization of projections from the mediodorsal nucleus of the thalamus to orbital and medial prefrontal cortex in macaque monkeys. *J Comp Neurol*. 337:1-31.
89. Bale TL, Vale WW (2004): CRF and CRF receptors: role in stress responsivity and other behaviors. *Annu Rev Pharmacol Toxicol*. 44:525-557.
90. Koob GF, Zorrilla EP (2012): Update on corticotropin-releasing factor pharmacotherapy for psychiatric disorders: a revisionist view. *Neuropsychopharmacology*. 37:308-309.
91. Coric V, Feldman HH, Oren DA, Shekhar A, Pultz J, Dockens RC, et al. (2010): Multicenter, randomized, double-blind, active comparator and placebo-controlled trial of a corticotropin-releasing factor receptor-1 antagonist in generalized anxiety disorder. *Depress Anxiety*. 27:417-425.

92. Zobel AW, Nickel T, Kunzel HE, Ackl N, Sonntag A, Ising M, et al. (2000): Effects of the high-affinity corticotropin-releasing hormone receptor 1 antagonist R121919 in major depression: the first 20 patients treated. *J Psychiatr Res.* 34:171-181.
93. Binneman B, Feltner D, Kolluri S, Shi Y, Qiu R, Stiger T (2008): A 6-week randomized, placebo-controlled trial of CP-316,311 (a selective CRH1 antagonist) in the treatment of major depression. *The American journal of psychiatry.* 165:617-620.
94. O'Rourke H, Fudge JL (2006): Distribution of serotonin transporter labeled fibers in amygdaloid subregions: implications for mood disorders. *Biol Psychiatry.* 60:479-490.
95. Paxinos G, Huang X, Petrides M, Toga A (2009): *The rhesus monkey brain in stereotaxic coordinates.* 2nd ed. San Diego: Academic Press.

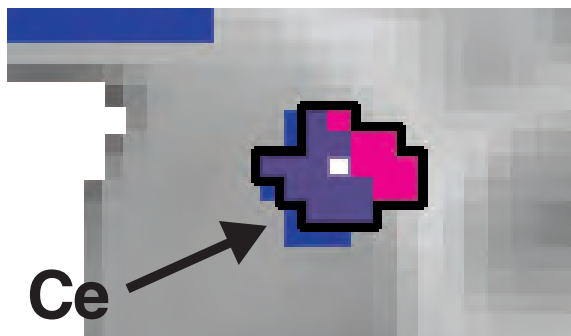
A Figure 1

Peak FDG-PET correlation with AT in Ce

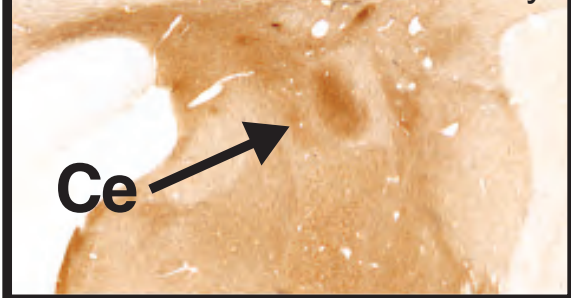


Oler et al., 2010, Nature

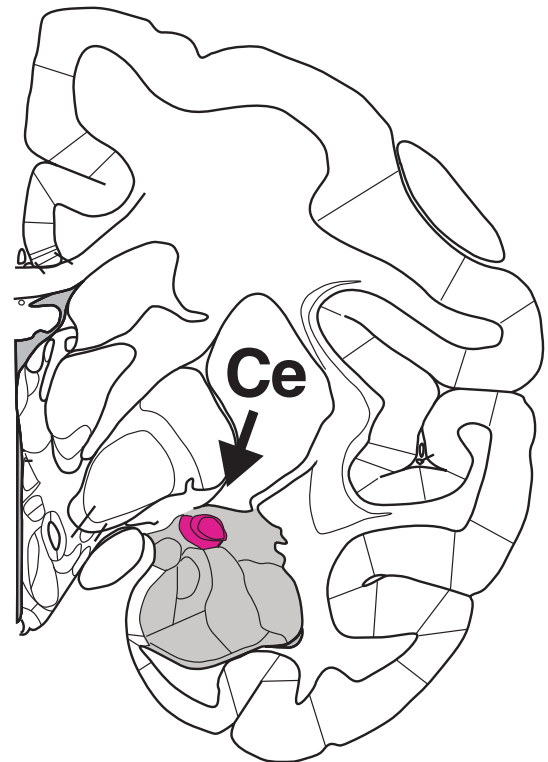
B Ce AT peak pinpointed by *in vivo* 5HTT binding



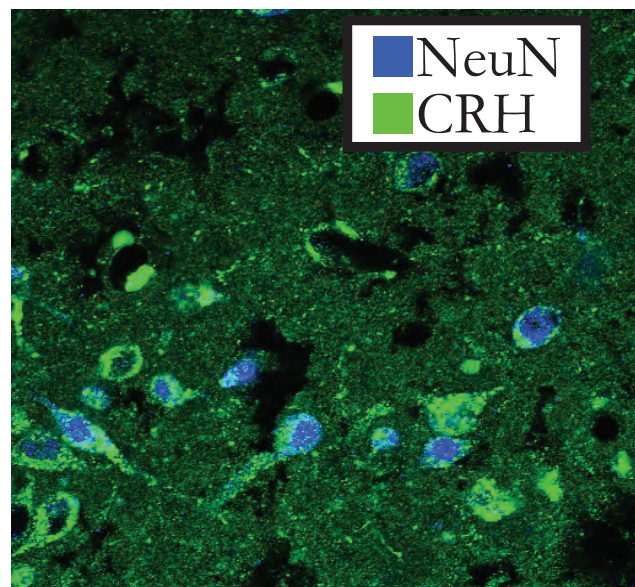
C 5-HTT Immunohistochemistry



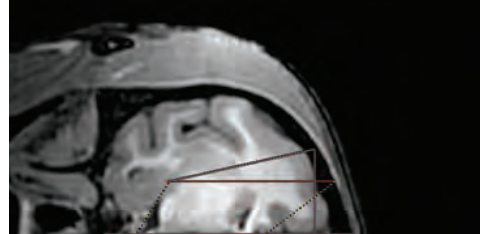
D



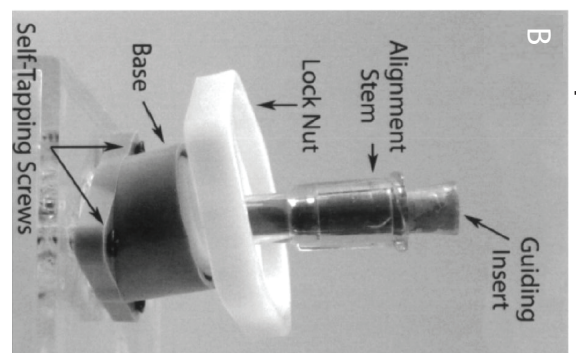
E



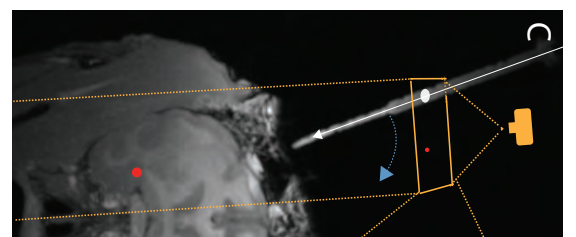
Preoperative targeting



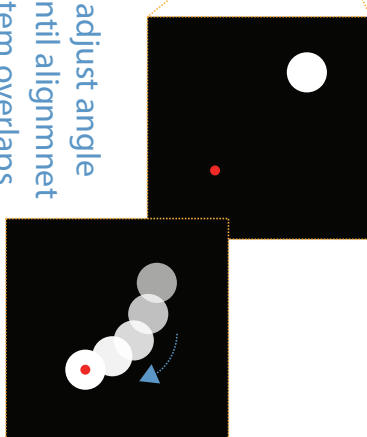
trajectory guide placement



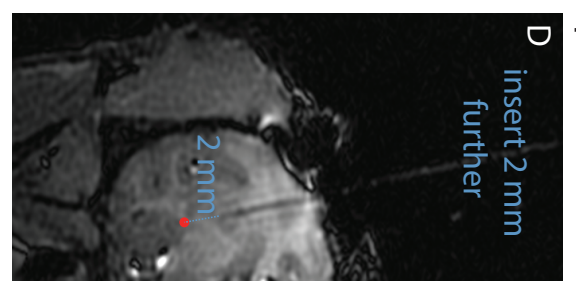
intraoperative trajectory planning



adjust angle until alignment stem overlaps with target



catheter insertion and depth assessment



D
insert 2 mm further

infusion area confirmation



Figure 3

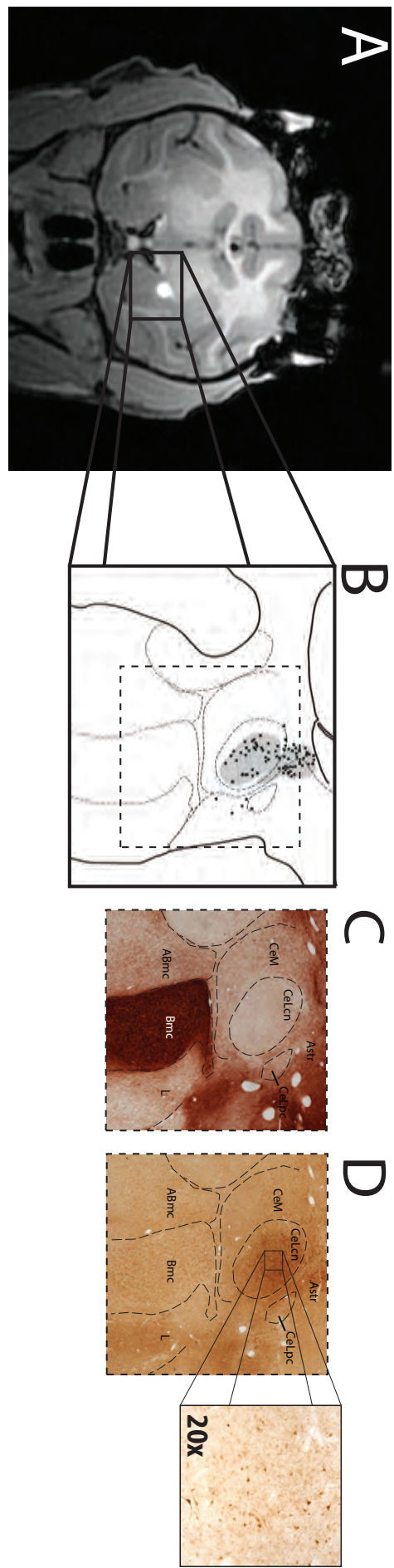


Figure 4

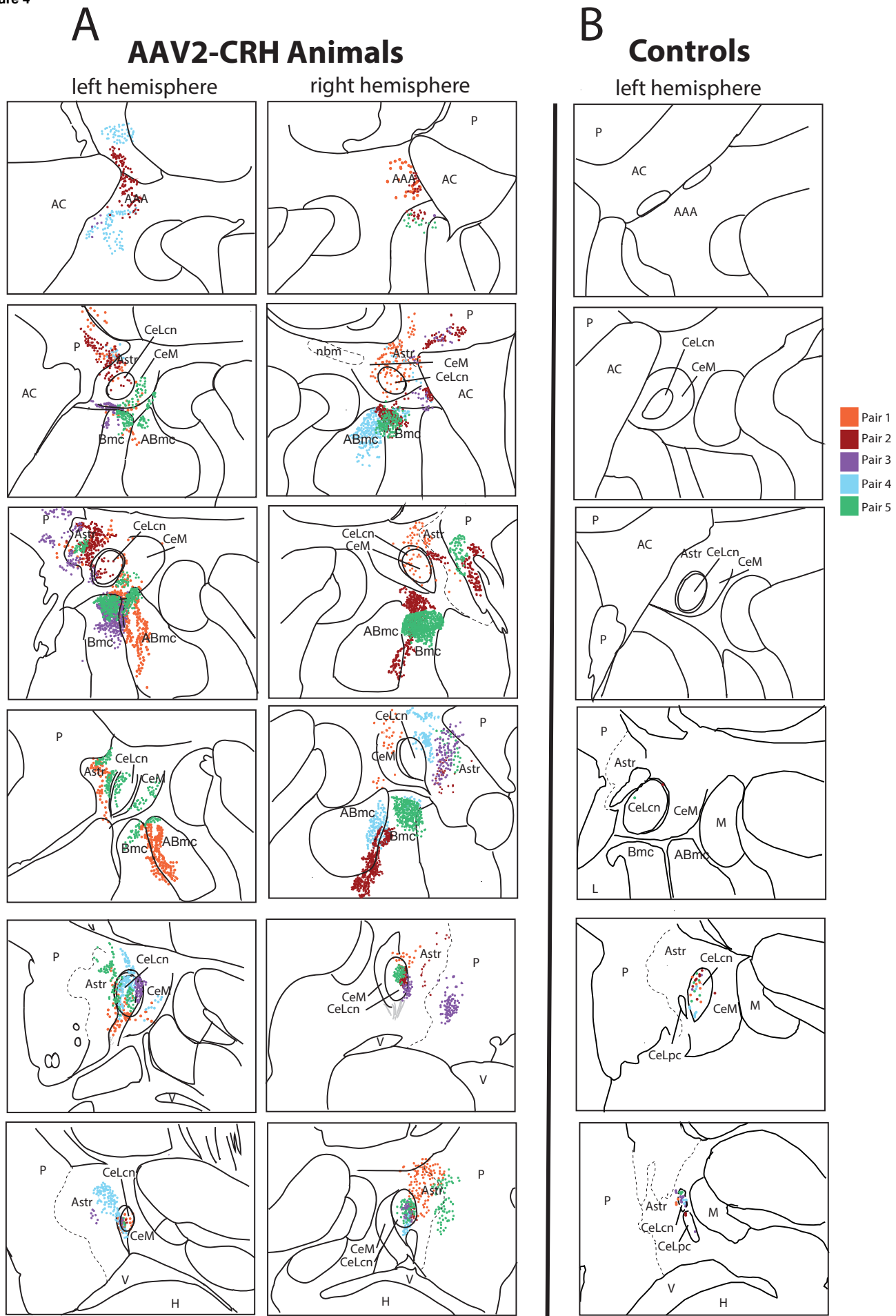


Figure 5

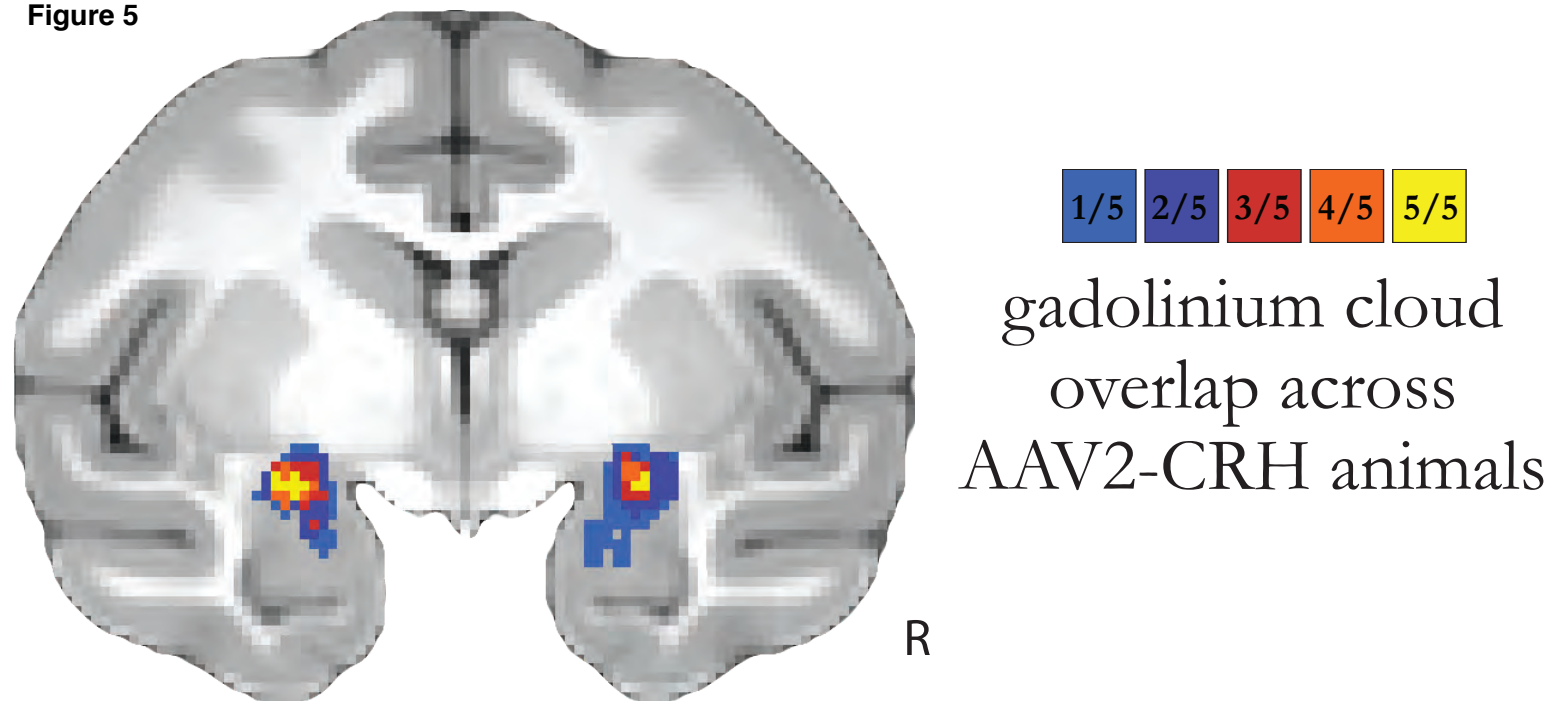


Figure 6

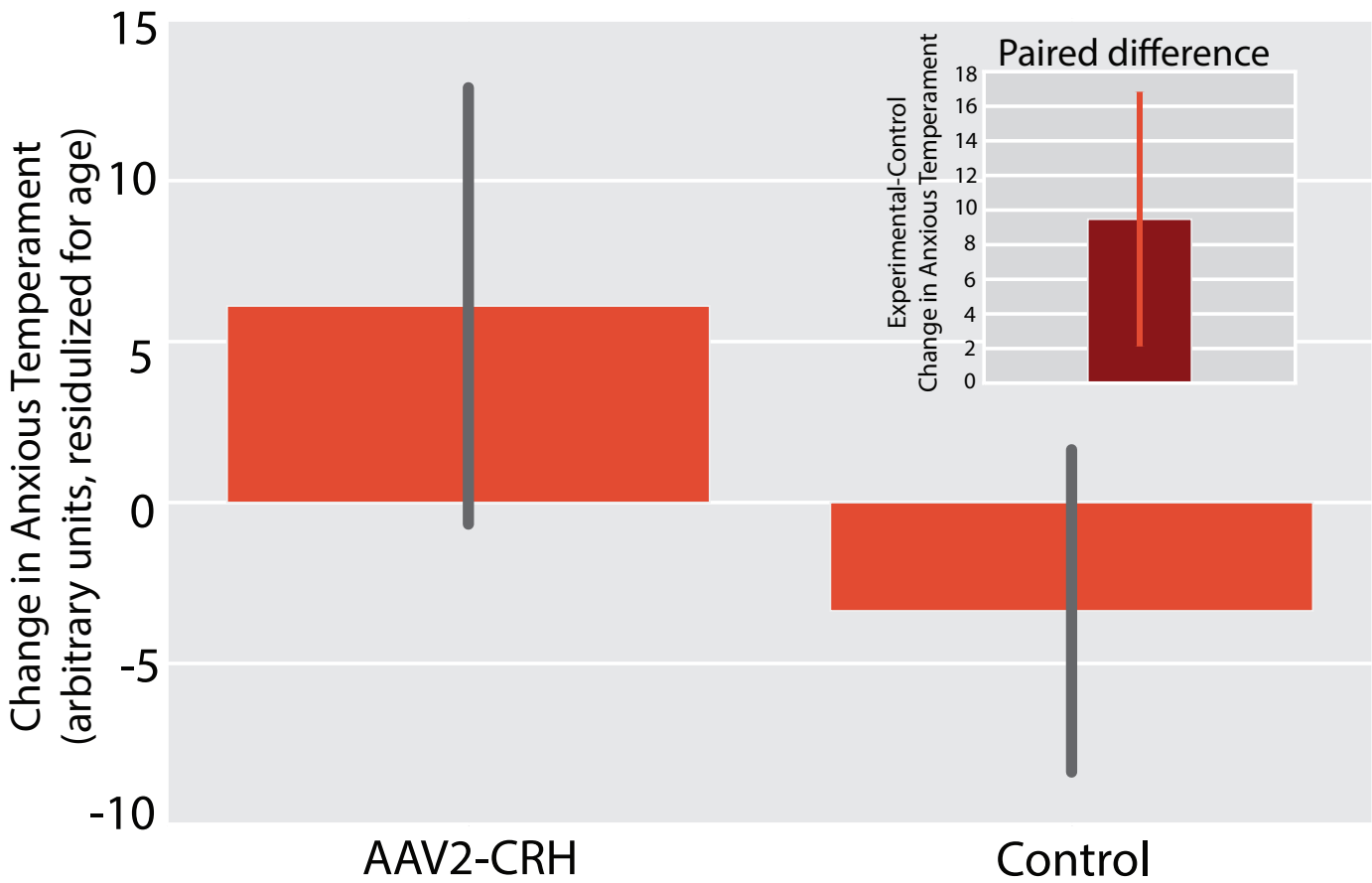
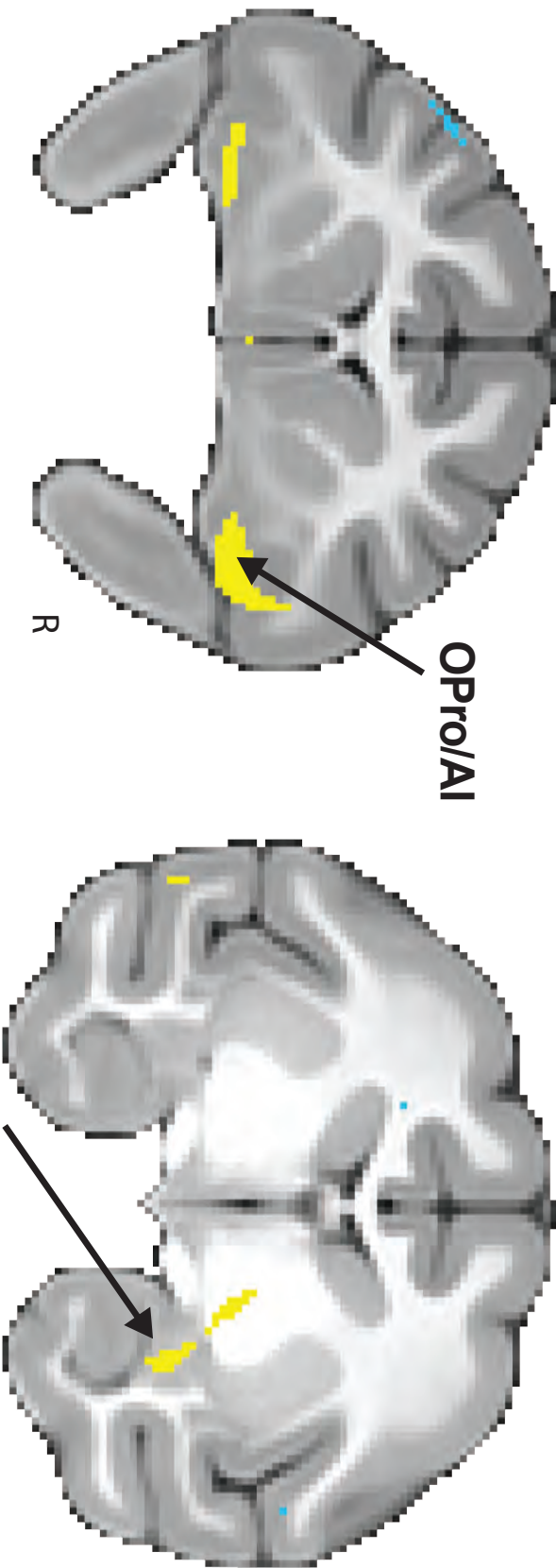


Figure 7

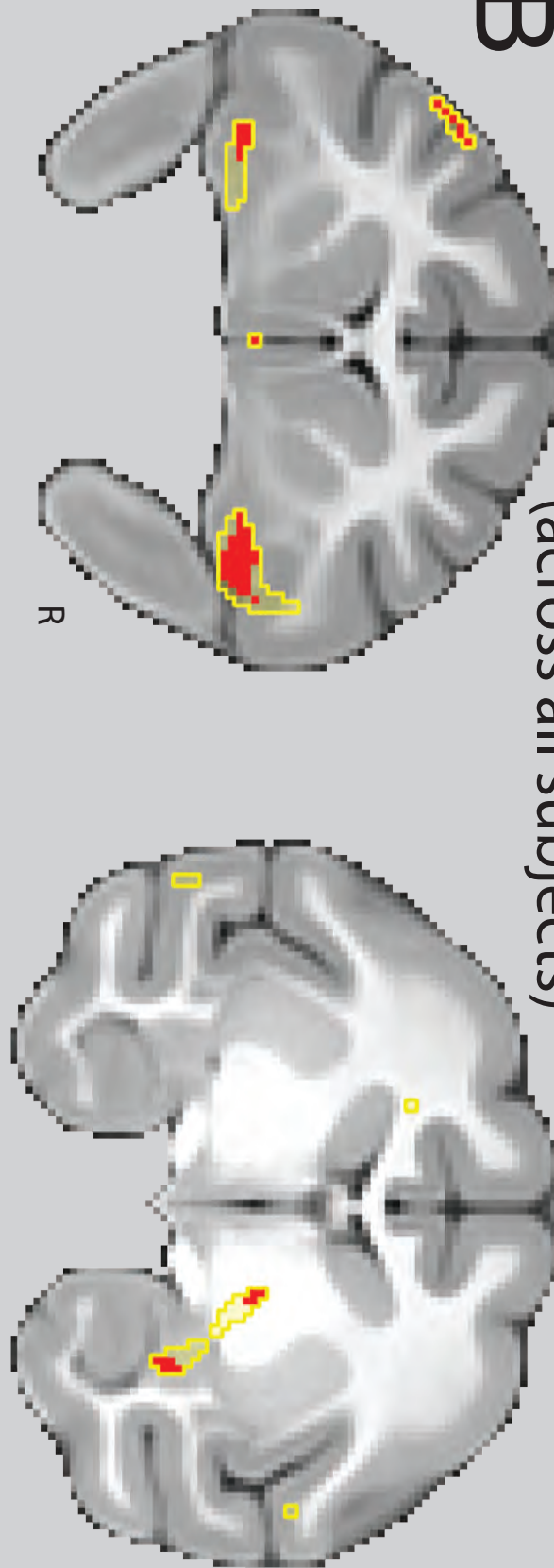
A AAV-2 CRH-related change in brain metabolism

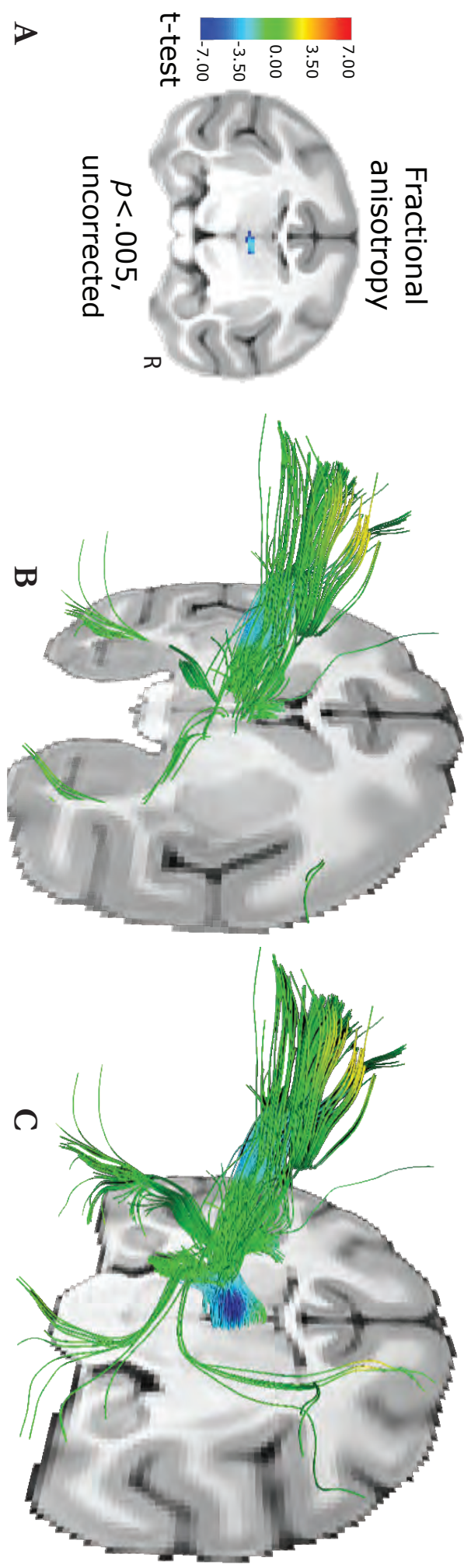


dorsal amygdala

Changes in brain metabolism correlated with changes in AT
(across all subjects)

B





Supplemental Information

[**Click here to download Supplemental Information: supplementFINAL.pdf**](#)

Supplemental information:

Overexpressing corticotropin-releasing hormone (CRH) in primate amygdala increases anxious temperament and alters its neural circuit

Ned H Kalin^{1,2,4}, Andrew S Fox¹, Rothem Kovner^{1,2}, Marissa K Riedel¹, Eva M Fekete¹, Patrick H Roseboom^{1,2}, Do P M Tromp^{1,2}, Benjamin P Grabow³, Miles E Olsen³, Ethan K Brodsky^{3,5}, Andrew L Alexander^{1,3,5}, Marina E Emborg^{2,3,4}, Walter F Block^{3,5}, Julie L Fudge⁶ and Jonathan A Oler¹

¹Department of Psychiatry, ²Neuroscience Training Program, ³Department of Medical Physics, University of Wisconsin, Madison, WI; ⁴Wisconsin National Primate Research Center, Madison, WI; ⁵inseRT MRI, Inc.; ⁶Departments of Neurobiology, Anatomy and Psychiatry, University of Rochester Medical Center.

Corresponding Author:

Jonathan A Oler, PhD
University of Wisconsin School of Medicine and Public Health
Department of Psychiatry
6001 Research Park Boulevard
Madison, WI 53719
e-mail: oler@wisc.edu

SUPPLEMENTAL METHODS AND RESULTS

Visualization of endogenous CRH expressing neurons

To identify Ce neurons that endogenously express CRH (see **Figure 1E** in the main manuscript), tissue sections (40 μ) through the amygdala from one cynomolgus monkey (*Macaca fascicularis*) were incubated in NeuN primary antibody raised in chicken (catalog #AB134014; Abcam, Cambridge, MA), followed by a fluorescently-labeled secondary antibody (Alexa Fluor 647 goat anti-chicken; Life Technologies). Sections were then washed, and treated with an avidin/biotin blocking kit (Vector Laboratories) and CRH-expressing neurons were then double-labelled with the same CRH antibody (catalog # T-4037; Bachem, Torrance, CA) used in the CRH viral vector studies. Sections were then treated with secondary antibody (biotinylated goat anti-rabbit, Vector Laboratories) followed by incubation with streptavidin-conjugated Alexa Fluor 488 (Life Technologies, Grand Island, NY). CRH signal was amplified with a biotinylated anti-streptavidin antibody (Vector Laboratories, Burlingame, CA) followed again by incubation with streptavidin-conjugated Alexa Fluor 488. To aid in localization of the Ce, sections were then incubated with a somatostatin primary antibody raised in mouse (catalog #sc-74556; Santa Cruz Biotechnology, Dallas, TX) followed by secondary antibody (Alexa Fluor 568 donkey anti-mouse; Life Technologies). To dampen the autofluorescence signal, tissue was then treated with the autofluorescence eliminator reagent (EMD Millipore, Billerica, MA). Finally, sections were mounted and cover slipped using ProLong Gold (Life Technologies) and slides were visualized with an A1R confocal microscope (Nikon, Melville, NY) at 20x magnification. Edges of the lateral division of the Ce were identified using the somatostatin stain.

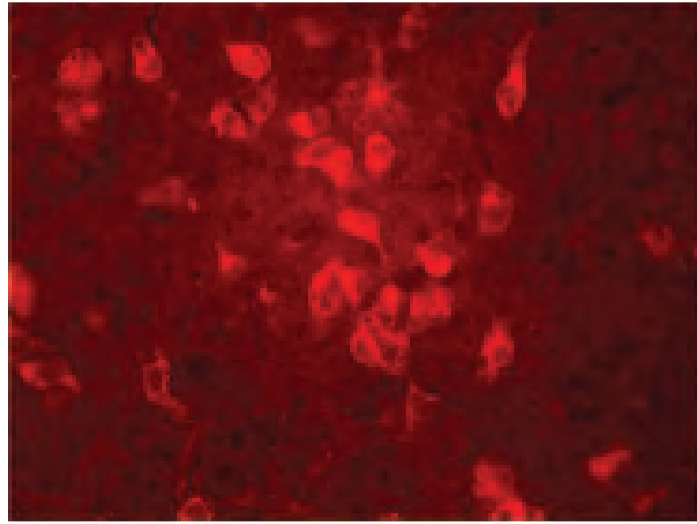
Development and validation of CRH viral vector construct

The DNA sequence corresponding to the entire open reading frame of rhesus prepro-CRH (GenBank accession #XM_001094433.2; bases 327 – 971) was inserted into the AAV2-MCS plasmid (Vector Biolabs, Philadelphia, PA). Expression of CRH from this plasmid was under control of the CMV promoter. In addition, the AAV2-MCS plasmid is thought to enhance expression by inserting an unrelated intronic intervening sequence upstream of the CRH sequence that is spliced out during processing to the mature mRNA.

The effectiveness of the plasmid at directing CRH expression was demonstrated by transfecting HEK-293 cells, followed by immunocytochemical detection of CRH expression using a commercially available CRH antibody produced in rabbit (T-4037; Bachem), followed by a fluorescently-labeled Alexa Fluor 568 conjugated goat anti-rabbit secondary antibody (Life Technologies, Grand Island, NY). CRH immunoreactivity was readily detected in the HEK-293 cells transfected cells (see **Supplemental Figure 1**). The plasmid sequence was then packaged into AAV2 at a titer of 3.1×10^{13} genome copies/ml (Vector Biolabs).

In vivo validation of CRH overexpression in a pilot cynomologus monkey

Using the methods described in the paper and detailed below, the effectiveness of the CRH AAV2 virus to direct CRH over expression *in vivo* was first demonstrated in a pilot monkey. For this study, 12 μ l of the virus solution was infused into two separate locations within the amygdala of a



CRH transfected cells *in vitro*

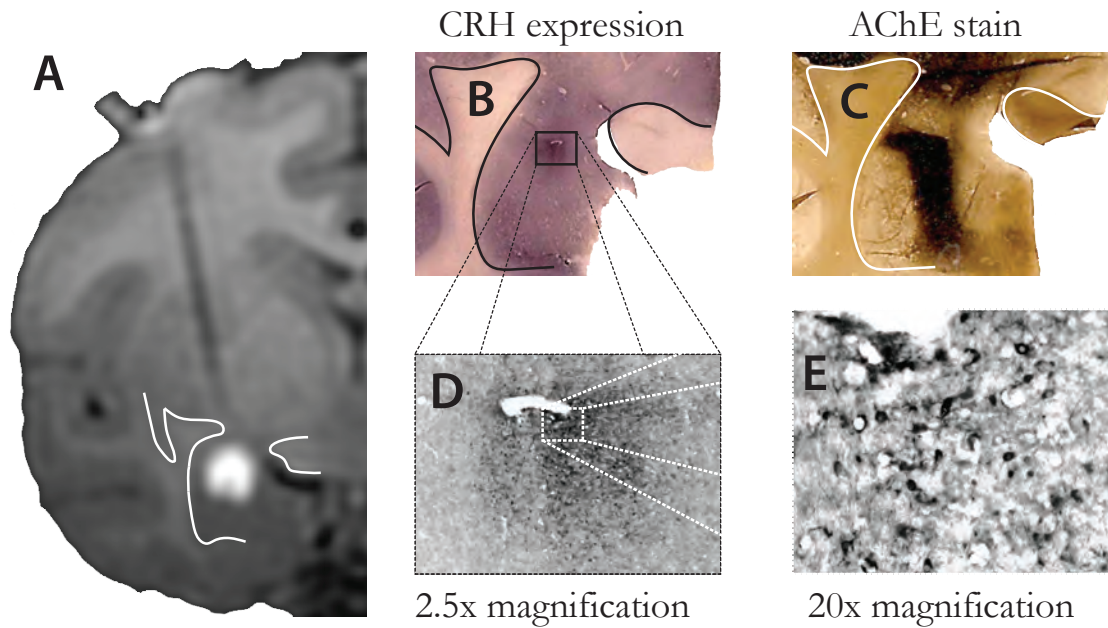
Supplemental Figure 1. Immunocytochemical detection of CRH expression in HEK293 cells transfected with a plasmid directing expression of CRH.

cynomolgus monkey (*Macaca fascicularis*). In this pilot animal, the RT-IMRI along with the *post mortem* analysis revealed that the major locus of infection was in the dorsal part of the basal nucleus, which is directly ventral to the Ce. In addition to establishing infusion parameters, this pilot animal allowed us to refine the targeting procedure. The animal was sacrificed 5 weeks following injection and was perfused with 0.9% heparinized-saline followed by 4% paraformaldehyde (PFA) in phosphate-buffered saline (PBS), pH 7.4. After overnight fixation in 4% PFA, the brain was cut into 14 mm thick slabs, cryoprotected in 20% sucrose/5% glycerol and 40 μ frozen sections were cut through the amygdala on a cryostat (CM3050, Leica Biosystems, Buffalo Grove, IL).

Sections were processed for immunohistochemistry with the same CRH antibody used in the *in vitro* studies. Signal was visualized with goat anti-rabbit biotinylated secondary antibody (Vector Laboratories; Burlingame, CA) using diamino-benzene (DAB) as the chromogen. Acetylcholinesterase (AChE) staining was used to identify the structural details of the amygdala nuclei (1). The method was based on a previously published procedure (2). Immunohistochemical examination of the brain from the pilot animal demonstrated that viral vector containing the CRH construct used with the optimized perfusion parameters effectively increased CRH expression in the infused region of the amygdala. (**Supplemental Figure 2**).

Assessing Behavior and Cortisol as Components of AT

A trained rater, who was blind to monkey group assignment, scored the animals' behavior during the no eye contact condition of the human intruder paradigm (NEC). Freezing was defined as a lack of movement for greater than 3-seconds, and was recorded in seconds



Supplemental Figure 2. RT-IMRI guided infusion of CRH viral vector effectively guides overexpression of CRH in the amygdala. In this pilot animal, the dorsal part of the basal nucleus was the primary region infected. A) Infusion location was verified using real-time imaging by adding gadolinium into the viral vector solution B) CRH expression was verified by staining for CRH. C) AChE staining in a slide adjacent to the CRH section was used to determine the location of amygdalar nuclei. D & E) CRF overexpression at 2.5x, and 20x magnification, respectively.

per 5-minutes of NEC exposure. Mean freezing scores were log-transformed and standardized after covarying for age and sex. Cooing was measured as the number of coo-vocalizations during each 5-min period of NEC-exposure. Mean cooing frequencies were square-root transformed, and standardized after removing the effects of age and sex. Plasma cortisol ($\mu\text{g}/\text{dL}$) was quantified based on samples taken immediately after NEC-exposure. Cortisol was quantified in duplicate using the DPC Coat-a-count radioimmunoassay (Siemens, Los Angeles, CA). Cortisol values were standardized after removing any effects of age, sex, and the time-of-day in which samples were taken. A composite measure of AT (3, 4) was computed as the combination of standardized freezing, cooing and cortisol measures, as in $(Z_{\text{freezing}} - Z_{\text{cooing}} + Z_{\text{cortisol}}) / 3$. Further details on the validation and methods used to assess AT has been previously described (3, 5, 6).

Placement of the Trajectory Guide Base

Before the procedure, the animals were anesthetized with ketamine (up to 20 mg/kg, intramuscular (IM)), prepared for surgery, and then placed in a MRI compatible-stereotaxic frame. The animals were intubated and received isoflurane anesthesia (1–3%, intratracheal (IT)). Atropine sulfate (0.01–0.3 mg/kg, IM) was administered to depress salivary secretion, and buprenorphine (0.01–0.03 mg/kg, IM) was given for analgesia. To maintain fluids and electrolytes, Plasmalyte (up to 10 mg/kg/hr, intravenous (IV)) was administered. Cefazolin (20–25 mg/kg, IM or IV) was administered as a prophylactic antibiotic one day prior to the

surgery. Cefazolin was also administered immediately prior to surgery, and then every 6 hours while under anesthesia. All drugs and treatments were given in consultation with veterinary staff. Vital signs (heart rate, respiration, oxygen saturation, and CO₂) were continuously monitored. Body temperature was monitored during the surgical procedure and maintained by wrapping the animals for warmth. To reduce intracranial pressure and prevent brain swelling, Mannitol (up to 2.0 g/kg, IV) was given as needed. Cefazolin (20-25 mg/kg, IM or IV) or Cephalexin (20-25 mg/kg, oral (PO)) was given twice daily for five days after surgery to prevent infection. The animals were allowed to recover and testing did not commence before 2 months after surgery.

Placement of the MRI-compatible trajectory guide bases followed previously reported methods (see refs (7, 8) for details) modified for Ce targeting. Prior to surgery the 3D T1W MRIs were used to visualize Ce in three planes (sagittal, axial, and coronal) and identify the entry point for the catheter. The anteroposterior (AP) zero plane was identified by visualization of the ear canals. The dorsoventral (DV) zero was defined as the surface of the brain at the site of insertion and the mediolateral (ML) zero was defined as the middle of the sagittal sinus. Based on the three sets of images a target point in the Ce was determined and a trajectory was planned to define the location of the entry at the skull (see **Figure 2A** in the main manuscript). The distance from entry point to target was calculated based on the zero coordinates previously defined, using GE MRI software. Intraoperative MRI guidance of the catheter was performed using a pivot point-based MRI compatible external trajectory guide (Navigus™ brain port, Medtronic Inc., Minneapolis, MN, see **Figure 2B** in the main manuscript). Modifications were made to this system to adapt it for the placement of catheters by the addition of a guiding insert, a customized base to fit the nonhuman primate skull and the addition of a laser alignment pointer that fastens to a micromanipulator. Placement of the MRI-compatible trajectory guide bases was performed in the surgical suite (adjacent to the MRI suite) under sterile conditions. Using stereotactic guidance, 11-12 mm in diameter craniotomies were performed bilaterally at the planned entry points. Each trajectory guide base was mounted on the skull over the craniotomy with three titanium AutoDrive self-tapping screws (OsteoMed, Addison, TX) and dental acrylic. Surgical gelfoam that was moistened with sterile saline was placed over the craniotomies and the bases were capped with sterile plastic base plugs (Navigus).

Catheter Trajectory Planning and Insertion

The animals were transported from the surgical suite to the MRI suite under anesthesia. Sterile conditions were maintained in the MRI suite during viral vector delivery. A 3-inch circular surface coil (MR Instruments, Minneapolis, MN) was positioned above the animal's head, transverse to the main magnetic field, with the Navigus brain port located near the center of the coil. A sterile MR-visible alignment guide was inserted into the trajectory guide base. A high-resolution, volumetric roadmap scan was acquired for later target identification using a 3D IR GRE MRI with a 12° flip angle, 256x224x248 acquisition matrix (0.35x0.35x0.80 mm voxels), 9.1/3.9 ms TR/TE, 450 ms inversion time, 97 Hz/pixel receiver bandwidth, 6.5 minute total acquisition time. The targeting was performed using a platform for

real-time MR-guided prospective stereotaxy (9) that was initially developed by the University of Wisconsin (10-13).

The brain port consists of a MR-visible fluid-filled alignment guide seated in a ball-and-socket pivot joint with two degrees of rotational freedom. The base constrains the guide such that its proximal tip passes the center of the pivot joint, and the distal end of the guide extends away from the skull. After identifying the desired target point in the brain and the location of the pivot point in the high-resolution 3D T1-weighted “roadmap” volume, the prospective stereotaxy tool calculates an “aiming point” outside the skull that is co-linear with the target and alignment guide pivot points and then performs real-time imaging (2D GRE, 384x384 acquisition matrix size, 1 mm slice thickness, 0.52 mm in-plane resolution, 25° flip angle, TR=16 ms, 650 Hz/pixel receiver bandwidth, 6 s/frame) of a plane perpendicular to and centered on the aiming point, allowing the operator to move the alignment guide until its image overlaps with the software-displayed aiming point. Once the alignment guide is in position, the base is locked into place and the catheter can be inserted.

This system is built on top of the RTHawk scanner interface (HeartVista, Palo Alto, CA), which permits the implementation of image-guided interventional procedures (14), and the VURTIGO toolkit (Visual Understanding of Real-Time Image Guided Operations, Sunnybrook Health Sciences Centre; Toronto, Canada), an open-source visualization platform that allows simultaneous display and interaction with multiple 3D and 2D datasets (15). The platform allows the surgeon to align the brain ports used to orient catheters with real-time feedback in an interactive manner (see **Figure 2C** in the main manuscript).

When the trajectory angle (anteroposterior, mediolateral direction) of the fluid-filled alignment guide was confirmed to be on target, the alignment stem was locked into position. The fluid-filled alignment guide was removed, the remote introducer (Navigus) was fastened to the stem, and the guiding insert was placed in the alignment stem. The catheter for the infusion was threaded through the remote introducer and the guiding insert, and was fastened to the remote introducer by a locking mechanism. FEP Teflon infusion lines (IDEX Health & Science, Oak Harbor, WA) were used to connect the catheter via a pressure sensor transducer to a 100 microliter (μ l) Hamilton syringe (Hamilton Company USA, Reno, NV) that was placed in a MRI-compatible syringe pump attached to the control mechanism of a standard Harvard apparatus PHD 2000 (Holliston, MA). Monitoring of the pressure in the infusion line was performed using the infusion pump controller system (Engineering Resources Group, Inc., Pembroke Pines, FL). A computer was connected to the pump controller for infusion protocol programming, and connected to a pressure sensor transducer to monitor infusion line pressure at the pump output port. The infusion line was primed with a loading line solution (Dulbecco's phosphate-buffered saline (D-PBS) without Ca^{2+} and Mg^{2+} with 5% glycerol) and the catheter was loaded with the viral vector containing the CRH construct and Gd. After pressure in the line was stabilized, the catheter was introduced into the brain, advancing the remote introducer at approximately 10-15 mm/minute. The catheter was advanced two-thirds of the measured depth towards the target for partial insertion, and another targeting 3D T1W MRI was performed to confirm the correct trajectory, and calculate the remaining distance from catheter tip to target (see **Figure 2D** in the main manuscript).

Once confirmed, the catheter was advanced to its final position and the stylet was slowly retracted. When the pressure reading on the infusion pump controller system stabilized, the infusion began.

Real-time scan control and visualization was conducted on a high-performance external workstation with two quad-core Intel Xeon E5620, 2.4 GHz CPUs, 12 GB of memory, an NVIDIA GF100 Quadro 4000 graphics card, and dual gigabit Ethernet controllers, running 64-bit Linux. Scanner interface was via an internal Ethernet switch. Visualization display was available on a screen in the control room, which was placed in the scanner room window so that an operator could lean into the bore and reposition the MR-visible fluid-filled alignment guide to the optimal trajectory angle.

The catheter (100mm Valve Tip Catheter, Engineering Resources Group, Inc., Pembroke Pines, FL) was a fused silica cannula with a polyimide tubing tip and was sealed with a retractable glass fiber stylet. Its dimensions were: tip—outer diameter (OD) = 0.40 mm, inner diameter (ID) = 0.345 mm, length = 3.0 mm; shaft—OD = 0.67 mm, ID = 0.45 mm, length = 97.0 mm from ferrule, stylet OD = 0.275 mm.

Different imaging sequences were performed during and immediately following the infusion depending on the intended monitoring goal. For rapid, qualitative monitoring of infusion progression, a time series of images of a single coronal slice containing the target and catheter/infusion track was acquired. The acquisition used a 2D SPGR sequence with 256 x 192 matrix size over a 140 mm FOV, for a resolution of 0.55 x 0.73 mm. The imaging used a slice thickness of 2.5 mm, TR/TE of 33.0/3.8 ms with two signal averages, flip angle of 50°, and a receiver bandwidth of 244 Hz/pixel. This sequence provides primarily infusate/anatomy contrast and allowed for early verification that the infusion was on target and that the infusion was not experiencing significant backflow along the catheter. For a qualitative visualization of the volumetric infusate delivery region, the previously described 3D roadmap was reacquired. This sequence provides sensitivity to the contrast-enhanced infusate and sufficient gray/white contrast for easy identification of the infusion's anatomical location.

The infusate consisted of AAV2-CRH vector in a solution of D-PBS without Ca²⁺ and Mg²⁺ with 5 % glycerol. To facilitate *in vivo* MRI visualization of the infusion, Gd was mixed with the viral vector to reach final concentration 0.66 mM (see **Figure 2E** in the main manuscript). A total volume of 12 μ l was infused at a steady rate of 1 μ l/min per infusion site, for a total of 24 μ l per hemisphere. After each infusion the catheter was removed, and after all infusions were complete the animal was transported back to the surgical suite and the craniotomies were closed in layers.

Details Regarding Imaging Methods

All behavioral (NEC) and brain imaging (FDG-PET, fMRI, and DTI) measures were assessed twice, once before surgery and again approximately 2 months later in the 5 CRH-overexpressing monkeys, and at similar intervals in their 5 matched unoperated controls.

Measuring glucose metabolism using [18-F] deoxyglucose PET

Subjects were exposed to the NEC-context for 30-minutes. Immediately prior to NEC exposure, subjects were restrained in a squeeze cage and received an intravenous injection of FDG. Thus, FDG-uptake occurred in metabolically active cells while animals freely behaved in the NEC context. Following 30-minute exposure to the NEC-context, subjects were anesthetized with a 15mg/kg intramuscular injection of ketamine, and plasma was collected for quantifying cortisol. The animals were intubated and placed in the PET scanner while anesthesia was maintained using 1-3% isoflurane gas. FDG and attenuation scans were acquired using a Siemens Focus 220 microPET scanner. Images were reconstructed using standard filtered-backprojection techniques with attenuation- and scatter-correction. This technique results in FDG-PET scans that represent the integrated brain metabolism throughout each NEC-exposure. FDG-PET images were transformed to standard space as described below, and intensity-normalized with SPAMALIZE (http://psyphz.psych.wisc.edu/~oakes/spam/spam_frames.htm) so that the mean brain value was equivalent across individuals. Each animal's FDG-PET images were aligned to the corresponding Pre/Post T1-anatomical image using a rigid body mutual information warp, and the transformation from T1 to template-space (described below) was then applied to the FDG-PET image. A 6mm FWHM Gaussian smoothing kernel was applied to account for individual differences in brain anatomy and registration.

MRI Acquisition and Analysis

Prior to MRI acquisition, the monkeys were anesthetized with ketamine (15 mg/kg, IM). The animals were placed in a MRI-compatible stereotaxic frame, administered dexmedetomidine (0.015 mg/kg, IM), and scanned for approximately one hour. Heart rate and oxygen saturation were monitored throughout the scan. Ketamine (up to 5 mg/kg, IM) was repeated as needed approximately every 20-40 minutes throughout the scan. At the end of the scan the dexmedetomidine was reversed with atipamezole (0.15 mg/kg, IM) and animals were removed from the scanner and monitored until they fully recovered from anesthesia.

All imaging was performed in a 3-Tesla GE 750 (GE Healthcare; Waukesha, WI) magnetic resonance imaging (MRI) scanner with a HD T/R Quad extremity coil (Invivo Corp, Gainsville, FL). The head was fixed in the sphinx position using a custom stereotaxic frame that fit inside the coil. Whole-brain anatomical images were acquired using an axial T1-weighted 3D inversion recovery prepared fast spoiled gradient recalled scan (IR-FSPGR; inversion time [TI] = 600 ms, repetition time [TR] = 11.45 ms, echo time [TE] = 5.4 ms, flip angle α = 10°, number of excitations [NEX] = 2, field of view [FOV] = 140 x 140 mm, matrix = 512 x 512, in-plane resolution = 0.27 mm, slice thickness/gap = 0.5/0 mm, 248 slices). Resting-state functional MRI's were acquired using an echo planar imaging sequence (EPI; TR/TE = 2000/25 ms, α = 90°, NEX = 1, FOV = 140 x 140 mm, matrix = 64 x 64, in-plane resolution = 2.19 mm, slice thickness/gap = 3.1/0.5 mm, 26 interleaved slices). Diffusion weighted imaging was performed using a two-dimensional, echo-planar, spin-echo sequence (TR/TE = 10000/85.3 ms, NEX = 1, FOV = 144 x 144 mm, matrix = 256 x 256, in-plane voxel

dimension = 0.56 x 0.56 mm², slice thickness/gap = 1.3/0 mm, 68 interleaved slices, echo-planar spacing = 816 µs. Diffusion-weighted imaging ($b = 1000 \text{ s/mm}^2$) was performed in 72 non-collinear directions with 6 non-diffusion weighted images). Images were acquired in the coronal plane through the entire monkey brain. A co-planar field map was also obtained using a gradient echo with images at two echo times: TE1 = 7 ms, TE2 = 10 ms.

Study-specific template creation and individual-subject registration

All pre-processing was performed using well-established methods for rhesus neuroimaging data (3, 5, 16-21). Prior to spatial normalization, T1 images were manually segmented into brain and non-brain tissue using SPAMALIZE. T1-brain images were then transformed to standard space (methods described below), and transformation parameters were saved. Study-specific T1-anatomical template creation was performed using an iterative procedure using Advanced Normalization Tools (ANTS; <http://sourceforge.net/projects/advants>; (22, 23). First, each subject's two T1-anatomical images were aligned to each other, and averaged to create a subject-specific average. Then, each subject's T1-anatomical average was aligned using a non-linear symmetric diffeomorphic image registration in ANTS to a predefined template-space (18) that was created from 592 T1-MRI images from young rhesus monkeys. Nonlinear registration was performed using a symmetric diffeomorphic image registration and a .25 gradient step-size; a pure cross correlation cost-function with window radius 2 and weight 1; the similarity matrix was smoothed with sigma=2; and this process was repeated at 4 increasingly fine levels of resolution with 30, 20, 20, and 5 iterations at each level respectively. The average of T1's in 'standard-space' was computed and taken to be the study-mean. Similarly, the non-linear deformation-field was also averaged and taken to be the deformation-mean. The deformation-mean was inverted and 15% of this deformation was applied to the study-mean, to obtain the first iteration of the study-specific template. To maintain comparability to other studies, and to printed brain atlases, the affine transformation was *not* inverted and applied to the study-mean. The same procedure was preformed aligning each subject's T1-anatomical images to the initial study-specific template. After averaging the images and deformations, a new study-specific template was created by applying 15% of the newest mean-deformation to the newest study-mean. This process was repeated 4 times, to obtain a final study-specific template. Each subject's original T1-anatomical images were then aligned to this study-specific template by combining the subject-specific and study-specific deformations. This procedure resulted in T1 images in standard space, along with corresponding deformations that could be applied to other modalities.

fMRI analytic methods

Intrinsic functional connectivity was assessed with previously published methods (16, 20). fMRI scans were performed using methods modified from prior work demonstrating the reliability of collecting resting fMRI data in anesthetized rhesus monkeys (24). All fMRI processing steps were carried out in AFNI (25), unless otherwise indicated. Resting state scans were slice timing and motion corrected, had the first 4 frames removed, and were

adjusted for field inhomogeneities with a field map correction. The preprocessed resting state scans were aligned to standard space using the deformations derived from the anatomical scans. In order to reduce the influence of non-neuronal fluctuations on functional connectivity estimates, average signal intensity time courses from the white matter and cerebrospinal fluid were regressed out of the EPI time series (26). The residualized resting state signal was further processed with a temporal bandpass filtering (low=0.01Hz high=0.1Hz).

We employed a standard *a priori* seed-based approach to quantifying group differences in intrinsic functional connectivity. The seed region was defined as the conjunction of the overlapping gadolinium infusion area within the dorsal amygdala (see yellow region in Figure 5 in the main manuscript), and the region of dorsal amygdala demonstrating significant CRH-induced change in brain metabolism (see Figure 7A in the main manuscript). For each subject, the BOLD time series was averaged across the voxels defining the seed, and a voxelwise temporal correlation between the extracted EPI time-series and the times-series throughout the rest of the brain was performed. Correlation maps were normalized (Fisher's *r*-to-*z* transformation) and spatially blurred with a 6mm FWHM Gaussian smoothing kernel. These images were used in voxelwise analyses to identify AAV2-CRH associated alterations in dorsal amygdala functional connectivity as described in the statistical analyses section below.

DTI analytic methods

DTI analysis included distortion corrections using FSL's tools for eddy and field distortions (27). Tensors were estimated using a robust estimation of tensors by outlier rejection (RESTORE, as implemented in Camino software; (28)). This method has been proven to increase reliability of the tensor estimation (29). Because standard intensity-based registration based on the T1-anatomical images does not preserve tensor orientation, tensor images were normalized using a high-dimensional registration method that incorporates the tensor orientation (DTI-TK (30)). This procedure is nearly identical to the iterative ANTS-procedure described above; with the exception that the alignment between scans was determined based on the tensor orientation as opposed to image intensity. The result of this procedure was a study-specific tensor-based template based on multiple registration iterations, and corresponding study-specific template-space tensor images for each scan. To ensure that DTI data were in the same space as other neuroimaging modalities, a final rigid-body transformation was performed to align the study-specific DTI template with the study-specific T1 template, and this transformation was applied to individual images to obtain standard-space tensor images. The resulting standard-space DTI images were used to quantify the local diffusion parameters: fractional anisotropy (FA), mean diffusivity (MD), axial diffusivity (AD) and radial diffusivity (RD). Images were smoothed with a 6mm FWHM Gaussian smoothing kernel. Peak region of significance resulting from analysis of FA was used as a seed for deterministic fiber tractography (see **Figure 8B** in the main manuscript), using Camino software (28).

Statistical analysis

The effects of CRH on neuroimaging measures was assessed using voxelwise paired-sample t-tests (CRH group _(post-pre) – Control group _(post-pre)) using fMRIStat (<http://www.math.mcgill.ca/keith/fmristat/>). To account for potential confounds, all regressions entered the variable age as a covariate. Whole-brain statistical analyses were performed on FDG-PET, resting fMRI, and DTI measures, and thresholded using a p<.01, two-tailed uncorrected statistical threshold. Follow-up across-group analyses of the FDG-PET data in relation to AT were thresholded at p<.05, two-tailed uncorrected.

CRH immunocytochemistry performed in Fudge laboratory

Approximately 1 year after AAV2 infusions, animals were euthanized by transcardiac perfusion with 0.9% heparinized-saline followed by 4% paraformaldehyde (PFA) in phosphate-buffered saline (PBS), pH 7.4. The brains were extracted and fixed overnight in 4% PFA, and were then put through an increasing gradient of sucrose (10%, 20% and 30%) followed by sectioning at 40 µm on a freezing microtome. All sections were stored in cryoprotectant solution (30% ethylene glycol and 30% sucrose in 0.1 M phosphate buffer, pH 7.2) at -20 °C. CRH expression was assessed by CRH immunoreactivity with the same commercial CRH antibody (Peninsula Labs, made in rabbit; 1:6000) used for the *in vitro* validation of the CRH viral vector construct described above (and see below for further details). Signal was visualized with biotinylated anti-rabbit secondary antibody and avidin-biotin reaction (Vector Laboratories). 1:12 sections through the brain were immunostained for CRH. Sections were mounted on subbed slides, dehydrated in an increasing gradient of alcohols, cleared in xylene for 45 minutes, and coverslipped with Permount (Sigma, St Louis, MO).

The antibodies used for detection of CRH (anti-CRH, gift of Dr. John Olschowska and anti-CRH, Peninsula Labs; T-4037, both made in rabbit), were previously characterized in rodents (31, 32). The commercial antibody is the same one used in all the above studies, and the Olschowska antibody is made against the ovine peptide (33). After determining the best dilution for each antibody, we examined the distribution of labeled cells and fibers in the central nucleus, bed nucleus of the stria terminalis, and PVN in the monkey resulting from each antibody, and found the labeling pattern to be equivalent between antibodies. We also compared labeling in the *Macaca mulatta* and *Macaca fascicularis*, and found the distribution of labeled cells and fibers in these structures to be similar between the species. Finally, we examined the distribution of labeled cells in sections immunoreacted with antibody to sections labeled for CRH mRNA using *in situ* hybridization (R. Kovner 2014, unpublished observations), and found a similar distribution of cells through the rostrocaudal extent of the Ce as was observed with immunocytochemistry.

Measuring CRH levels in cerebrospinal fluid

A radioimmunoassay established in our laboratory with an antibody (rC68 – 5/31/83 bleed) generously provided by Dr. Wylie Vale (Salk Institute for Biological Studies, La Jolla, CA) was used as previously described (34). All samples were run in triplicate in a single assay.

Supplemental Table 1. significant peaks in the FDG_PET analysis

clusters demonstrating significant [CRH(post-pre) – Control(post-pre)] interaction			Local maxima for distinct brain regions within clusters			Location relative to anteriro commissure			
Direction of effect	Hemisphere	Cluster	Cluster volume (mm ³)	Regions within cluster	Maximum t-value	p-value	x	y	z
Positive effect	Right	posterior hippocampus / visual cortex / pulvinar	296.63 posterior hippocampus / visual cortex / pulvinar	V1	55.78	6.34E-06	15.000	-15.625	-4.375
				WM dorsal to hippocampus	19.89	1.39E-04	13.750	-23.125	1.875
	Crosses midline	prefrontal cortex	261.47 orbitofrontal cortex (Area 13W)	anterior pulvinar boarding on the WM	15.99	2.66E-04	16.875	-10.625	-3.750
				ventromedial prefrontal cortex (Area14M)	12.04	6.17E-04	10.625	-11.875	5.625
				posterior orbitofrontal cortex (Area 47O) / OPro	64.07	4.19E-06	-13.750	13.750	0.625
				orbitofrontal cortex (Area 14O)	46.70	1.08E-05	0.625	18.750	-1.250
			100.34 dorsal amygdala / external globus pallidus	frontopolar cortex (Area10)	35.18	2.53E-05	-17.500	10.000	-3.125
				ventrolateral prefrontal cortex (Area47)	21.83	1.05E-04	-3.125	15.625	-1.250
				dorsal amygdala (Ce region) / putamen	16.70	2.34E-04	-15.625	19.375	5.000
				external globus pallidus	109.53	8.39E-07	-12.500	-1.250	-6.875
Left	Right	dorsal amygdala / globus pallidus	62.01 Area 13M	46.08	1.13E-05	-7.500	-0.625	-1.250	
				orbitofrontal cortex	52.80	7.48E-06	12.500	13.750	0.000
				cerebellum	40.08	1.71E-06	0.000	-19.375	-11.875
				anterior temporal lobe	27.83 temporopolar cortex	26.66	5.79E-05	-13.125	6.250
				mid-cingulate cortex	22.22 cingulate sulcus (Area23C)	15.54	2.89E-04	6.875	-6.250
	Left	mid-cingulate cortex / visual cortex	20.75 ventral V4	20.75 ventral V4	110.18	8.24E-07	-10.000	-18.125	-6.875
				ventral V3	13.03	4.88E-04	-6.250	-19.375	-4.375
				ventral temporal cortex	19.53 temporal area TL (36R)	18.95	1.60E-04	-16.250	-9.375
				superior temporal gyrus	11.23 superior temporal sulcus area 1 (ST1)	24.62	7.35E-05	26.250	1.250
				temporopolar protoscorortex (TPPro)	7.01	2.98E-03	23.125	4.375	-11.250
Negative effect	Left	posterior parietal lobe	73.00 dorsal V4	dorsal parietal area PG	-53.39	7.24E-06	-18.750	-25.625	14.375
				dorsal parietal cortex	-36.76	2.21E-05	-20.625	-24.375	13.125
				V2	-16.03	2.64E-04	-11.250	-28.750	18.750
				temporoparietal area	-7.65	2.32E-03	-8.125	-35.625	16.875
				left somatosensory cortex	-6.00	4.64E-03	-23.750	-20.625	10.000
	Right	posterior frontal lobe / frontal lobe	16.11 S2 / Area3b	14.89 Area 8A	-37.89	2.02E-05	-25.000	-3.125	4.375
				frontal lobe	-14.33	3.68E-04	-18.750	3.125	13.750
				8.30 Area 8A / principal sulcus	-12.20	5.92E-04	18.750	8.750	14.375

WM, white matter; OPro, orbital protoscorortex

Supplemental Table 2. significant peaks in the $\Delta\Delta T - \Delta PET$ correlation

Direction of effect	Clusters demonstrating significant [$[CRH(\text{post-pre}) - \text{Control}(\text{post-pre})]$] interaction	Cluster	Cluster volume (mm^3)	Local maxima for distinct brain regions within clusters			Location relative to anterior commissure		
				Regions within cluster	Maximum t-value	p-value	x	y	z
Positive	Right	posterior hippocampus / inferior pulvinar / parahippocampal gyrus	58.35	inferior pulvinar / parahippocampal gyrus	6.85	3.19E-03	10.625	-14.375	-3.125
	Left	orbitofrontal cortex	50.05	WM dorsal to hippocampus	5.30	6.54E-03	17.500	-13.125	-4.375
				Area 13M	6.38	3.90E-03	-16.875	8.125	-3.125
				temporopolar/priocortex	6.12	4.39E-03	-10.000	15.000	1.250
				gustatory cortex	5.77	5.18E-03	-19.375	8.125	-4.375
				Right	4.07	1.34E-02	-21.250	8.125	-1.250
				orbitofrontal cortex	4.04	4.55E-03	13.125	16.875	2.500
				posterior hippocampus	7.01	2.98E-03	-16.250	-12.500	-8.125
				cerebellum / pons	5.41	6.18E-03	-0.625	-20.000	-13.750
				temporal cortex	6.11	4.41E-03	-16.875	-8.125	-15.000
				globus pallidus	6.69	3.41E-03	-7.500	-2.500	0.625
				dorsal amygdala	6.90	3.12E-03	-13.125	3.125	-5.625
	Right	caudate / claustrum / ventral pulvinar	9.28	claustrum	6.75	3.32E-03	11.875	-9.375	6.250
	Left	ventromedial prefrontal cortex	9.03	Area 14O	6.24	4.15E-03	-1.250	18.125	-0.625
Negative	Left	visual cortex	10.25	V4D	-6.75	3.33E-03	-9.375	-32.500	18.125
	Left			V2	-5.30	6.57E-03	-7.500	-35.625	16.875

BLD, basal nucleus of the amygdala, dorsal part; IPAC, interstitial nucleus of the posterior limb of the anterior commissure, AA, anterior amygdala area; V4D, visual area V4, dorsal part

Supplemental Table 3. significant peaks in the functional connectivity analysis

Clusters demonstrating significant [CRH (post/pre) – Control (post/pre)] interaction Direction of Hemisphere effect	Cluster	Cluster volume (mm ³)	Local maxima for distinct brain regions within clusters				Location relative to anterior commissure		
			Regions within cluster	Maximum t-value	p-value	x	y	z	
Positive Right	posterior orbitofrontal cortex	53.96	Oro / Al	129.44	5.08E-07	12.500	7.500	-4.375	
Left	dorsal amygdala	49.56	anterior amygdalar nucleus/ medial nucleus	22.35	9.80E-05	8.125	1.250	-6.875	
Left	cerebellum	39.31	cerebellum	9.77	1.14E-03	-5.000	-30.000	-9.375	
Left	globus pallidus / thalamus	37.35	ventral anterior thalamic nucleus	53.90	7.03E-06	-5.000	-5.000	1.875	
Left	posterior orbitofrontal cortex	34.91	Oro / Al	18.85	1.63E-04	-11.875	8.125	-6.875	
Right	prefrontal cortex	10.01	WM ventral to Area8B	8.95	1.47E-03	7.500	13.750	15.625	
Negative Left	temporal cortex	184.81	superior temporal sulcus	-73.45	2.78E-06	-17.500	-0.625	-10.000	
			Area TE	-23.23	8.74E-05	-18.125	1.250	-16.250	
Right	visual cortex	105.47	temporopolar proisocortex (TPPro)	-20.26	1.31E-04	-21.250	5.000	-11.250	
Right	anterior temporal lobe	95.70	WM lateral to ventral putamen	-78.90	2.24E-06	18.750	-33.750	5.625	
			Area TE	-56.24	6.19E-06	16.875	-2.500	-7.500	
			LGN / WM dorsal to hippocampus	-31.51	3.51E-05	21.250	-5.625	-16.875	
			superior temporal sulcus	-24.06	7.87E-05	13.750	-7.500	-6.250	
				-6.58	3.57E-03	21.875	-5.625	-11.875	
Right	temporoparietal WM	85.45	deep WM of superior temporal gyrus	-51.24	8.19E-06	16.875	-15.000	2.500	
			WM ventral to intraparietal sulcus	-18.78	1.65E-04	10.625	-15.000	10.000	
Right	visual cortex	79.10	V1	-96.53	1.23E-06	13.125	-41.875	7.500	
Left	posterior ventral temporal lobe / cerebellum	59.57	cerebellum	-34.91	2.58E-05	-11.875	-18.125	-8.750	
Left	brain stem	19.29	posterior hippocampus	-32.09	3.32E-05	-15.625	-17.500	-4.375	
Left	mid-hippocampus / ventral putamen	16.85	cerebral peduncle	-14.19	3.79E-04	-5.000	-16.250	-10.000	
Left	parietal cortex	16.60	WM dorsal to hippocampus	-41.15	1.58E-05	-15.000	-7.500	-5.625	
Right	striatum	8.79	opercular part of parietal Area PG	-21.56	1.09E-04	-20.625	-20.000	13.125	
			lateral putamen	-30.80	3.76E-05	17.500	-1.250	3.125	

AI, anterior insular cortex; WM, white matter; OPro, orbital proisocortex; LGN lateral geniculate nucleus

Supplemental Table 4. significant peaks in the DTI analysis (MD)

Clusters demonstrating significant [CRH (post-pre) – Control (post-pre)] interaction		Local maxima for distinct brain regions within clusters		location relative to antero commissure					
Direction of effect	Hemisphere	Cluster	Cluster volume (mm ³)	Regions within cluster	Maximum t-value	p-value	x	y	z
Positive	Left	visual cortex	61.52 V1		38.74	1.89E-05	-4.375	-39.375	6.875
				V2	11.98	6.22E-04	-8.125	-33.750	6.250
	Right	caudate / septum / stria terminalis / fornix	55.18 lateral septum / caudate		20.34	1.30E-04	2.500	1.875	5.000
	Left	cerebellum	33.20 cerebellum		62.99	4.41E-06	-5.625	-17.500	-11.250
	Right	visual cortex	32.47 dorsal V4 / TEO		23.81	8.12E-05	28.750	-23.125	-0.625
	Left	parietal cortex	17.58 PGOp		26.33	6.01E-05	-25.000	-16.875	13.750
	Right	precuneus	16.36 PGM		19.18	1.55E-04	1.250	-30.000	16.875
	crosses the midline	cerebellum	16.11 cerebellum		10.90	8.26E-04	2.500	-25.625	-10.625
	Left	visual cortex	10.74 V2		15.40	2.97E-04	-18.750	-33.125	9.375
	Right	ventral temporal cortex	9.77 superior temporal gyrus		23.11	8.87E-05	27.500	-5.000	-10.625
Negative	Right	frontal cortex	296.14 Area 8A, dorsal part		-109.75	8.34E-07	15.000	9.375	19.375
	Right	visual cortex	10.25 V1	Area 9 / Area 46, dorsal part	-6.16	4.31E-03	16.250	15.625	13.750
	Right				-43.81	1.31E-05	3.750	-46.875	-3.125

TEO, temporal area TE, occipital part; PGOp, parietal area PG, opercular part; PGM parietal area PG, medial part

Supplemental Table 5. significant peaks in the DTI analysis (RD)

Clusters demonstrating significant [CRH (post-pre) – Control (post-pre)] interaction		Cluster (mm ³)	Local maxima for distinct brain regions within clusters			Location relative to anterior commissure		
Direction of effect	Hemisphere		Regions within cluster	Maximum t-value	p-value	x	y	z
Positive	Right	caudate / septum / stria terminalis / fornix	231.93 lateral septum / caudate	51.77	7.94E-06	2.500	1.250	5.000
			WM dorsal to putamen	25.29	6.78E-05	13.125	-5.000	9.375
			caudate / internal capsule	19.46	1.48E-04	10.000	-3.125	7.500
	Left	visual cortex	55.18 V1	24.35	7.59E-05	-4.375	-38.750	7.500
			V2	8.28	1.88E-03	-8.125	-32.500	5.625
Right		dorsal thalamus	52.25 ventral lateral thalamic nucleus	12.26	5.85E-04	8.125	-6.875	6.875
Left		cerebellum	29.05 cerebellum	18.33	1.77E-04	-5.625	-17.500	-8.750
		cerebellum	26.86 cerebellum	15.41	2.97E-04	5.000	-25.625	-11.875
	Left	motor cortex	26.12 Area 4	17.84	1.92E-04	-17.500	-1.250	15.000
			Area 6	10.22	9.99E-04	-16.875	1.875	14.375
Left		visual cortex	18.80 V2	22.85	9.18E-05	-18.750	-33.125	9.375
Right		prefrontal cortex	15.87 Area 47	36.75	2.22E-05	18.750	23.750	6.875
Right		precuneus	14.65 PGV	18.89	1.62E-04	0.625	-30.625	17.500
Right		cerebellum	13.43 cerebellum	30.69	3.80E-05	5.000	-30.000	-20.000
Right		motor cortex	13.18 Area 6	9.92	1.09E-03	16.875	20.625	
Right		temporal cortex	8.30 superior temporal gyrus	26.17	6.12E-05	27.500	-5.000	-11.250
Negative	Right	frontal cortex	260.50 Area 8	-80.34	2.13E-06	13.125	15.625	16.875
	Right	visual cortex	9.77 V1	-43.70	1.32E-05	3.750	-46.875	-3.125

WM, white matter; PGV parietal area PG, medial part

Supplemental Table 6. significant peaks in the DTI analysis (ΔD)

Direction of effect	Clusters demonstrating significant [CRH (post-pre) – Control (post-pre)] interaction		Cluster volume (mm ³)	Local maxima for distinct brain regions within clusters			Location relative to anterior commissure		
	Hemisphere	Cluster		t-value	Maximum p-value	x	y	z	
Positive	Right	temporal cortex	84.96 TPO	105.05	9.51E-07	25.000	-17.500	8.125	
	Right	temporal cortex	49.07 TEO	35.80	2.40E-05	29.375	-25.000	-3.750	
	Left	cerebellum / pons	32.23 cerebellum / pons	14.18	3.80E-04	-3.750	-17.500	-8.750	
	Left	parietal cortex	27.34 PGOp	24.53	7.43E-05	-23.750	-14.375	13.125	
	Left	temporal cortex	24.41 entorhinal cortex	15.65	2.83E-04	-8.750	-2.500	-18.125	
	Left	visual cortex	TLR(36R)	12.16	5.98E-04	-12.500	-1.250	20.625	
	Left	visual cortex	23.93 V1	38.24	1.97E-05	-8.125	-35.000	7.500	
	Left	visual cortex	18.31 V1	14.44	3.60E-04	-5.625	-40.000	5.625	
	Right	precuneus	18.31 PEC	21.81	1.06E-04	0.625	-30.000	16.875	
	Left	visual cortex	17.82 V2	28.70	4.64E-05	-21.875	-28.750	-3.750	
	Right	temporal cortex	16.85 TE	16.54	2.40E-04	24.375	-5.625	-14.375	
	Right	motor cortex	15.87 Area 6	9.82	1.12E-03	17.500	1.250	20.625	
	Right	caudate / septum / stria terminalis / fornix	12.45 lateral septum / caudate	8.55	1.68E-03	1.875	2.500	5.625	
	Right	somatosensory cortex	8.79 Area 2	20.61	1.25E-04	26.875	-4.375	8.125	
	Left	motor cortex	8.30 Area 6	25.84	6.36E-05	-10.625	-0.625	18.125	
Negative	Right	frontal cortex	359.62 Area 8	-137.56	4.24E-07	14.375	8.750	18.750	
	Left	frontal cortex	Area 6	-56.20	6.20E-06	8.125	9.375	18.750	
	Left	cerebellum	28.81 cerebellum	-31.42	3.54E-06	-14.375	-29.375	-17.500	
	Right	visual cortex	24.90 V1	-19.54	1.46E-04	16.875	-38.125	-3.125	
	Left	temporal cortex	11.96 superior temporal gyrus	-35.88	2.38E-05	-26.875	0.000	-8.750	
	Right	visual cortex	10.25 V1	-37.15	2.14E-05	4.375	-46.875	-3.125	

TPO, temporal parieto-occipital association area; TEO, temporal area TE, occipital part; PGOp, parietal are PG, opercular part; TLR(36R), temporal area TL, rostral part; PEC, parietal area PE, caudal part
TE, temporal area TE;

Supplemental Table 7. significant peaks in the DTI analysis (FA)

Clusters demonstrating significant [CRH (post-pre) – Control (post-pre)] interaction		Local maxima for distinct brain regions within clusters		Location relative to anterior commissure					
Direction of effect	Hemisphere	Cluster	Cluster volume (mm ³)	Regions within cluster	Maximum t-value	p-value	x	y	z
Positive	Right	visual cortex	18.31 V1		61.74	4.68E-06	10.625	-38.125	15.000
	Right	visual cortex	17.58 collateral sulcus / ventral V3		28.16	4.91E-05	15.625	-33.125	-3.750
	Right	primary motor cortex	17.33 Area 4		8.30	1.84E-03	15.625	-4.375	18.125
	Right	visual cortex	10.50 V1 / V2		28.32	4.83E-05	15.625	-22.500	0.000
Negative	Right	visual cortex	48.34 V3A		-30.76	3.77E-05	12.500	-33.125	10.000
	Left	visual cortex	41.50 V2		-28.05	4.97E-05	-15.000	-34.375	13.125
	Left	intraparietal sulcus	32.23 V3A		-19.57	1.46E-04	-12.500	-26.875	6.875
	crosses midline	midline thalamus	16.11 mediodorsal thalamic nucleus		-10.73	8.66E-04	-1.875	-6.250	2.500
Right	corpus callosum	mediodorsal thalamic nucleus	-6.03		4.58E-03	4.375	-6.875	1.875	
	Right	splenium	12.70 splenium		-17.10	2.18E-04	3.750	-16.250	5.000
	Right	visual cortex	8.30 V1		-10.39	9.51E-04	10.625	-43.750	-5.625
Left	visual cortex	8.06 V1 / V2			-16.95	2.24E-04	-24.375	-34.375	4.375

References

1. Paxinos G, Huang X, Petrides M, Toga A (2009): *The rhesus monkey brain in stereotaxic coordinates*. 2nd ed. San Diego: Academic Press.
2. Lim MM, Hammock EA, Young LJ (2004): A method for acetylcholinesterase staining of brain sections previously processed for receptor autoradiography. *Biotechnic and Histochemistry*. 79:11-16.
3. Fox AS, Shelton SE, Oakes TR, Davidson RJ, Kalin NH (2008): Trait-like brain activity during adolescence predicts anxious temperament in primates. *PLoS ONE*. 3:e2570.
4. Shackman AJ, Fox AS, Oler JA, Shelton SE, Davidson RJ, Kalin NH (2013): Neural mechanisms underlying heterogeneity in the presentation of anxious temperament. *Proceedings of the National Academy of Sciences of the United States of America*. 110:6145-6150.
5. Oler JA, Fox AS, Shelton SE, Rogers J, Dyer TD, Davidson RJ, et al. (2010): Amygdalar and hippocampal substrates of anxious temperament differ in their heritability. *Nature*. 466:864-868.
6. Fox AS, Kalin NH (2014): A Translational Neuroscience Approach to Understanding the Development of Social Anxiety Disorder and Its Pathophysiology. *The American journal of psychiatry*.
7. Emborg ME, Joers V, Fisher R, Brunner K, Carter V, Ross C, et al. (2010): Intraoperative intracerebral MRI-guided navigation for accurate targeting in nonhuman primates. *Cell transplantation*. 19:1587-1597.
8. Emborg ME, Hurley SA, Joers V, Tromp do PM, Swanson CR, Ohshima-Hosoyama S, et al. (2014): Titer and product affect the distribution of gene expression after intraputaminal convection-enhanced delivery. *Stereotact Funct Neurosurg*. 92:182-194.
9. Truwit CL, Liu H (2001): Prospective stereotaxy: a novel method of trajectory alignment using real-time image guidance. *Journal of magnetic resonance imaging : JMRI*. 13:452-457.
10. Brodsky EK, Block WF, Alexander AL, Emborg ME, Ross CD, Sillay KA (2011): Intraoperative device targeting using real-time MRI. *Biomedical Sciences and Engineering Conference (BSEC)*, 2011, pp 1-4.

11. Grabow B, Block W, Alexander AL, Hurley S, CD R, Sillay K, et al. (2012): Extensible real-time MRI platform for intraoperative targeting and monitoring. *ISMRM Nineteenth Annual Scientific Meeting and Exhibition, poster presentation #1585*. Melbourne, Australia.
12. Grabow BP, Oler JA, Riedel M, Fekete EM, Kovner R, brodsky EK, et al. (2014): Alteration of Molecular Neurochemistry: MRI-guided Delivery of Viral Vectors to the Primate Amygdala. *ISMRM Twenty-First Annual Scientific Meeting and Exhibition, oral presentation #672*. Milan, Italy.
13. Brady ML, Raghavan R, Block W, Grabow B, Ross C, Kubota K, et al. (2015): The Relation between Catheter Occlusion and Backflow during Intraparenchymal Cerebral Infusions. *Stereotact Funct Neurosurg*. 93:102-109.
14. Santos JM, Wright GA, Pauly JM (2004): Flexible Real-Time Magnetic Resonance Imaging Framework. 1048-1051.
15. Radau PE, Pintilie S, Flor R, Biswas L, Oduneye SO, Ramanan V, et al. (2012): VURTIGO : Visualization Platform for Real-Time , MRI-Guided Cardiac Electroanatomic Mapping. 244-253.
16. Birn RM, Shackman AJ, Oler JA, Williams LE, McFarlin DR, Rogers GM, et al. (2014): Evolutionarily conserved prefrontal-amygadalar dysfunction in early-life anxiety. *Mol Psychiatry*. 19:915-922.
17. Fox AS, Oakes TR, Shelton SE, Converse AK, Davidson RJ, Kalin NH (2005): Calling for help is independently modulated by brain systems underlying goal-directed behavior and threat perception. *Proc Natl Acad Sci U S A*. 102:4176-4179.
18. Fox AS, Oler JA, Shackman AJ, Shelton SE, Raveendran M, McKay DR, et al. (2015): Intergenerational neural mediators of early-life anxious temperament. *Proc Natl Acad Sci U S A*. 112:9118-9122.
19. Kalin NH, Shelton SE, Fox AS, Oakes TR, Davidson RJ (2005): Brain regions associated with the expression and contextual regulation of anxiety in primates. *Biol Psychiatry*. 58:796-804.
20. Oler JA, Birn RM, Patriat R, Fox AS, Shelton SE, Burghy CA, et al. (2012): Evidence for coordinated functional activity within the extended amygdala of non-human and human primates. *Neuroimage*. 61:1059-1066.

21. Oler JA, Fox AS, Shelton SE, Christian BT, Murali D, Oakes TR, et al. (2009): Serotonin transporter availability in the amygdala and bed nucleus of the stria terminalis predicts anxious temperament and brain glucose metabolic activity. *J Neurosci*. 29:9961-9966.
22. Avants BB, Tustison NJ, Song G, Cook PA, Klein A, Gee JC (2011): A reproducible evaluation of ANTs similarity metric performance in brain image registration. *Neuroimage*. 54:2033-2044.
23. Avants BB, Yushkevich P, Pluta J, Minkoff D, Korczykowski M, Detre J, et al. (2010): The optimal template effect in hippocampus studies of diseased populations. *Neuroimage*. 49:2457-2466.
24. Vincent JL, Patel GH, Fox MD, Snyder AZ, Baker JT, Van Essen DC, et al. (2007): Intrinsic functional architecture in the anaesthetized monkey brain. *Nature*. 447:83-86.
25. Cox RW (1996): AFNI: software for analysis and visualization of functional magnetic resonance neuroimages. *Comput Biomed Res*. 29:162-173.
26. Jo HJ, Saad ZS, Simmons WK, Milbury LA, Cox RW (2010): Mapping sources of correlation in resting state fMRI, with artifact detection and removal. *Neuroimage*. 52:571-582.
27. Woolrich MW, Jbabdi S, Patenaude B, Chappell M, Makni S, Behrens T, et al. (2009): Bayesian analysis of neuroimaging data in FSL. *Neuroimage*. 45:S173-186.
28. Cook PA, Bai Y, Nedjati-Gilani S, Saunarine KK, Hall MG, Parker GJ, et al. (May, 2006): Camino: Open-Source Diffusion-MRI Reconstruction and Processing. *14th Scientific Meeting of the International Society for Magnetic Resonance in Medicine*. Seattle, WA, USA, pp 2759.
29. Chang LC, Jones DK, Pierpaoli C (2005): RESTORE: robust estimation of tensors by outlier rejection. *Magnetic resonance in medicine : official journal of the Society of Magnetic Resonance in Medicine / Society of Magnetic Resonance in Medicine*. 53:1088-1095.
30. Zhang H, Yushkevich PA, Alexander DC, Gee JC (2006): Deformable registration of diffusion tensor MR images with explicit orientation optimization. *Medical image analysis*. 10:764-785.
31. Olschowka JA, O'Donohue TL, Mueller GP, Jacobowitz DM (1982): The distribution of corticotropin releasing factor-like immunoreactive neurons in rat brain. *Peptides*. 3:995-1015.

32. Tagliaferro P, Morales M (2008): Synapses between corticotropin-releasing factor-containing axon terminals and dopaminergic neurons in the ventral tegmental area are predominantly glutamatergic. *J Comp Neurol.* 506:616-626.
33. Vale W, Spiess J, Rivier C, Rivier J (1981): Characterization of a 41-residue ovine hypothalamic peptide that stimulates secretion of corticotropin and beta-endorphin. *Science.* 213:1394-1397.
34. Raper J, Stephens SB, Henry A, Villarreal T, Bachevalier J, Wallen K, et al. (2014): Neonatal amygdala lesions lead to increased activity of brain CRF systems and hypothalamic-pituitary-adrenal axis of juvenile rhesus monkeys. *J Neurosci.* 34:11452-11460.